Fall 2012

Flame structure and thermo-acoustic coupling for the low swirl burner for elevated pressure and syngas conditions

Majid Emadi
University of Iowa

FLAME STRUCTURE AND THERMO-ACOUSTIC COUPLING FOR THE LOW

SWIRL BURNER FOR ELEVATED PRESSURE AND SYNGAS CONDITIONS

by

Majid Emadi

An Abstract

Of a thesis submitted in partial fulfillment
of the requirements for the Doctor of
Philosophy degree in Mechanical Engineering
in the Graduate College of
The University of Iowa

December 2012

Thesis Supervisor: Associate Professor Albert Ratner

ABSTRACT

Reduction of the pollutant emissions is a challenge for the gas turbine industry. A solution to this problem is to employ the low swirl burner which can operate at lower equivalence ratios than a conventional swirl burner. However, flames in the lean regime of combustion are susceptible to flow perturbations and combustion instability. Combustion instability is the coupling between unsteady heat release and combustor acoustic modes where one amplifies the other in a feedback loop. The other method for significantly reducing NO_x and CO_2 is increasing fuel reactivity, typically done through the addition of hydrogen. This helps to improve the flammability limit and also reduces the pollutants in products by decreasing thermal NO_x and reducing CO_2 by displacing carbon.

In this work, the flammability limits of a low swirl burner at various operating conditions, is studied and the effect of pressure, bulk velocity, burner shape and percent of hydrogen (added to the fuel) is investigated. Also, the flame structure for these test conditions is measured using OH planar laser induced fluorescence and assessed.

Also, the OH PLIF data is used to calculate Rayleigh index maps and to construct averaged OH PLIF intensity fields at different acoustic excitation frequencies (45-155, and 195Hz). Based on the Rayleigh index maps, two different modes of coupling between the heat release and the pressure fluctuation were observed: the first mode, which occurs at 44Hz and 55Hz, shows coupling to the flame base (due to the bulk velocity) while the second mode shows coupling to the sides of the flame. In the first mode, the flame becomes wider and the flame base moves with the acoustic frequency. In the second mode, imposed pressure oscillations induce vortex shedding in the flame shear layer. These vortices distort the flame front and generate locally compact and sparse flame areas. The local flame structure resulting from these two distinct modes was markedly different.

Abstract Approved: _____
                   Thesis Supervisor

                   _____
                   Title and Department

                   _____
                   Date

FLAME STRUCTURE AND THERMO-ACOUSTIC COUPLING FOR THE LOW

SWIRL BURNER FOR ELEVATED PRESSURE AND SYNGAS CONDITIONS

by

Majid Emadi

A thesis submitted in partial fulfillment
of the requirements for the Doctor of
Philosophy degree in Mechanical Engineering
in the Graduate College of
The University of Iowa

December 2012

Thesis Supervisor: Associate Professor Albert Ratner

www.manaraa.com

Graduate College
The University of Iowa
Iowa City, Iowa

CERTIFICATE OF APPROVAL

_____

PH.D. THESIS

_____

This is to certify that the Ph.D. thesis of

Majid Emadi

has been approved by the Examining Committee
for the thesis requirement for the Doctor of Philosophy
degree in Mechanical Engineering at the December 2012 graduation.

Thesis Committee: _____

           Albert Ratner, Thesis Supervisor

           _____

           Patrick Butler

           _____

           William Eichinger

           _____

           Ching-Long Lin

           _____

           H.S. Udaykumar

ACKNOWLEDGEMENTS

First, I would like to express my sincere gratitude to my advisor, Professor Albert Ratner, for all of his help and support throughout my PhD study. His guidance, understanding and encouragement have provided a foundation for the present thesis.

I would like to express my sincere thanks to my thesis committee members, Prof. Butler, Prof. Lin, Prof. Udaykumar, and Prof. Eichinger.

I thank all the members in our lab; in particular Yun Huang, Neeraj Mishra, Taleb Salameh, Doug Karkow, Matt Zanker, Tim Gentry, Matt Burkhalter, and Jianan Zhang for making my time here so enjoyable.

I would like to thank the University of Iowa, the Richard B. Stewart Thermal-Fluids Graduate Scholarship foundation, the Lawrence Berkeley National Laboratory (R.K. Cheng as the project monitor), and Siemens (Scott Martin as the project monitor), for financial support.

Finally, I want to thank my dear wife and family for their love and encouragement.

ABSTRACT

Reduction of the pollutant emissions is a challenge for the gas turbine industry. A solution to this problem is to employ the low swirl burner which can operate at lower equivalence ratios than a conventional swirl burner. However, flames in the lean regime of combustion are susceptible to flow perturbations and combustion instability. Combustion instability is the coupling between unsteady heat release and combustor acoustic modes where one amplifies the other in a feedback loop. The other method for significantly reducing NO_x and CO_2 is increasing fuel reactivity, typically done through the addition of hydrogen. This helps to improve the flammability limit and also reduces the pollutants in products by decreasing thermal NO_x and reducing CO_2 by displacing carbon.

In this work, the flammability limits of a low swirl burner at various operating conditions, is studied and the effect of pressure, bulk velocity, burner shape and percent of hydrogen (added to the fuel) is investigated. Also, the flame structure for these test conditions is measured using OH planar laser induced fluorescence and assessed.

Also, the OH PLIF data is used to calculate Rayleigh index maps and to construct averaged OH PLIF intensity fields at different acoustic excitation frequencies (45-155, and 195Hz). Based on the Rayleigh index maps, two different modes of coupling between the heat release and the pressure fluctuation were observed: the first mode, which occurs at 44Hz and 55Hz, shows coupling to the flame base (due to the bulk velocity) while the second mode shows coupling to the sides of the flame. In the first mode, the flame becomes wider and the flame base moves with the acoustic frequency. In the second mode, imposed pressure oscillations induce vortex shedding in the flame shear layer. These vortices distort the flame front and generate locally compact and sparse flame areas. The local flame structure resulting from these two distinct modes was markedly different.

TABLE OF CONTENTS

LIST OF TABLES

LIST OF FIGURES

viii

ix

CHAPTER 1

INTRODUCTION

1.1 Background and Motivation

Gas turbine engines have a key role in human being's life as the heart of power plants in power generation process. Most of the industries in the world depended on the power produced by these engines. Natural gas in the most common fuel used in these systems but to increase the efficiency and to broaden the fuel options other reactive gases such as hydrogen; carbon monoxide are being considered as fuel additive/substitutes. The combustion process in an industrial gas turbine engines takes place at high temperature, high pressure and with high reactant flow rates. The hot pressurized product gases of this chemical reaction, which consists mostly of water vapor, carbon dioxide, and nitrogen (pollutions like carbon monoxide, lead, nitrogen oxides, particulate matter, sulfur dioxide, and volatile organic are also present in the ppm range) drive the turbines and generate power.

The two major challenges for the gas turbine engine designers are improving the thermal efficiency of the engine and also reducing the pollutant emissions. Since the passage of clean air in 1970 (which is updated every four years) the EPA tracks the six principle air pollutants mentioned above, and industry has successfully reduced all of them to acceptable levels except for the oxides of nitrogen. NO_x, consisting of NO and NO_2, is a contributor to stratospheric ozone depletion, acid rain, and smog. Stricter government regulations regarding pollutant emissions, and in particular for oxides of nitrogen, continue to be inacted. As a result, the gas-turbine industry is seeking new ways to reduce NO_x emissions.

Several solutions have been previously employed in industry to reduce NO_x emissions and meet EPA regulations. Catalytic combustion, rich-burn/quick-quench/lean-burn (RQL), exhaust stream clean-up using ammonia, fuel staging, water or steam

injection, and lean premixed combustion are some of these techniques. Of these, lean premixed combustion is garnering the most interests of late. In this regime of combustion the flame temperature is reduced due to an excess of air (combustion occurs at low equivalence ratios) and result in a decrease in Zeldovich mechanism (thermal) for NO_x formation (Turns, 2001; Littlejohn et al., 2002). For instance, GE in 2005 utilized a dry low NO_x combustion system for their 12 MW class 10-2 gas turbine reduced NO_x emissions from 25 to 15 ppm.
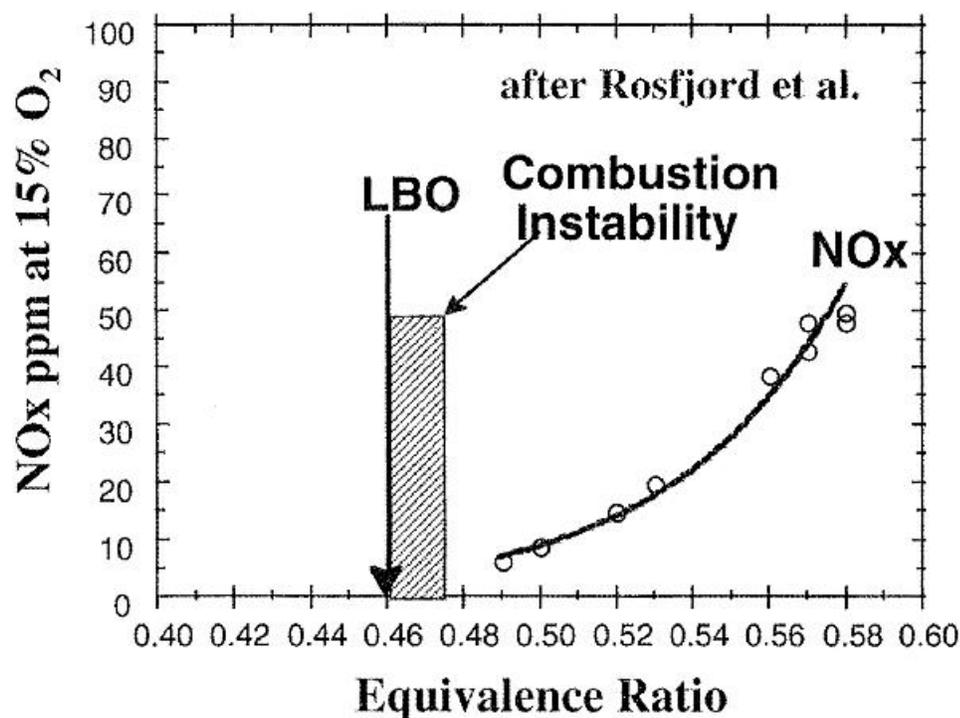
Figure 1.1 As the equivalence ratio decreases, NO_x formation reduces.

Source: Rosfjord, 1994

Several approaches for designing new burners to obtain better performance and pollution reduction have been undertaken. One new burner design that seems to meet

many of the desired criteria is the low swirl burner (LSB) developed by Robert K. Cheng (Cheng et al., 2000) at the Lawrence Berkeley national lab (LBNL). This burner creates a flame that has a shorter chemical residence time and operates at lower equivalence ratios than the current industrial burners (high swirl burners). Being able to operate in a leaner regime decreases the NO_x production of this burner.
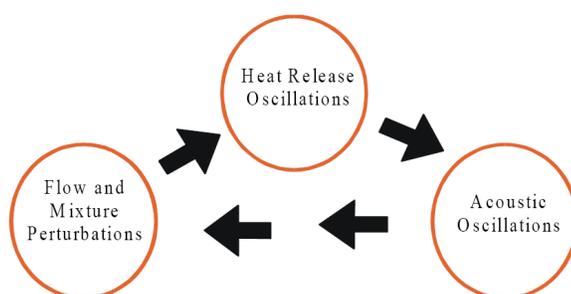
Figure 1.2 Feedback mechanism responsible or combustion instability

However, lean premixed combustion is susceptible to flow field fluctuations. As shown in figure 1.2, these perturbations can alter the combustion process and cause an unsteady heat release in the system which results in excitation of the chamber acoustic modes. If these self-excited acoustic fluctuations couple with the heat release, combustion instability occurs. The large pressure fluctuation generated in the combustion system as the result of acoustic and combustion coupling can cause serious problems for both the chamber and the flow fields, reducing the life-time of system components or increasing pollutant production. Part life-time is affected by the enhanced heat transfer due to the unsteady heat release, particularly for components operating near high temperature limits, such as the combustor liner or turbine blades, and can lead to a catastrophic failure. Also, instability can trigger the flame to become unstable and blow-

off. It was reported that the cost for the repair and replacement of hot section components, where much of the damage was directly attributable to combustion instability, now exceeds $1 billion annually and constitutes up to 70% of the nonfuel costs for F-class gas turbines. Combustion instability is not only seen in gas turbines. It has been encountered in a variety of combustors, for example, propulsion systems (rockets, ramjets, and afterburners), power generation (land-based gas turbines), boiler and heating systems, and industrial furnaces (Lieuwen and Yang, 2006).

The fuel used for most gas turbines is natural gas which mainly consists of methane. One solution to reduce NO_x formation is to add a small amount of other fuels which are more reactive (with a burning rate higher than methane). One of these candidate additive fuels is hydrogen. Hydrogen enrichment of fuel helps to broaden the flammability range and enables operation at lower equivalence ratios (Emadi et al., 2012). Since hydrogen increases the global reactivity and the mixture's resistance to the flow oscillations, it can improve combustion stability. However, the effect of adding hydrogen on flame dynamics and its structure is not well understood.

1.2 Objectives and Outline

This thesis examines the effect of hydrogen enrichment (in the low swirl burner) on flame dynamics and structure and also on the flammability range. Even though many studies have examined combustion instability, and specifically instability in low swirl burners, this phenomenon is still not well understood. Measurement of the flame response to acoustic forcing at various frequencies, while maintaining the amplitude of the perturbation nearly constant is the other goal of this research.

Chapter 2 presents a literature review of combustion instability mechanisms, models, criteria and measurement techniques. Chapter 3 introduces the experimental arrangement; including the 3.81 cm low swirl burner, combustion chamber, acoustic excitation system, laser diagnostics and PLIF technique. In chapter 4 the flame structure

of pure methane flame, and hydrogen enriched flame are examined. Flame surface curvature and density for various conditions are calculated and the effect of adding hydrogen and elevating the pressure on the flame structures is examined. Chapter 5 examines thermoacoustic instability in the low swirl burner and different modes of instability are categorized. In chapter 6 a comparison between methane flame response and hydrogen-methane flame response to acoustic forcing is carried out. Chapter 7 presents the proposed future works, including examination of the effect of mean pressure, amplitude of acoustic perturbations and bulk velocity on the acoustic modes of the chamber and flame response to the acoustic excitation. Chapter 7 also includes results and conclusions.

CHAPTER 2

LITERATURE REVIEW

Combustion instability and flame dynamics are broad topics in combustion research. Large numbers of studies have been gain a better understanding of these phenomena. In this chapter, a review of the literature related to flame dynamics and structures is presented. The first part of this chapter is about low swirl burner. Then combustion instability is introduced and the physical factors which lead to amplification of system fluctuations are presented. Various theoretical models utilized as tools in CFD to predict instability in a combustion system are then reviewed. The fourth section focuses on flame structures and their importance in flame dynamics research. And the last part is a brief review of visualization methods and measurement techniques applied by other researchers.

2.1 Low Swirl Burner

One of the solutions applied to reduce the pollutant emission over the last decade is the lean premixed combustion, but stabilizing the flame at the lean combustion regime due to the lack of inherent damping (Syred, 2006) is still a challenge for the designers. Swirling flow burners have been employed in the combustion systems as an option because of their significant beneficial on flame stability, combustion intensity, and engine performance. In the swirl burners, the circulating motion generated by the injectors or vanes (figure 2.1) produces internal toroidal recirculation zones at the entrance of the combustor, as seen in figure 2.2. These vortical structures circulate heat and active chemical radicals like CH and OH to the root of the flame and cause the flame to stabilize in regions of relative low velocity where flow and flame velocity can be matched.

In figure 2.2 the processing vortex core (PVC) and central recirculation zone (CRZ) are also shown. PVC and CRZ usually develop in high swirl flows and can affect the combustion stability. The CRZ flow field shows a large acceleration which increases

the shear stress and turbulence intensities at this region (Gupta et al., 1984). This effect causes better mixing and stabilizing the flame in a wider range of equivalence ratios.
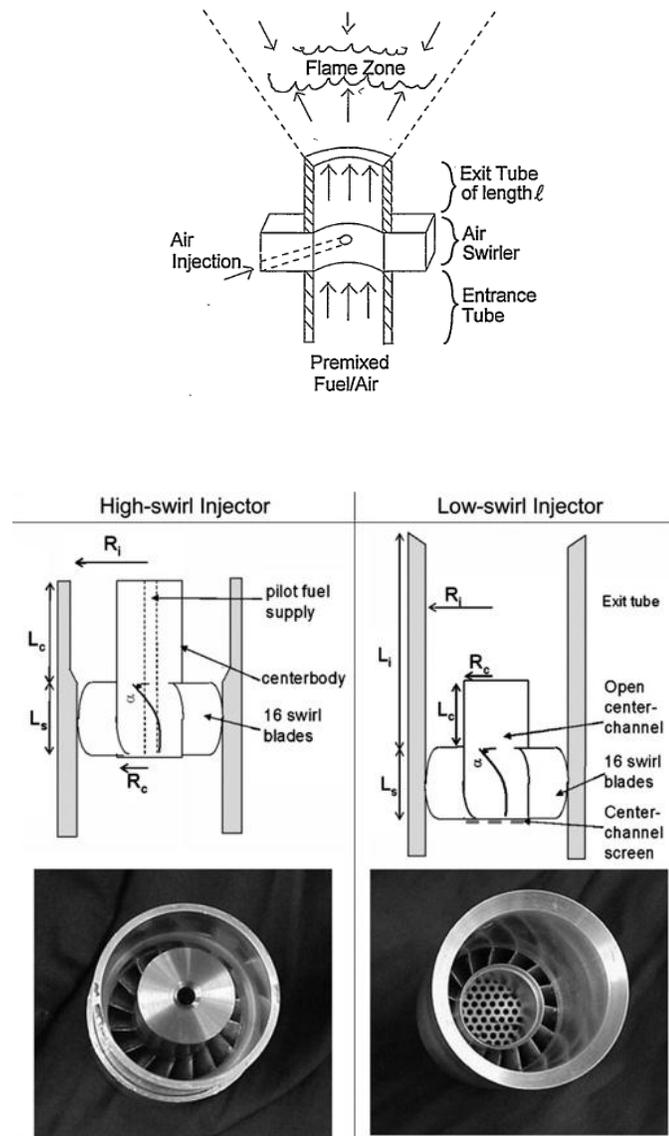
Figure 2.1 Two ways for generating the swirl flow

Source: Left: Cheng et al., 2000, Right: Johnson et al. 2005
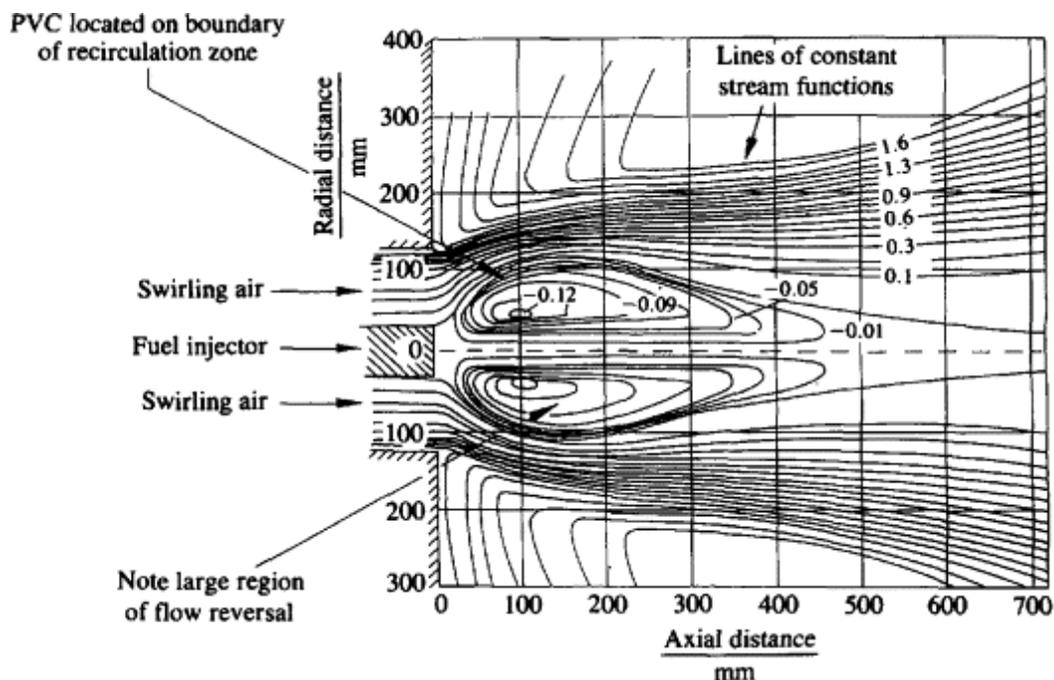
Figure 2.2 Stream line and PVC location of a swirl burner swirl number 1.57

Source: Chigier and Beer, 1964

Central vortical structures in the center of high swirl burners exhibit a highly non-axisymmetric, low-frequency instability, known as the precessing vortex core PVC (Yazdabadi et al., 1994; Griffiths, et al. 1998). The PVC is a quasi-periodic motion of the core of the main vortical structure about the cyclone's geometrical center. Experimental studies of swirling flow reveal the strong impact of vortex core precession on the level of the velocity fluctuations (Wunenburger et al., 1999). It can also affect the flame shape and size and alter the heat release pattern inside the chamber. To eliminate the PVC and its unfavorable effects on combustion process, the idea of the low swirl burner was introduced by Robert Cheng. In the low swirl burner, some of the reactants flow axially through the center of the burner and the rest pass through the vanes and are swirled (figure 2.3).
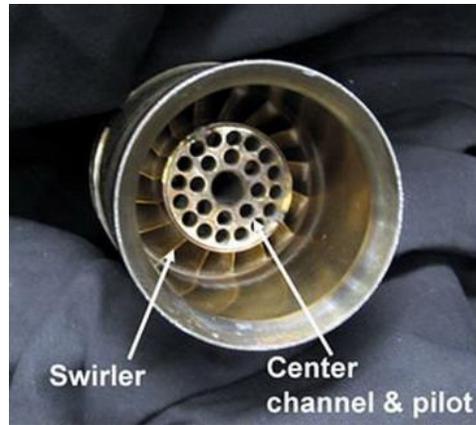
Figure 2.3 Low swirl burner designed by Robert Cheng (from LBL website)

The low swirl burner generates a non-recirculating flow described by a flow divergence region where the axial flow velocity decays linearly with the distance away from the burner exit (Cheng et al. 2000; Littlejohn et al. 2007). Figure 2.4 shows the flow field measurements with Particle Image Velocimetry (PIV) method in a LSB.
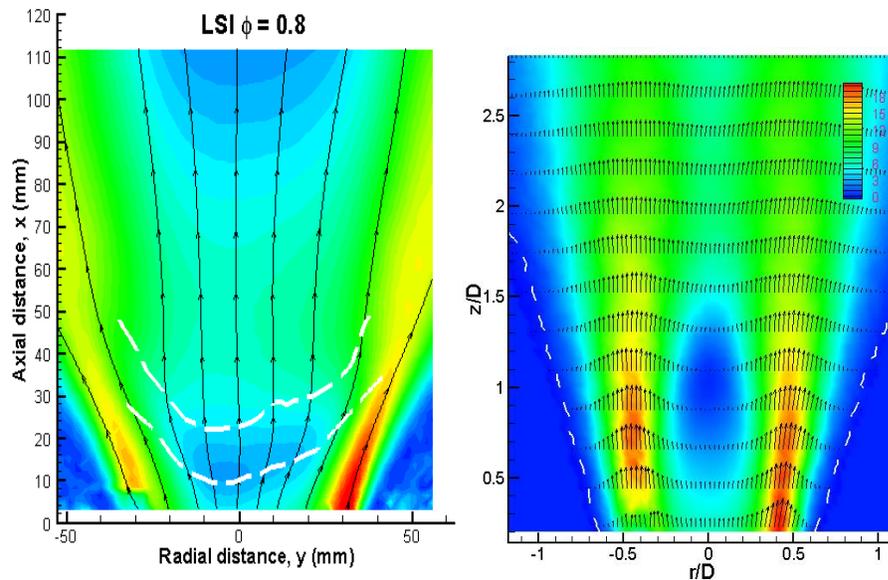
Figure 2.4 Flow field in the low swirl burner by Robert Cheng

The flow field of low swirl burner shows a self-similar behavior like the turbulent jet flow (Cheng et al., 2006). Nazeer et al. in 2006 showed the NO_x emission of this burner in a full scale engine is much smaller than that of the high swirl burner. Because of this, low swirl burner technology won the 2007 R&D 100 Award. However, the interaction between combustion and acoustics in this burner is not well understood. The goal of this study is to give a better understanding of the flame and acoustic interaction in a 3.81 cm low swirl burner which is relatively large (close to the industrial scales) and to identify the various coupling modes in the combustion chamber. The effect of pressure and fuel composition on the flame structure of LSB will also be addressed.

2.2 Combustion Instabilities

Combustion instability phenomenon is characterized as large amplitude fluctuations of natural acoustic modes of the combustor due to the coupling between flame dynamics and combustion chamber acoustics. For decades it has been an obstacle in development of power generation and propulsion systems, industrial boiler and furnaces. Combustion instability is maintained and amplified by the feedback loop mechanism between the unsteady heat release process and acoustic fluctuations. Perturbations in the flow field or thermodynamic variables can induce unsteadiness into heat release pattern. This oscillatory heat release excites acoustic fluctuations that propagate away from the flame. These acoustic pressure and velocity fluctuations interact with the flow field and thermodynamic variables and close the feedback loop. The large amplitude acoustic pressure and velocity oscillations resulting from combustion instability can cause serious problems in a combustion system such as flame blow-off or flash back, severe vibration and fatigue stresses in combustors components, structural failures (figure 2.5), and thermal stresses due to the heat transfer enhancement.
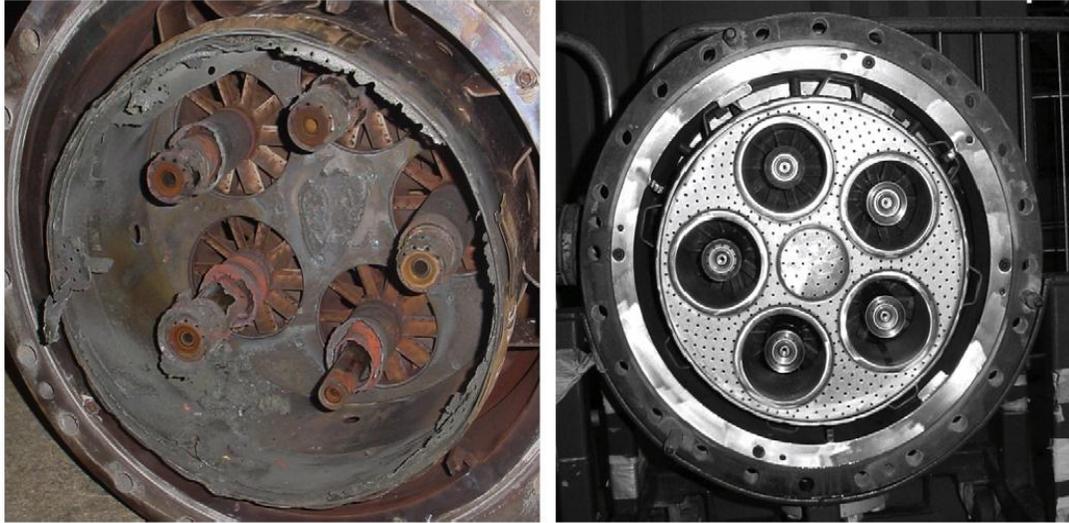
Figure 2.5 Burner assembly (left) damaged by combustion instability and new burner assembly (a non-premixed jet flame with acoustic perturbation (Goy et al., 2005)

In industry, combustion instabilities are categorized by their frequencies and grouped into the following categories: low frequency, intermediate frequency and high frequency (Sutton and Biblarz, 2000). Low frequency instabilities are in the frequency range of 10 to 50 Hz. In the industry these types of oscillations are referred to as "cold tone" because their amplitude increase as the flame temperature decreases. These fluctuations are often observed at the lean regime of combustion and close to blowout limits. Low frequency unstable modes are audible and may sound like a passing freight train running through the plant. Seasonal tuning in spring and fall is necessary for engines with this type of instability. In the fall as the temperature is lower and air is denser, the combustion occurs in a leaner regime. The mid-range frequency instabilities are usually observed in the range 100-250 Hz. These fluctuations are usually referred to as "hot tones" because their amplitudes increases with the flame temperature and engine load. High frequency oscillations are usually above 1000 Hz and occasionally observed in industrial gas turbines.

2.2.1 Combustion Instability Deriving Mechanisms

Several mechanisms are known to be capable of triggering combustion instabilities in gas turbine engines. The first mechanism is the coupling between the fuel feeding system and the acoustics (Kendrick et al. 1998). Pressure fluctuations inside the chamber affect the pressure drop through the fuel nozzles or injectors. If the nozzles are unchecked, this variation in pressure drop can negatively affect the fuel flow rate passing through them. The unsteady fuel flow rate causes unsteadiness of the heat release in the chamber, which results in excitement of the acoustic modes of the combustor and produces more pressure oscillations. In this case the feedback loop of instability is closed and the combustion system becomes unstable.

The interaction of equivalence ratio fluctuations and chamber acoustics could be another driving mechanism of instability. Equivalence ratio oscillations can be generated either by incomplete mixing of the reactants in the premixer or by the fluctuations which fuel and air supply systems induce to the system. The inhomogeneity in the reactant mixture results in unsteady heat release in the chamber. The pressure fluctuations excited by the heat release modulate the mixing process and they form a feedback loop of instability. Lieuwen et al. (1998) theoretically showed that the fluctuations of the equivalence ratio in low NO_x gas turbines can perturb the acoustic field and amplify the oscillations. Kang et al. (2009) investigated a non-premixed jet flame with acoustic perturbation. They demonstrated that the level of mixing and the local equivalence ratio are sensitive to the excitation frequency and that flame response is a function of frequency.

In liquid fuel engines, the processes of atomization, evaporation and mixing could be a source of instability. Acoustic interaction with the fuel spray from injectors might affect the spray pattern and produces an oscillatory fuel injection. The shape and size of the droplets and the mixing process might also be altered due to the acoustic coupling. All these periodic behaviors can cause unsteady heat release in the chamber and make a

closed feedback loop with the acoustic perturbations. In this situation the instability can be triggered in the combustion system.

The other mechanism that can be responsible for triggering instability is the interaction between the flame and coherent vortical structures. These vortices could be created by the flow separation from the flame holder, rapid expansion in the dump combustors and/or vortex break down in swirl combustion systems. The formation of vortical structures in the combustors is known to be an important source of coupling between the acoustic field and the flame. Vortices usually form at the shear layers due to the velocity gradient between the different layers. In combustion chambers the roll-up of the mixing layer between cold reactants and hot gas products can lead to the formation of a coherent vortical structure (figure 2.6). The fresh gases inside are convected by the mean flow downstream of the chamber and are also simultaneously mixed with the burnt product gases. This pocket of fresh reactants burns downstream of the chamber and causes unsteady heat release.
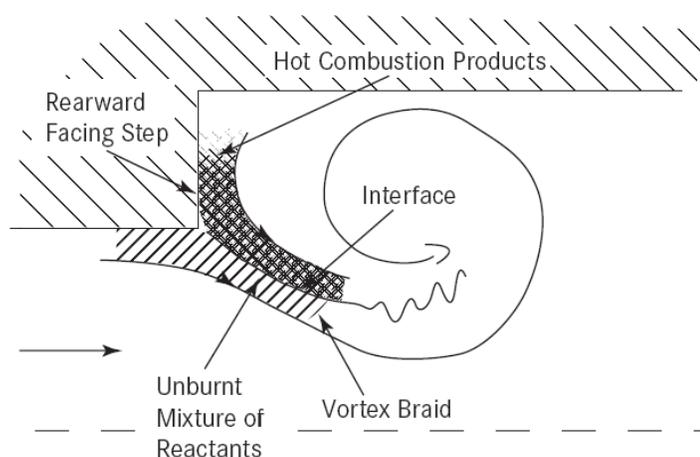
Figure2.6 Vortex roll-up in a dump combustor

Source: Schadow and Gutmark, 1992
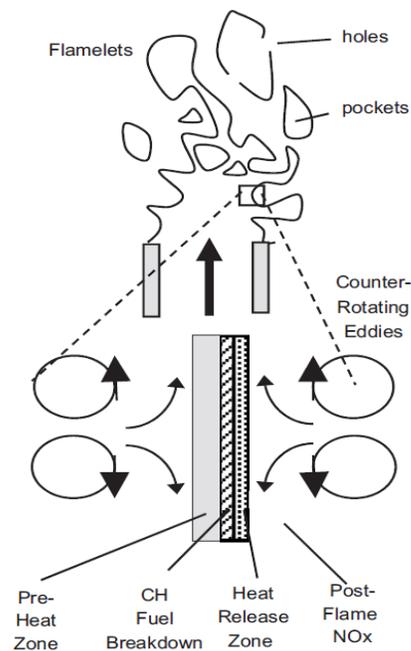
Figure2.7 Structure of turbulent premixed flame

Source: Driscoll, 2008

The vortical structures alter the flame surface (and in results the combustion process) too. It can stretch the flame surface which leads to increase in heat release (heat release is proportional to the flame surface) or distort it in a way that cause quenching in some portion of the flame and forms holes in it as shown in figure 2.7.

In 1987 Poinsot and coworkers calculated the phase difference between heat release and pressure oscillations by measuring the emission of C_2 in a dump combustor and showed that the phase relationship is a function of delay times due to vortex formation, convection and combustion. Gutmark et al. (1989) and Keller (1995) reported the same observation. Generally, it seems that, in the combustion zone, if the frequency

of vortex shedding is close to the frequency of acoustic field (or natural modes of the chamber), it can amplify the acoustic fluctuations. In addition, if the amplitude of acoustic perturbations is large enough, a feedback loop can be formed and the combustion process can become unstable.

The other factors which might affect the instability are reactants density and mean pressure. Both of these properties have a role in flame speed. By increasing the mean pressure of the chamber, the speed of flame will increase and cause change in blow-off limits (change the flame stability). The same scenario may happen as the density varies. Also the acoustic characteristics of the combustion chamber may be altered by changing the mean pressure and density, and as a result the acoustic field will show a different behavior. By changing the flame speed the position which flame stabilized there will vary, and causes change in flame dynamics.

2.2.2 Instability Suppression Methods

To suppress combustion instability, the feedback loop between the active acoustic modes and unsteady heat release should be interrupted. Two methods are employed in industry to mitigate these instabilities: passive and active control. In passive control the geometrical parameters of the unstable system, the type of fuel or the combustor hardware are changed to reduce the rate of energy transferred to the unstable modes. In active control the goal is to minimize the changes in the system design. Generally the fluctuations in active control are tracked by the sensors and then if they show an unusual behavior in the system, the feedback control loop modifies the input parameters to restore the system to the desirable conditions.

Energy of an unstable mode can be removed via three processes. The first process is to transfer the acoustic energy to vortical or entropy disturbances through viscous dissipation and heat transfer respectively. The energy of acoustic waves can be dissipated through boundary layer losses near the rigid surfaces (Temkin, 1981) or the flow

separation losses at sharp edges or during rapid expansions (Robertson, 1993). The other way to dissipate the acoustic energy is convection or radiation of acoustic energy out of the system. The mean fluid motion can convect the acoustic energy to the outside of the system boundaries. Transferring energy to the stable modes can also help to damp unstable modes.

2.3 Theoretical approach to Combustion Instabilities

One of the early theoretical approaches to combustion instability is the Rijke tube. When the air inside an open-end tube is locally heated, acoustic oscillations are generated in the tube (figure 2.8). Rijke observed that the acoustic fluctuations created by the heated wire screen would stop if the top of the tube were closed. This change in behavior shows that the air convection upward in the pipe is a necessary condition for generating sound in Rijke tube. The maximum amplitude of oscillations is observed when the heated screen is located at a quarter of the length of the tube from bottom. When the screen is positioned a quarter of the pipe length from the top of the tube, damping instead of driving is observed (Bisio, G. and Rubbato, G., 1999).

Simple models of acoustic field in confined combustors have been proposed based on the similarity of systems to the Rijike tube. Dowling and Stow (2003) calculated the acoustic modes of a simple 1D duct. The pressure field in the duct was modeled by following equation:

$$\frac{1}{c^2}\frac{D^2 p'}{Dt^2} - \nabla^2 p' = \frac{\gamma-1}{c^2}\frac{Dq'}{Dt}$$

(2.1)

Here, p' is the pressure fluctuation, q' is heat release fluctuation, γ is the specific heat ratio and c is the velocity of sound. If no heat release occurs in the system, the acoustic pressure and velocity fields can be obtained as:

$$\hat{p}(x) = \hat{f}e^{-i\omega x/\bar{c}} + \hat{g}e^{i\omega x/\bar{c}}, \ \hat{u}(x) = \frac{1}{\bar{\rho}\bar{c}}\left(\hat{f}e^{-i\omega x/\bar{c}} - \hat{g}e^{i\omega x/\bar{c}}\right)$$

(2.2)

In equation (2.2) f and g are arbitrary functions of time, x is the axial direction, ω is the frequency and i is the square root of negative one. The frequency of natural modes of the combustor is calculated based on the boundary conditions. For example if the chamber has one end open (open to the atmosphere or attached to a large plenum) and one end closed, the frequency ω of the plane wave is:

$$\omega_n = \frac{(2n-1)\pi\bar{c}}{2l} \tag{2.3}$$
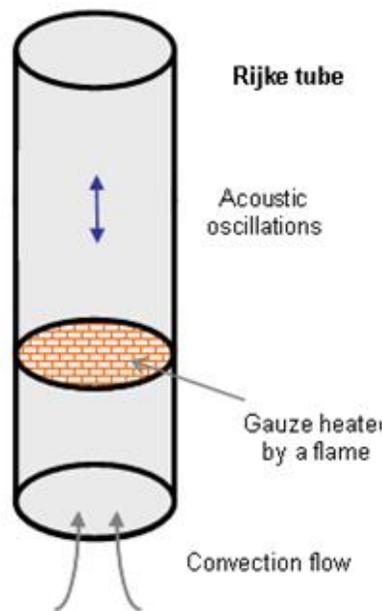
Figure2.8 Rijke tube

However, to find the acoustic field in existence of flame, heat release fluctuations should be modeled. Several models for heat release are proposed by Crighton et al. (1992). The frequencies calculated by this method (even in non-uniform ducts) matches very well with the experimental results.

The results presented above are all calculated for 1-D geometries, but to have a better sense of real systems, equation 2.1 should be solved for 3-D geometries. A 3-D analysis of acoustic field in a cylindrical geometry in the absence of flame was conducted by Culick and Yang (1995). The pressure perturbation resulting from separation method is introduced in equation (2.4).

$$p' = \sum_{l,m,n} A_{lmn} J_m(k_{rmn} r) \cos(m\theta + \gamma_{lmn}) \cos(k_{zl} z) e^{j\omega_{lmn} t} \tag{2.4}$$

Where l, m, and n are integers, J_m is the Bessel function of the first kind of order m, , k_{rmn} is the wave number in the radial direction; γ_{lmn} is the wave number in the azimuthal direction; k_{zl} is the wave number in the longitudinal direction which satisfies $k_{zl} L = l\pi$ where L is the chamber length. And the frequency of pressure fluctuations is determined by:

$$\omega_{lmn} = \bar{c}(k_{rmn}^2 + k_{zl}^2)^{1/2} \tag{2.5}$$

In equation (2.1), if $m=n=0$ and $l\neq 0$, longitudinal modes is given. If $l=m=0$, $n\neq 0$, it represents radial modes and finally tangential modes or azimuthal modes are described if $l=n=0$ and $m\neq 0$. Culick (2001) showed the frequencies of acoustic modes calculated by equation (2.5) are within 10-15% of results from the experimental observation.

2.3.1 Instability Criteria

In 1945, Lord Rayleigh was the first to state the instability criteria:

"If heat be communicated to, and abstracted from, a mass of air vibrating (for example) in a cylinder bounded by a piston, the effect produced will depend upon the phase of the vibration at which the transfer of heat takes place. If heat be given to the air at the moment of greatest condensation, or be taken from it at the moment of greatest rarefaction, the vibration will be encouraged. On the other hand, if heat be given at the moment of greatest rarefaction, or abstracted at the moment of greatest condensation, the vibration will be discouraged."

Rayleigh criterion describes the conditions under which the periodic heat release in the chamber can amplify the acoustic perturbations and add energy to the acoustic field. Putnam formulized this criterion as follow:

$$\iint_{V\,T} p'q'\,dt\,dV > 0 \qquad (2.6)$$

Where, *p'* and *q'* are pressure and heat release oscillation, *V* is the volume and *T* is the period of fluctuations. Equation (2.6) says the heat release process adds energy to the acoustic field when the phase between unsteady heat release and pressure oscillations is less than 90 degree and when they are out of phase; the combustion process damps the acoustic perturbations. Nicoud and Poinsot (2005) extended the Rayleigh criterion. First they introduced the acoustic energy equation:

$$\frac{\partial}{\partial t}\int_V \left(\frac{1}{2}\bar{\rho}\vec{u}^2 + \frac{1}{2}\frac{p'^2}{\overline{\rho c}} \right) dV = \int_V \frac{(\gamma-1)p'q'}{\gamma\bar{P}} dV - \int_S p'\vec{u}.d\vec{S} \qquad (2.7)$$

Here ρ is the density, *u* is the velocity, and *S* is the area. The term on the left hand side of (2.7) represents the change in acoustic energy. The first term on the right hand side is the expected Rayleigh term as a source term and the second term at the right hand side represents the acoustic fluctuations transferred through the system boundaries. It is obvious that the acoustic energy growth rate depends not only on the Rayleigh term, but also on the acoustic fluxes. So the Rayleigh criterion is only a necessary condition for instability to initiate and the following acoustic energy criterion can predict instability more accurate than the Rayleigh criterion:

$$\int_V \frac{(\gamma-1)p'q'}{\gamma\bar{P}} dV > \int_S p'\vec{u}.d\vec{S} \qquad (2.8)$$

This criterion basically says that the amplification of the acoustic energy inside the system must be greater than the damping due to acoustic flux from the physical boundaries, otherwise the system become unstable.

The other criterion proposed by Nicoud and Poinsot is the "fluctuating energy". In this approach the effects of non-isentropic flow field and linear entropy fluctuations on the initiation of instability is being included. The energy equation has the following form:

$$\frac{\partial}{\partial t}\int_V \left(\frac{1}{2}\overline{\rho}\vec{u}^2 + \frac{1}{2}\frac{p'^2}{\overline{\rho c}} + \frac{\overline{P}s'^2}{2RC_p}\right)dV = \int_V \left(\frac{T'q'}{\overline{T}} - \frac{\overline{P}s'}{RC_p}\vec{u}.\nabla\overline{s}\right)dV - \int_S p'\vec{u}.d\vec{S} \qquad (2.9)$$

Where R is the gas constant, C_p is the specific heat, s is the entropy, and T is the temperature. If the flow is isentropic equation (2.9) and (2.7) are identical. The fluctuating energy equation suggests that the classic Rayleigh criterion should be replaced by:

$$\int_V \left(\frac{T'q'}{\overline{T}} - \frac{\overline{P}s'}{RC_p}\vec{u}.\nabla\overline{s}\right)dV > \int_S p'\vec{u}.d\vec{S} \qquad (2.10)$$

This criterion extends the Rayleigh and acoustic criterions to the case where the net flux of energy through the boundaries is not negligible and the entropy perturbations are important. However measurement of pressure fluctuations and entropy fluctuations (experimentally) at the boundaries is still difficult. So in experimental studies of combustion instability the Rayleigh criterion is still broadly used. To construct the Rayleigh index maps, pressure can be measured by a transducer and to measure heat release, several diagnostic mechanisms can be applied including chemiluminescence, fluorescence. The last two criteria introduced are new tools for numerically examining instability in combustion systems.

Pun (2001 and 2003) measured the Rayleigh index maps of two different flames using OH PLIF and chemiluminescence techniques. He showed the bluff-body stabilized flame is less sensitive to chamber acoustic excitation due to the flames ability to anchor to a surface. Lee et al. (2003) calculated Rayleigh index maps using CH chemiluminescence. They observed two distinct regions of acoustic damping and driving. In 2007 Kang et al. measured the Rayleigh index in a 1 inch low-swirl burner and detect

the shear-layer coupling. Huang et al. (2009) measured the Rayleigh index maps at higher pressures for 1 inch low-swirl burner. All of these examples show that the Rayleigh criterion is still a reliable method to study combustion instability.

It is important to recognize that all the criteria above are based on a linear analysis of instability growth and the non-linear effects are not included. These criteria are useful in predicting the initiation of instability, but not the growth and behavior of the unstable parameters of the system. In figure 2.9, the region which these analyses are valid is shown.
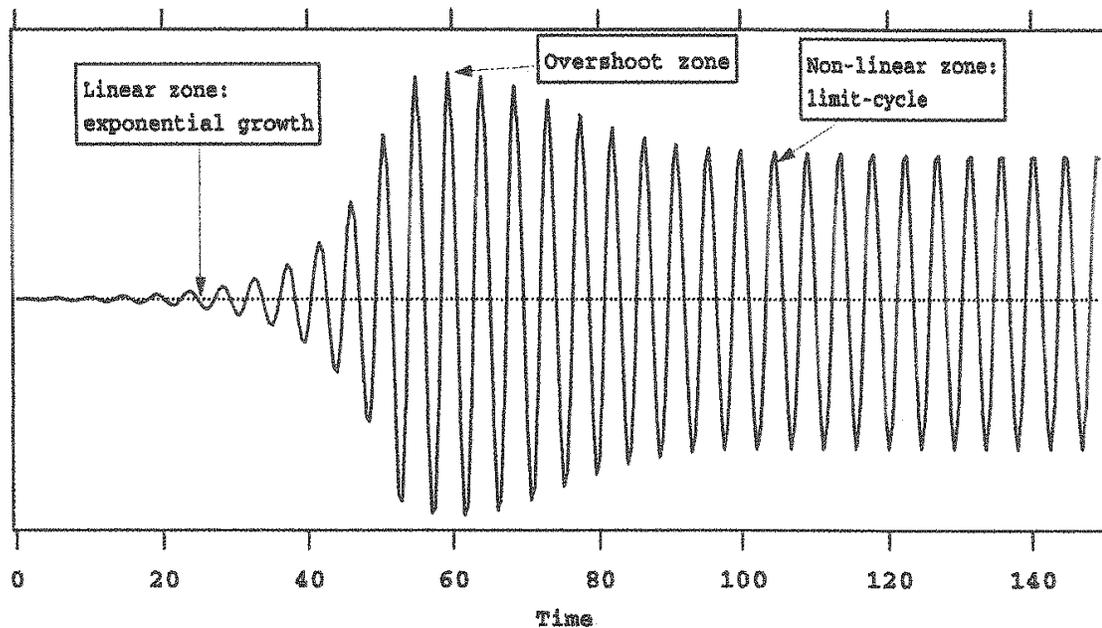
Figure2.9 Growth of instability (Linear zone, non-linear zone)

Source: Poinsot and Veynant, 2005

Figure 2.9 shows the typical time evolution of pressure oscillations in a combustion system. An instability is triggered at time $t=0$. In the linear region, acoustic

energy added to the system is larger than the energy dissipation and the oscillations increase linearly. However amplitudes of fluctuations do not grow infinitely; a limit-cycle is reached which non-linear phenomena are dominant. In this region the growth rate becomes zero and the amplitude of the fluctuations do not change. The non-linearities may cause by flow and combustion processes inside the control volume or at its boundaries. Non-linear terms are not generally important when the amplitude of fluctuations are low (less than 10% of the mean values), but when large amplitude fluctuations occur in the system, these non-linear processes strongly affect the characteristics of instability (Zinn et al., 1970; Culick et al., 1995).

2.3.2 The Darrieus-Landau Instability

The Darrieus-Landau Instability, or hydrodynamic instability, can occur in exothermal reacting flows due to the acceleration of the burning gases. A small disturbance can alter the flame front and cause flame wrinkling. Therefore, with respect to the reactants, convex and concave regions will be present. These gases accelerate normal to the flame front. In convex regions, the streamlines have to diverge toward the flame front and converge after the flame front. The opposite is true for the concave region of the flame. Because the reactants velocity drops as approaching the flame and the burning velocity stays approximately constant, the convex parts tend to grow (figure 2.10).

Darrieus and Landau utilized flamelet theory for their analysis (the flame is infinitesimally thin and propagates normal to itself at a constant speed S_L, laminar flame speed, relative to the cold unburned gas). The growth rate of hydrodynamic instability can be formulated as:

$$\omega = S_L k \omega_{DL}, \ \omega_{DL} \equiv \frac{-\sigma + \sqrt{\sigma^3 + \sigma^2 - \sigma}}{\sigma + 1} \tag{2.11}$$

Here k is the transverse wave number and $\sigma \equiv \rho_u/\rho_b$ is the unburned-to-burned density ratio. When σ is close to 1, it is assumed that the density of reactants and products are the same, and based on (2.11) the flame front does not change and flame is hydrodynamically stable (Pocheau, 1994; Denet, 1997).
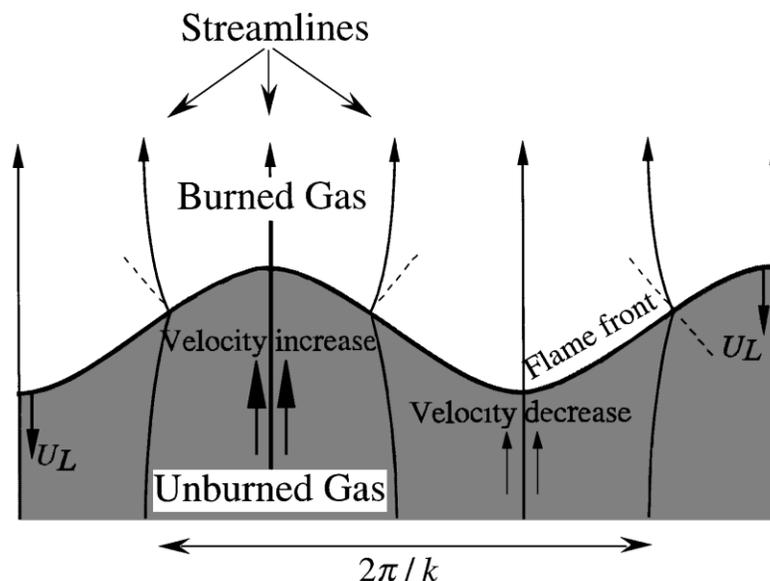
Figure 2.10 Deviation of flow lines leading to the Darrieus-Landau instabiltiy

Source: Clanet and Searby, 1998

In reality, thermal expansion is typically as large as $\sigma = 5 \sim 8$, so the flame front modifies the flow and is subjected to the hydrodynamic, Darrieus-Landau (DL) instability (Boughanem and Trouve, 1998). The analysis of Landau, for an infinitely thin flame sheet, gives a positive amplification for all wavenumbers, but it is noted that this only holds for wavenumbers that correspond to wavelengths k larger than the flame thickness. For given k, the growth rate increases with the expansion.

2.3.3 Thermal Diffusive Instability

Thermal diffusive instabilities are known to occur in both premixed and non-premixed combustion. These types of instabilities depend on thermal diffusion of heat, relative to the diffusivity of reactants, which is expressed by the Lewis number *Le* (ratio of thermal diffusivity to mass diffusivity). If the Lewis number is not equal to one there is an imbalance between thermal and mass diffusion. Heat conduction from the flame front in convex regions will cool the flame and cause in a decrease in burning velocity and flame surface area. These effects stabilize the flame (figure 2.11). It occurs when the *Le>1* and the mass diffusion of reactants is faster than thermal diffusion. When the Lewis number is less than one, diffusion of reactants to the flame front is faster than heat diffusion to them from the products. At the locations where the flame front is convex towards the hot gases, reactants diffuse into a region that is larger than the reference planar case, and cause in a decrease of laminar flame speed. On the other hand, when the flame front is convex towards the cold flow, reactants are focused into a smaller region and more heat is conducted to them, and as a result the laminar flame speed increases. This mechanism causes an increase in flame surface and amplifies the perturbations (Giacomazzi et al., 2007; Bastiaansy et al., 2007).

Barenblatt et al. (1962) reported linear analysis of thermal-diffusive instability of a plane flame front subject to long-wave perturbations, and derived the dispersion relation:

$$\sigma = \alpha\left[\tfrac{1}{2}\beta(1-Le)-1\right]k^2 \quad , \qquad \beta = E(T_b - T_u)/RT_b^2 \qquad (2.12)$$

Here σ is the rate of instability parameter, α is the thermal diffusivity, k is the wave number, E is the activation energy, T_b is the temperature of hot products and T_u is the reactants temperature. Here the theory assumes that combustion can be described with single-step chemistry, specified by an activation temperature.
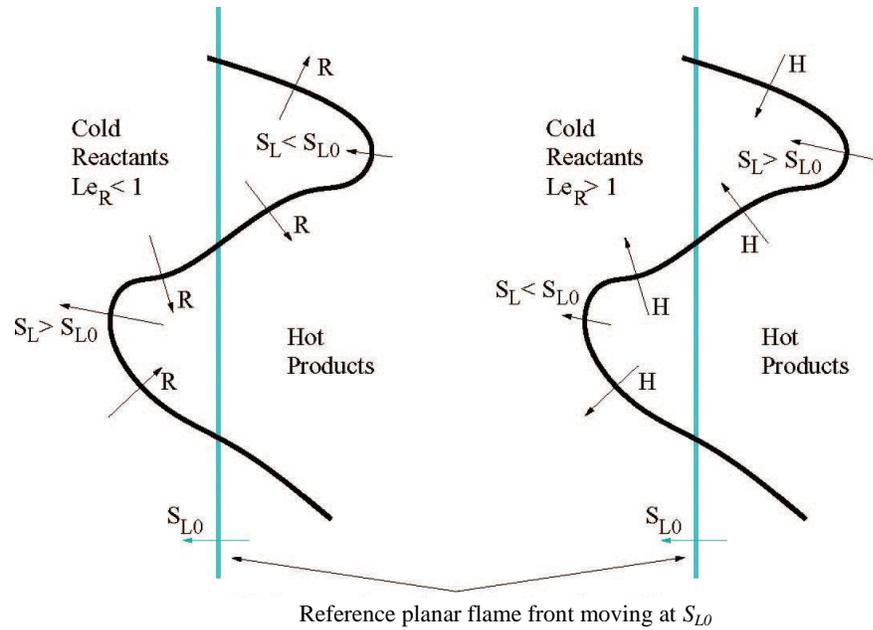
Figure 2.11 Schematic of thermal diffusive instabilities.

Source: Giacomazzi et al., 2007

At the beginning of this section, it was mentioned that the *Le=1* is the critical Lewis number. But in reality the critical Lewis number (*Le$_c$*) can be obtained from:

$$Le_c = 1 - 2/\beta \tag{2.13}$$

This critical Lewis number is slightly less than one. In a typical flame, *β ~15*, and so *Le$_c$*=0.87. The dispersion relation incorporating the relaxation effect of short-wave disturbances around the critical Lewis number was studied by Sivashinsky (1977).

$$\sigma = \alpha\left[\tfrac{1}{2}\beta(1-Le)-1\right]k^2 - 4\alpha\ell_D^2 k^4 \tag{2.14}$$

Where l_D is the diffusive length. Hence, when the flame is unstable (*Le < Le$_c$*) there is a critical wave number k_c that matches with the fastest growing mode of the perturbation.

Sivashinsky used a constant density model and employed a high activation energy asymptotic limit in order to study the linear stability of one-step chemistry flames.

However in his model hydrodynamic effects are neglected, but it has been demonstrated that Sivashinsky's model correctly captures thermal-diffusive effects on flame dynamics.

In this thesis, pure methane flame, methane-hydrogen mixture flames, and hydrogen flame will be discussed. The Lewis number of the mixture of methane and air is approximately unity, but as the ratio of hydrogen in the fuel mixture increases, Lewis number decreases and the possibility of thermal-diffusive instabilities occurrence in the system rises.

<u>2.4 Flame Structures</u>

Flame surface density (flame surface area per unit volume), flame curvature, flame brush thickness and stretch factor are usually introduced in the literature as the flame structures. Flame structures are important because turbulent burning velocity S_T depends on the flame wrinkling process which is geometry-dependent (Driscoll, 2008). In real systems flame wrinkling is a function of geometry of shear layers, walls, flame–flame interactions and the location where the flame is anchored and it has a memory of any wrinkling that might have happened upstream of the flame. The ratio of the fluctuations of the heat release to the mean heat release is proportional to the ratio of the changes in the flame surface area to the average flame surface area:

$$\frac{q'}{\overline{q}} \cong \frac{A'}{\overline{A}}$$
(2.15)

Perturbations in the system may cause flame front wrinkle (for example interaction of eddies with the flame front) and result in an enhanced flame front area and initiate Darrieus-Landau instability or thermal-diffusive instabilities which have been explained before.

The mean reaction rate of a turbulent flame can also be calculated as a function of flame surface density:

$$\overline{\dot{\omega}} = \rho_u \overline{S}_c \Sigma$$
(2.16)

Here $\bar{\bar{\omega}}$ is the mean reaction rate, ρ_u is the unburned gas density, S_c is the average flame consumption speed along the flame surface and Σ is the flame surface density. A high flame surface density at a given location in the flow corresponds to a high turbulence reaction rate (Marble and Broadwell, 1977). In this model, the turbulent flame is viewed as a combination of small laminar flame elements (flamelet), which are assumed to have a structure similar to the laminar stagnation point flame (flamelet theory). In the current study flame structures for different conditions will be measured and compared. The effects of hydrogen enrichment, pressure elevation, and variation of equivalence ratio on flame structures will be investigated.

2.5 Diagnostic Techniques in Combustion

To characterize the complicated process of combustion, key variables such as pressure, velocity, temperature, species concentrations and reaction rates are required to be known spatially at any time in the control volume or field of interest. Several techniques have been used to measure these variables and new methods are being developed for more accurate measurements. These methods are also applicable to detect combustion instability. In this section some of these techniques will be reviewed.

Measuring the dynamic pressure utilizing high frequency response (up to 250 kHz), water-cooled piezoelectric pressure transducers is a common way to detect unstable combustion in industry (Richards and Straub, 2003). Growth of pressure fluctuations amplitude shows occurrence of instability in the combustor. The instability mode can be determined by using several sensors. To capture longitudinal modes at least three sensors for the inlet, the outlet, and the middle of combustor is required. To identify and characterized transverse modes, several transducers should be installed at specific circumferential locations. Transducers can also be used for active control of instability. Continuous measurement of pressure is capable of capturing any deviation of the combustion system from normal operation, and upon detecting instability, proper

treatment can be made via the active control system to suppress unstable modes. A piezoelectric transducer can measure the pressure only at a single point, but infrared-absorption technique can be applied to obtain the pressure distribution over the whole flow field. In this method a laser beam with known wavelength and intensity is passed through the combustion field. The decrease in light intensity due to resonance absorption by specific atoms or molecules can be calibrated to calculate pressure, temperature, velocity, and gas concentration (Lieuwen and Yang, 2005).

Thermocouples are traditional instruments to measure the temperature at a single point. Usually, however, they can't measure the temperature at high frequencies. In combustion instability studies which deal with high frequency oscillations thermocouples are not reliable. New methods like Rayleigh scattering can be used to find the temperature of the combustion field at high frequencies (Haumann and Leipertz, 1984). In this method, a laser beam of an Nd-Yag laser system is used to excite the flame and an ICCD camera is used to take images the flame. From these instantaneous images, temperature and density field can be obtained. Halter et al. (2007) measured the flame temperature field in a Bunsen burner with this technique to characterize flame boundaries and calculated the flame surface density. An example of temperature field measured by Rayleigh scattering technique is shown in figure 2.12.

Velocity measurements in turbulent flows have been a challenge for researchers. In combustion systems interaction between the flame and flow field makes this task harder. Several velocimetry techniques have been applied, including hot wire anemometry, laser doppler velocimetry (LDV), particle image velocimetry (PIV) and etc.

Hot wire anemometry is an old technique to measure instantaneous fluid velocity. In this method a very thin wire (a few micrometers in diameter) is electrically heated up to above the ambient temperature. Flow passing the wire has a cooling effect on it. As the electrical resistance of the wire depends on its temperature, a relationship can be obtained between the resistance of the wire and the flow speed.
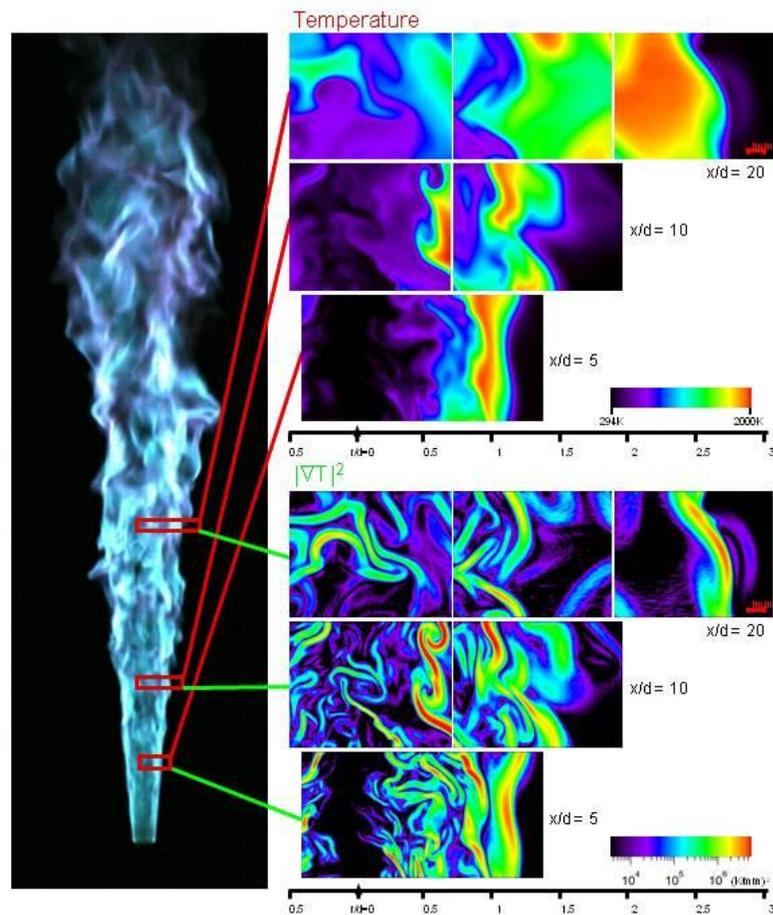
Figure 2.12 Highly resolved Rayleigh scattering measurements reveal the fine-scale structure of the temperature and thermal dissipation fields in turbulent jet flames.

Source: Sandia National Lab Website, http://crf.sandia.gov

Velocity measurements with hot wire make it possible to collect data up to several hundred kHz. The output signal from hot wire is analogue, continuous, and it has a very low level of noise. For collecting data, though, it is necessary to place hot wire in the flow path. This can alter the flow field and the wire may fail in a hostile environment like the combustion zone. Hot wire is unable to fully map the velocity and can only record the velocity at a single point.

Laser Doppler Velocimetry (LDV) is another method used to measure the instantaneous velocity of a flow field. This technique is non-intrusive and can measure the 3-D velocity vectors. In LDV method two monochromatic laser beams are sent to the point of interest and the radiated reflection of these beams from the target point is collected. Based on the Doppler Effect, the change in wavelength of the reflected beams is a function of the targeted object's relative velocity. Thus, the object's velocity can be acquired by measuring the change in wavelength of the reflected laser lights, which is accomplished by forming an interference fringe pattern. For this purpose, the flow field is seeded with small neutrally buoyant particles that scatter light and do not react with the fluid. The particles are then illuminated by laser beams having a known wavelength; the scattered lights are detected by a photomultiplier tube and the change in wavelength is analyzed to calculate the velocity (Ainsworth et al., 1997).

Particle Image Velocimetry (PIV) is a newer method for measuring flow field velocity. Compared to LDV, which usually measures the velocity at only one point, PIV is capable of measuring instantaneous velocity vectors in a cross section of control volume. The fluid is seeded with tracer particles which are generally oil drops in the range 1 μm to 5 μm. The fluid with entrained particles is illuminated with two back to back laser pulses so that particles are visible. Flow field images are recorded and analyzed to calculate the flow field velocity. By applying stereoscopic approach, all three component of velocity for each point can be measured. An example of PIV measurement in low swirl burner is shown in figure 2.4. This technique is broadly used in combustion study because PIV is a non-intrusive method which is capable of measuring velocities in the range of zero to supersonic.

Several techniques have been applied to visualize the combustion field for flame structure and combustion instability studies. Chemiluminescence and PLIF are two popular methods for visualizing phase resolved combustion, and measurement of species involved in combustion. Chemiluminescence is the electromagnetic emission radiated

from the de-excitation of electronically excited species, generated by chemical reactions in the combustion zone (Nori and Seitzman, 2008). The chemiluminescence process can give information regarding the concentration of active radicals such as OH, CH, C_2, and the fuel-to-air ratio in the reaction zone. An OH-chemiluminescence image of flame in a 2.54cm low swirl burner is displayed in figure 2.13.
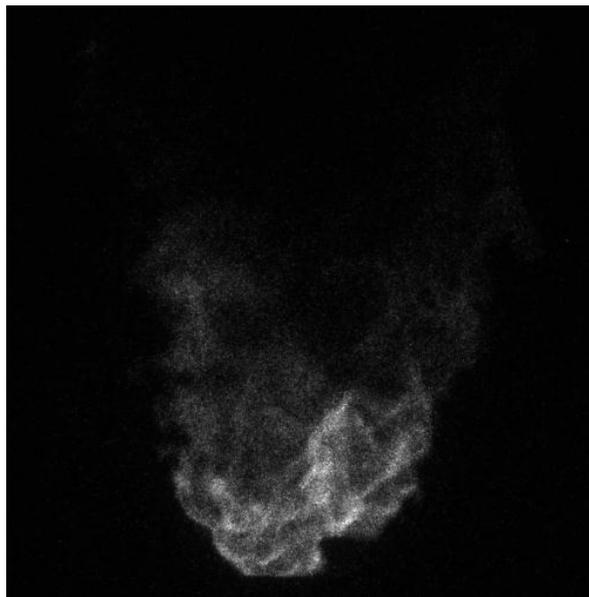
Figure 2.13 OH chemiluminescence in a 2.54 cm low swirl burner.

Unlike the other methods previously discussed, chemiluminescence doesn't utilize a laser beam source for excitation. However, capturing small-scale structures with this method is relatively hard. Due to simplicity of chemiluminescence, it has been broadly used in combustion studies (Lee and Santavicca 2003; Hardalupas and Orain, 2004; Taupin et al., 2007).

Laser-Induced Fluorescence (LIF) is an established, selective and sensitive approach for identifying species concentration and the flame shape and structure from

reactive-flow systems without perturbing the flow field. LIF is a sequence of molecules or atoms being excited to higher electronic energy states via laser absorption and is followed by spontaneous emission producing fluorescence. The spectral absorption regions are discrete, because the energy states of molecules and atoms are quantized. Typically, fluorescence occurs at wavelengths greater than or equal to the laser wavelength. Thus, LIF offers the possibility to investigate species of interest by selecting the appropriate wavelength. Planar Laser-Induced Fluorescence (PLIF) is a derivative of the LIF technique, which requires the generation of a laser sheet from the laser beam in order to facilitate imaging of the fluorescence. For capturing the fluorescence, usually an ICCD camera is used. PLIF techniques were first utilized in 1970's for combustion studies and have been improved since. In figure 2.14 a sample of OH PLIF imaging is shown.
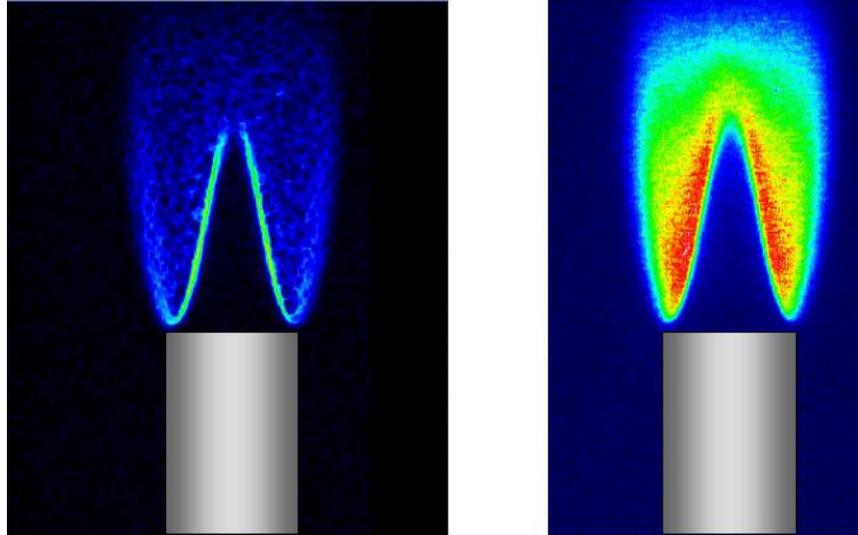
Figure 2.14 OH radical concentration distribution of a Benson flame measured by PLIF. The first image (left) is the flame front calculated from the OH concentration gradient.

Source: http://engine.princeton.edu

Driscoll (2008) overviewed the studies in which the flamelet structures were captured using PLIF technique. In Driscoll's review OH, CH, and CH_2O PLIF images were used to characterize the turbulence effects on combustion and the flame structures. In this thesis OH PLIF is applied to capture the flame shape and as a result flame surface density and curvature. Also OH PLIF is used to measure the ratio of heat release fluctuations over mean heat release for combustion instability examination.

CHAPTER 3

EXPERIMENTAL SYSTEM AND TECHNIQUES

The experimental rig which has been used in this study contains multiple subsystems. In this chapter function of each component and its role during the tests will be explained. The first section describes experimental setup and unique features of the system including the acoustic chamber, swirl burner, air and fuel flow-meters and laser system. In the second section the PLIF diagnostic method, its benefits and the details of OH-PLIF technique are introduced. Finally the experimental procedure and the data analysis methodology are explained.

3.1 Test Facilities

Experimental investigation of combustion instability requires significant hardware and a complex arrangement. In figure 3.1 a schematic diagram of combustion instability test setup is shown. This experimental system consists of air and fuel feeding subsystems, combustion chamber, burner, mixer, cooling system, acoustic driving mechanism, laser, and ICCD camera.

3.1.1 Air and Fuel Feeding System

Air is provided by a compressor and is measured with a Hastings HFC-D-307 flow meter. The air flow rate can be controlled by a Hastings PowerPod 400. The accuracy of this flow meter is 0.2% of full scale (2000slpm) plus 0.5% of reading value. Methane is supplied from the city natural gas line and measured by a Hastings HFC-D-303 and controlled with software. The accuracy of the methane flow meter is the same as the air flow meter. Hydrogen cylinders are used for supplying H_2 to the system and its volumetric flow rate is measured and controlled by an Omega FMA5500 flow meter. The flow meter has an error about 1% of full scale reading (45slpm).
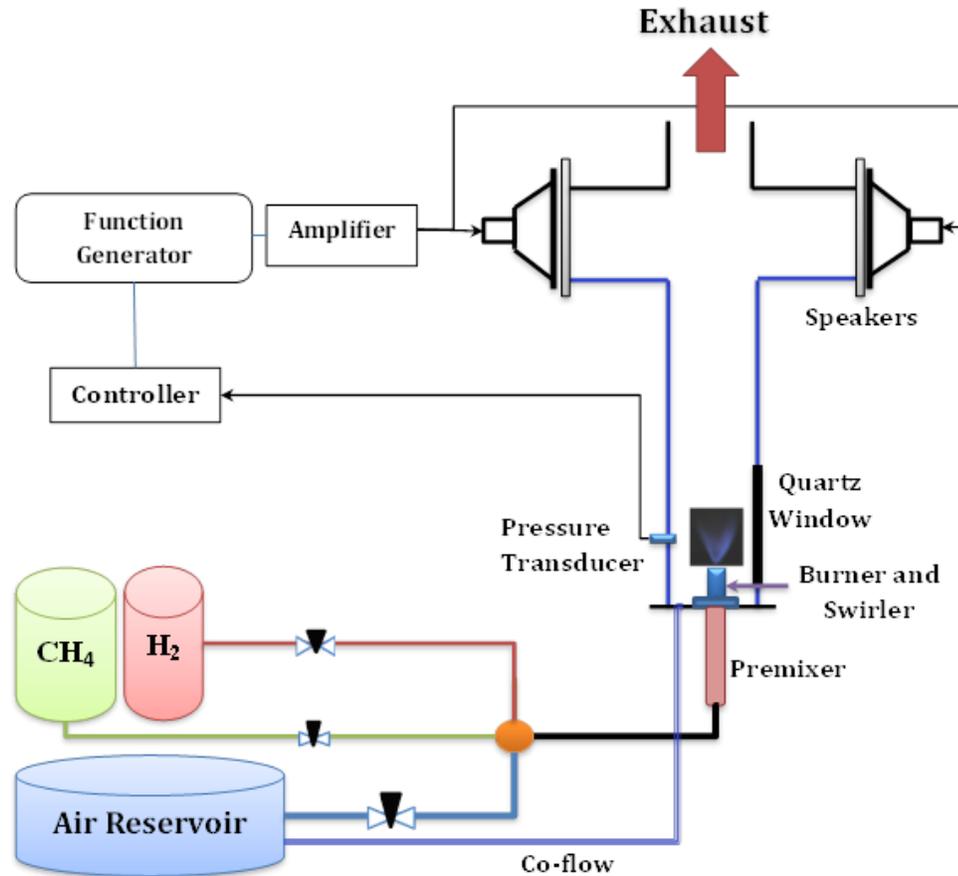
Figure 3.1 Experimental system schematic

3.1.2 Combustion Chamber and Acoustic Driving mechanism

The combustion chamber is made of five stainless steel cylinders which are bolted together and sealed. The inner diameter of the chamber is 30cm, and its height is 185cm. The burner is placed at the center of the chamber. The bottom section of chamber is wrapped with copper tubing for cooling purposes. The temperatures and pressures of cooling water running in copper tubes are monitored for safety. Optical access to the flame is provided by 4 quartz windows in the bottom part of the chamber. The upper section of the chamber is acoustically closed (no fluctuation of pressure or velocity is

allowed) and the exhaust flow is controlled by three electronic adjustable valves which give the capability of pressurizing the chamber continuously.

A: Loudspeakers   B: Speaker Section C: Quartz Window
D: Pressure Transducer E: Swirl Burner   F: Adjustable Premixer
G: Fuel/Air Inlets   H: Nitrogen Co-flow
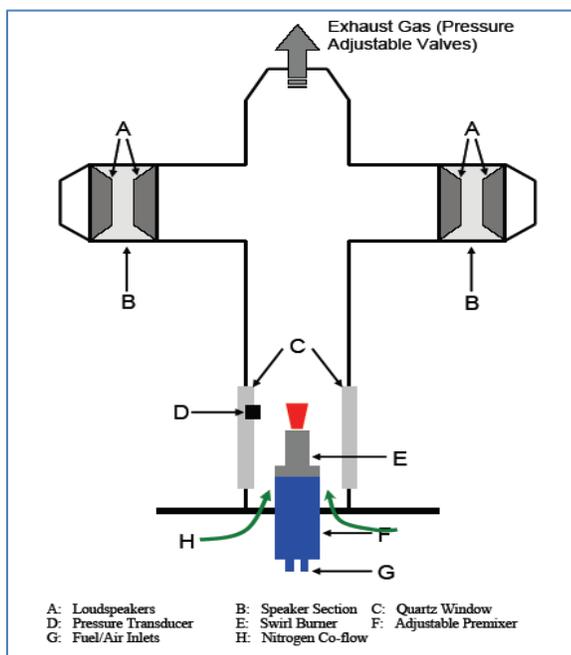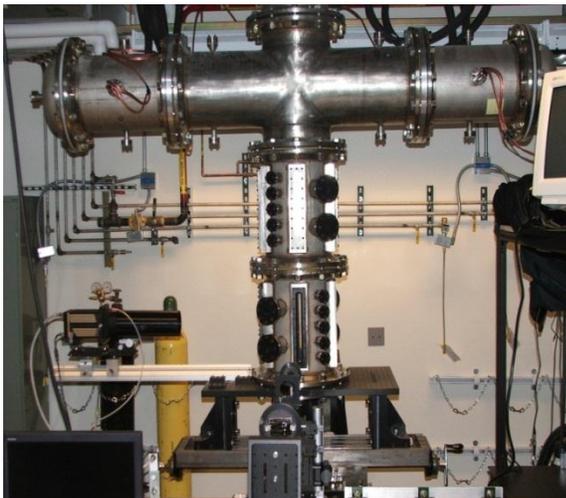
Figure 3.2 Combustion Chamber

In the most practical combustion system (airplane engines, power plant engines), reaction occurs at an elevated pressure. Running the combustion instability tests and examining the flame dynamics at above-atmospheric pressures and conditions produces a more realistic simulation. For safety purposes, the chamber can withstand pressures up to 10 bar, but is normally operated at pressures under 5 bar.

For the systems in which walls and flame interact, significant unsteady heat transfer occurs due to a very large temperature gradient (flame temperature is usually in the range of 1500 K to 2500 K while the wall temperature remains between 400 K to 600 K because of cooling). This can affect the efficiency and pollution formation of the flame and also the life time of the chamber (Delataillade et al., 2002; Dabireau et al., 2003). As mentioned above the inner diameter of the chamber (30 cm) is much bigger than the size of the burner (3.81 cm) and the flame width (roughly 6-9 cm). As a result, the flame and wall interactions in this chamber are eliminated because the flame is smaller than the chamber. In addition, the chamber geometry is quite different from that of traditional dump combustor systems. Dump combustor systems have been used in many combustion instability studies (Geoniem et al., 2002 and 2005) but produce a limited range of phenomena. The other outstanding advantage of the current configuration is that the acoustic driving mechanism is installed downstream of the combustion chamber. In most of combustion instability test rigs, the acoustic wave generated by the acoustic driving mechanisms (generally speakers or actuators) upstream of the flame and it can directly affect the reactants' supply and mixing, which can cause unsteady heat release. But in the current chamber, the speakers are far downstream from the flow meters and premixer (Figure 3.2), so acoustic perturbations only interact with the flame and do not disturb the reactants flow rate or alter the mixing process.

The acoustic driving mechanism consists of a signal generator, amplifier, and four speakers. Sine wave signals are generated by a Wavetek 171 function generator. This signal is amplified through a 2000_W Machie M2600 amplifier and the output signal is

translated to pressure waves by means of four 12-inch dual coil CVR Kickers speakers. The frequency response range and the RMS power of these speakers are 25-500 Hz and 400 Watts, respectively.

To measure the pressure inside the chamber, a high resolution piezoelectric pressure transducer (PCB 106B) is employed. This sensor is installed into one of flanges on the chamber wall, and its face is tangent to the inner surface of the chamber. This type of transducer can only operate at low temperatures (less than 121° C), so during hot tests, water cooling is necessary. An amplifier intensifies the output of the sensor by 100 times, and is then digitalized by an A to D data acquisition board. To record and save the data, LabVIEW 7.1 is utilized. The pressure transducer measures pressure at only one point and the pressure wave is assumed to be nearly uniform over the entire extent of the flame. This uniformity allows the single pressure reading to be applied at all of the flame spatial locations. This hypothesis is true when the frequency is not too high. Equation 3.1 shows the relation between frequency and wavelength. Here, c is the speed of sound, f is the frequency of excitation, and λ is the wavelength. At standard conditions, the speed of sound is about 330 m/s. At the excitation frequency of 200 Hz (the worst case scenario in the combustion instability experiments), the wave length will be on the order of 1.5 m, 7 times larger than the flame length. Because of this, the assumption of uniform pressure wave over the flame length seems reasonable. Increasing the temperature will increase the speed of sound, and the variation in the pressure wave along the flame length will become smaller in the hot test than the cold tests.

$$\lambda = \frac{c}{f} \tag{3.1}$$

As mentioned before in chapter two, the low swirl burner is an innovative technology for stabilizing lean-burning, premixed combustion as the flame is stabilized by flow divergence, not through the recirculation which is commonly seen in industrial high swirl burners (Cheng et al., 2006). Compared to other lean, premixed combustors, in

low swirl burners, the flame has a shorter chemical residence time and lower NO_x formation (Littlejohn et al., 2007). The low swirl burner used in the current study was designed and built by Robert Cheng at the Lawrence Berkeley National Lab. The flow field in this type of burner shows a self-similarity behavior like turbulent jet flow and changing the dimensions of this burner does not affect the flow field pattern. The CAD model of this burner is shown in Figure 3.3. The inner diameter, the outer diameter and the height of the burner are 3.81 cm (1.5 inch), 4.27 cm, and 8.92 cm, respectively. The swirler was installed at the bottom of the burner.
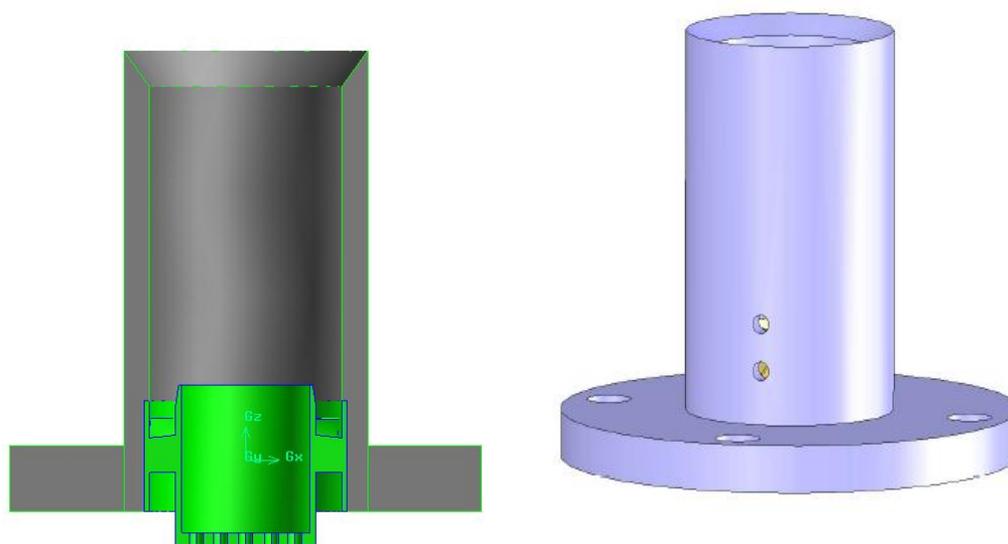
Figure 3.3 Schematic views of the burner and swirler

The center part is equipped with a screen which has 25 holes with the diameter of 2.8 mm in it. By changing the size of these holes, the effective area in the central part of the swirler can be adjusted and in result the swirled and axial portion of the reactants flow

through the swirler (the intensity of the swirl) can be set. Figure 3.4 illustrate more details of the swirler and the screen.

Vanes

Screen
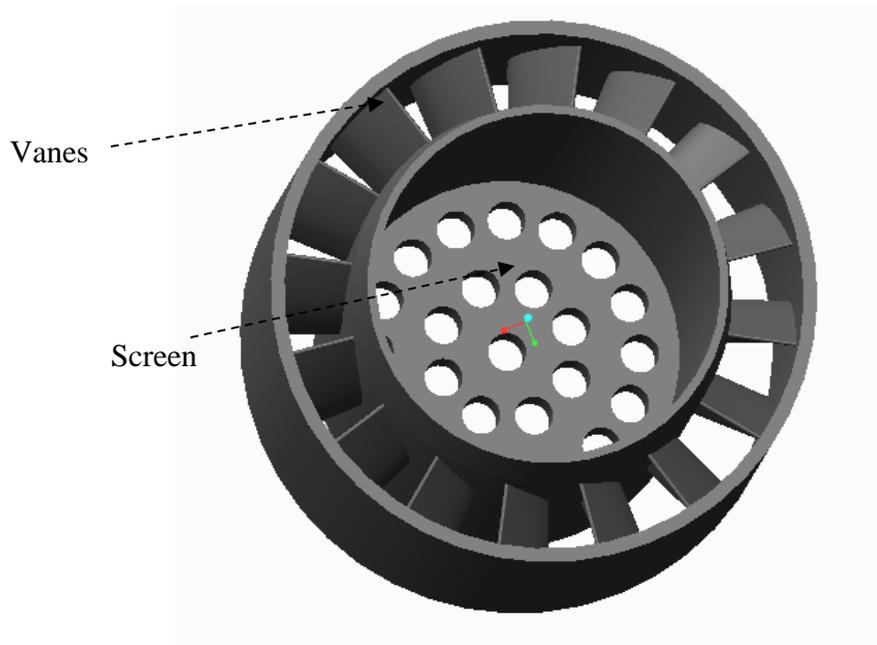
Figure 3.4 swirler

3.1.3 Premixer

To provide a uniform mixture of fuel and air a premixer was designed. This premixer consists of a 20 cm long tube with an inner diameter of 4.61 cm and outer diameter of 5.41 cm. As shown in figure 3.5, the bottom half of the tube is filled with small steel balls. The diameter of each ball is 7mm and they are compacted to avoid any balls movement during the tests. A thin plastic mesh and an aluminum honeycomb layer sit on the top of the balls and a steel sleeve secures the mesh and honeycomb in their place. Fuel and air from the flow meters go to the premixed and the mixing process occur in the porous media in between the balls. Then the large turbulent structures will be

dissipated by the mesh and honeycomb. The vortical structures which are smaller than the size of the holes in honeycomb will be dissipated in the empty space at the top of the premixer and at the end of the tube the flow become fully developed. This uniform fully developed mixture will be the input to the burner and swirler.

20 cm long tube

Honeycomb

Metal Balls
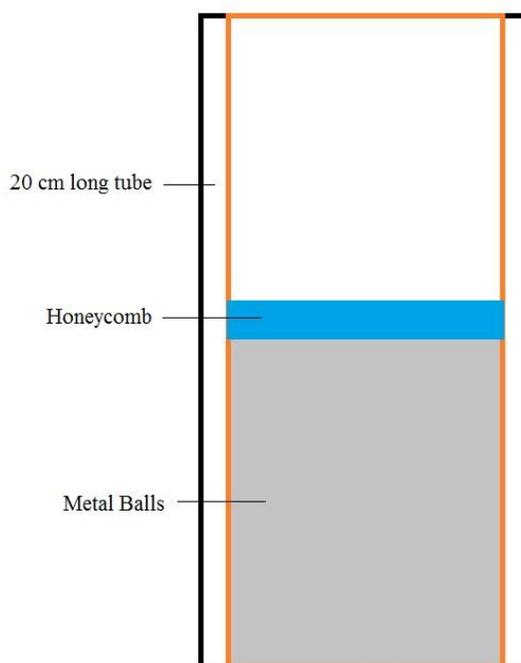
Figure 3.5 Premixer

3.1.4 Laser System

The laser system in this experiment is used to excite the OH radicals in the flame. This system includes a pump laser, a dye laser, and a frequency doubler. The pump laser is a high power Nd:YAG laser (Continuum Powerlite 9010). The YAG laser is capable of producing 1064 nm (infrared) or 532nm (green) beams. Nd:YAG lasers are commonly

used in PLIF measurements and PIV experiments. The Continuum YAG laser produces a 532 nm beam at 10 Hz with 500-600 mJ per pulse. The pump laser pulse runs the tunable dye laser, which contains a Rodamine 590-based solution. This chemical is a toxic dye; careful precautions are taken when mixing the solution. The role of the dye solution is to shift the laser's wavelength from a 532 nm beam to a 564 nm wavelength beam. With the dye, the beam's power drops to 130 mJ/pulse.
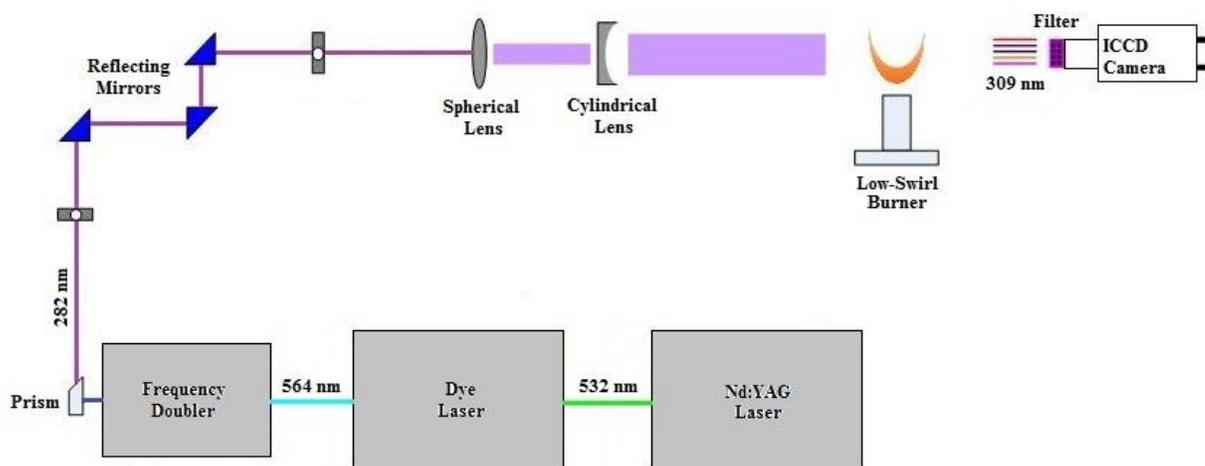
Figure 3.6 System for PLIF measurement

The tuned, pulsing laser signal then enters the frequency doubler, cutting the wavelength in half, resulting in a 282 nm beam with a power of about 30 mJ/pulse. The beam consists of a few red and green low frequency residuals which are separated from the UV beam and absorbed by a Pellin-Broca prism. The filtered UV light is then directed towards the optics configuration, which consists of a combination of spherical and cylindrical lenses, which optimize the position, strength, and uniformity of the laser sheet entering the combustion chamber. The beam height at the flame position is 5 cm and its thickness is between 300 μm to 500 μm. A Princeton Instruments ICCD camera is

employed to measure the fluorescence from OH PLIF. The camera is facilitated by a 105mm f/1.2 ultra violet (UV) lens and has a resolution is 512×512 pixels; data is taken at an angle of 90°from the laser sheet. The length of the laser sheet enforces the field of view to be a 4 cm by 4 cm square. The ICCD camera is triggered synchronously with the laser pulse and a Lattice Eletro Optics (LEO) band pass filter (312.6F10-10) is attached to cut off all scattered light. Only OH-fluorescence in the 300-320nm range passes through the filter. To interact with the camera WINview data acquisition software is used. The camera gate time (150ns) and gain (100) can be adjusted through the software.

3.2 General description of PLIF

There are a number of technical approaches for the measurement of combustion dynamics; PLIF is one outstanding technique that can be applied to image the intensity of specific species. Laser-induced fluorescence imaging is a species-specific imaging technique that holds several significant advantages over line-of-sight imaging methods like laser tomography or spontaneous emission imaging. In this method the laser beam excites chemical species of interest to a higher energy state during the laser absorption process (Eckbreth, 1996; Hassel and Linow 2000). After the species is excited it reverts, or decays, back to its lower energy level, which results in the spontaneous emissions of photons, known as fluorescence. The radiation emitted is collected by the ICCD camera and the processed images may then be used to obtain a variety of properties of the flow. OH planar laser-induced fluorescence is commonly used for imaging and characterizing combustion processes. There is good separation between its rovibronic lines and little spectral interference has been encountered for most of the combustion environments in which OH-PLIF has been applied. OH-PLIF has been shown to be a very effective two-dimensional visualization tool for examining flow uniformity and mixing.

The OH radical is usually excited by a weak transition of the A–X (1–0) band to avoid saturation and the combined fluorescence of A–X (0–0) and (1–1) bands are

monitored at 305–330 nm. The process is well understood, the data evaluation is relatively straightforward and all of the spectral information needed is available.

Figure 3.7 shows the OH spectrum from Hult et al. (2005) and shows that the excitation is quite narrow and has multiple peaks. The sharp response in the OH spectrum exhibits that choosing a right laser beam for excitation is critical. In reality, if the dye solution is too old, then the wavelength may be skewed, affecting the fluorescence signal. Figure 3.8 shows the OH spectrum obtained in the current experiment. Due to the operation range of the dye laser, only a small range of the wavelength was examined. It verifies that the OH fluorescence signal is sensitive to the UV beam wavelength.

When pressurized experiments are involved, the effect of pressure on OH PLIF signal has to be considered. Quantitative interpretations of linear laser induced fluorescence require accurate accounting of collision-induced phenomena. These phenomena, which include absorption line shape broadening, radiative trapping and collisional deactivation or quenching, can be severe at elevated pressure (Allen, 1995; Battles, 1995). Figure 3.9 gives the measured OH fluorescence intensity of a methane-air flame at various pressures and at two locations above the burner by Katharina et al (1990).

The OH fluorescence intensity is not linearly related with pressure. In addition, it changes at different locations in the flame region. In a word, OH fluorescence at higher pressures tends to be difficult and quantitative calibration of its relation to pressure is not available yet.
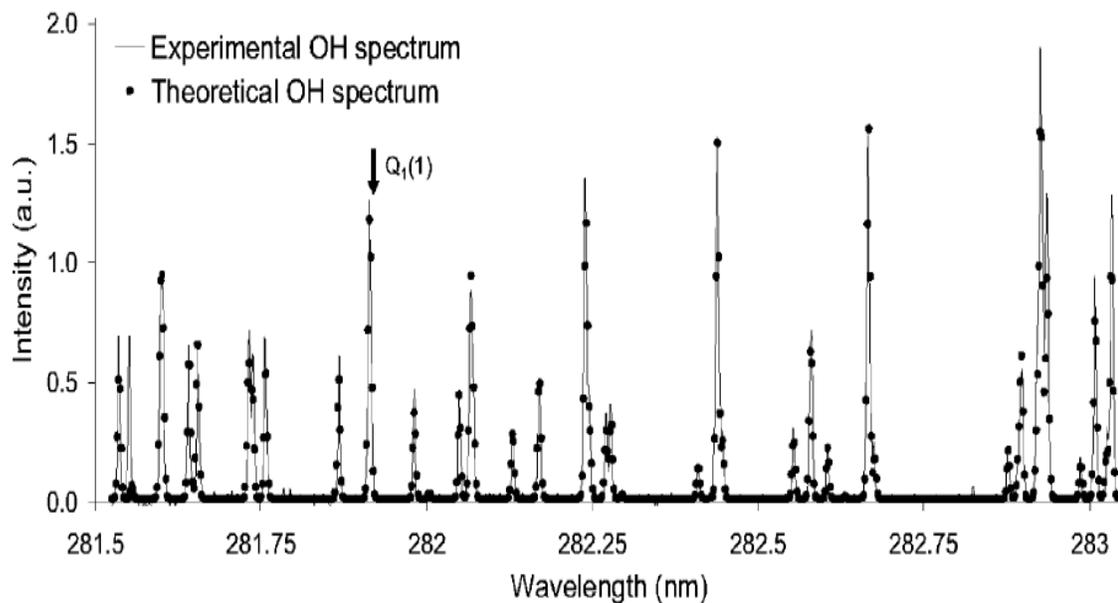
Figure 3.7 OH spectrum

Source: Hult, 2005
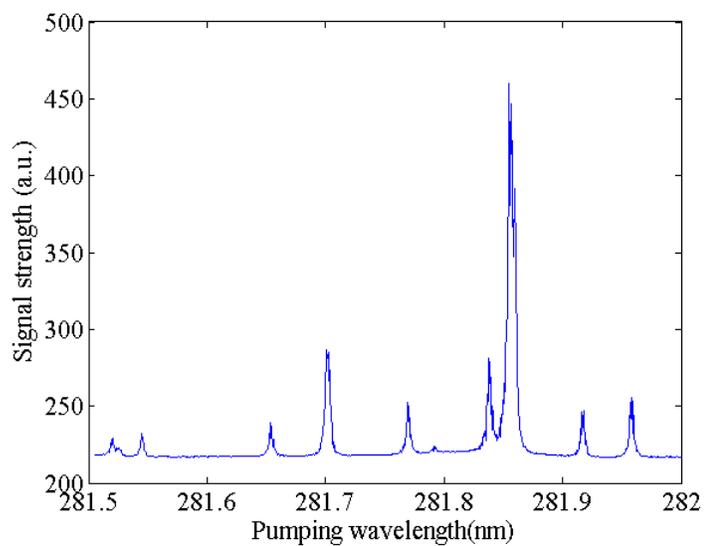
Figure 3.8 Measured OH spectrum
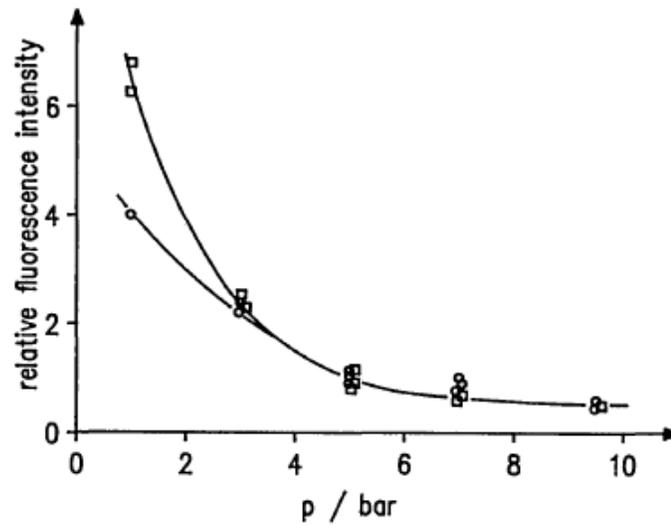
Figure 3.9 OH fluorescence intensity S_{21} vs. pressure at 3mm (squares) and 6 mm (circles) above the burner surface

Source: Katharina et al., 1990

3.3 Experiment Procedure and Data Acquisition

Combustion instability experiments can be very dangerous if the safety regulations are not observed. To avoid any mistake during the test an experiment procedure outline is provided which all the people involved in the test must follow step by step by.

1. Laser system check up

    a. Turn on the water tap for laser cooling. Make sure the water flow rate is enough.

    b. Turn on the dye pump

    c. Turn on the power of the laser

    d. Turn on the key switch when the LED changes from red to green

e. Operate the control box –shoot the laser and set it to program 1 to warm up for at least 30 minutes

f. Measure the beam power from the Nd:YAG, Dye laser and the final UV beam

2. Optics alignment

   a. Maximize the power of the UV beam by adjusting the position of the crystal in the frequency doubles.

   b. Check the pass of the beam and have it pass through the center of the burner

3. Turn on all the measurement equipment.

   a. Pressure monitor: Oscilloscope, pressure transducer power supply and amplifier

   b. Acoustic system: set the function generator to the right frequency, turn on the amplifier and the data box.

4. Beam profile calibration

   a. Use low power laser. Set delay time as 85µs

   b. Set camera gain to 250, and gate width to 100ns.

   c. Turn off the room light

   d. Allow laser sheet to impinge on fluorescent card and acquire the beam profile.

   e. Finally, cap the camera, turn on the room light, take the card out of the chamber and seal the window

5. Setup reactants flow rates and cooling lines

   a. Open the electric valve at the door. This valve controls all the electro-magnetic valves for the cylinders.

   b. Make sure the exhaust valves are open.

    c. Turn on the air, nitrogen and water lines for cooling the speakers and chamber walls

    d. Open the valves for the gas supply (Fuel, Oxidizer, co-flow, nitrogen for Camera, and cooling nitrogen for speakers).

    e. Turn on the flow meters and the controller and wait at least for 2 minutes.

6. Ignite the flame

    a. Loosen one of the small flanges on the combustion chamber which are close to the burner. And practice to stick the igniter into the chamber from the flange. Simultaneously turn on the spark plugs.

    b. Set the flow rates for air and fuels (methane and hydrogen) based on the excel sheets provided open.

    c. First let the air flow meter run and then the fuel flow meters. Stick the igniter in the chamber, and ignite the reactants. Waiting too long before igniting can be dangerous since too much fuel can accumulate in the chamber.

    d. If a flame could not be achieved with a couple of sparks, take out the igniter and spark plugs, shut off the fuel supply value, and turn on the exhaust fan to completely remove the fuel from the combustion chamber. Repeat the entire process until a flame is established.

7. Enforce acoustic perturbation

8. Turn off the light of the room

9. Shoot the laser and take the data

10. Change the frequency of the acoustic forcing and repeat

11. End experiment

    a. Stop the laser.

    b. Turn off the camera and turn on the light

c. Shut off the fuel valves, but let the air and co-flow still run. Discharge the fuel lines. After 5 minutes shut of the air valves and also co-flow. Discharge the air tube. Turn of the air, nitrogen and water cooling lines.

d. Turn off all the measurement equipment and the.

e. Cover the optics.

For each test condition three sets of data (each set contains 300 images) are taken and simultaneously the chamber pressure is recorded. All the data collected will be analyzed with a MATLAB code. The corresponding pressure for each image is extracted and at the end the FFT (Fast Fourier Transform) of pressure inside the chamber, power spectrum density of the pressure data, Rayleigh index map, flame average image, flame surface curvature, flame surface density and … is calculated.

<u>3.4 Summary</u>

In this chapter the experimental system and its features are described. In the first section different subsystems of the test system are introduced and the uniqueness of our experimental system is explained in comparison to other laboratory scale combustion test facilities. Then the OH-PLIF diagnostic technique is briefly described and finally the experiment procedure outline is presented.

CHAPTER 4

FLAME STRUCTURES IN THE LOW SWIRL BURNER

In this chapter the stability map of 3.81cm low swirl burner for different operating conditions are obtained. The effect of hydrogen enrichment and pressure elevation on the flame surface density and curvature are also examined. The results of this chapter are then compared to other studies.

4.1 Introduction

Lean, premixed methane (CH_4) combustion is currently considered a promising strategy for reducing NO_x production; it has become an important technology option for decreasing pollutant emissions. In lean, premixed combustion, the flame temperature is reduced by use of excess air. In turn, the lower temperature in the combustor facilitates a lower NO_x formation rate. However, lean methane combustion regimes are more susceptible to perturbations, resulting in a higher likelihood of flame instability. Adding small amounts of more reactive fuels to the methane is a solution to this problem. Fuel enrichment increases the range of flame stability and causes blow-off to occur at lower equivalence ratios, enabling the engine to operate at leaner conditions, decreasing the production of NO_x. One of these additive fuels used to improve and extend the flammability limits of methane combustion is hydrogen, which has been widely studied both experimentally and numerically (Dowling and Morgan, 2005). Mandilas et al. (2007) showed that the laminar burning velocity (S_L) of methane-hydrogen mixtures is increased in comparison to a pure methane flame because of a faster hydrogen reaction rate and a higher laminar burning velocity. DNS results of Hawks and Chen (2004) demonstrate a higher turbulent burning velocity for the hydrogen-enriched lean premixed methane flame as well as an increase in the ratio of turbulent burning velocity to laminar burning velocity (S_T/S_L) as s_L rises. This is due to a larger rise in the turbulent burning velocity.

Adding hydrogen to methane flames causes more wrinkling in the flame surface and causes an overall increase in flame area. Halter et al. (2007) showed that the distribution of 2-D flame surface curvature is broadened in enriched flames, indicating the enhancement of smaller scale flame front wrinkling. This is in agreement with DNS results of Han and Huh (2008) and experimental results of Zhu et al. (2010). However, in different experimental systems, other reported results of flame surface density measurements to show contradictory trends. Halter observed that adding hydrogen to a Bunsen burner increased the flame surface density, while Guo et al. (2010) showed, for their V-shape flame, the flame surface density decreased as the ratio of hydrogen was increased.

Real systems operate at elevated pressures in order to achieve a higher thermal efficiency. Increasing the efficiency can also be accomplished by reducing the overall dimensions of the combustion chamber. Experiments by Boschek et al. (2005) showed that for pure methane and methane-hydrogen mixtures, lean blow-off occurs at lower equivalence ratios as the pressure is increased. This effect was attributed to the reduction in the flame radical pool concentration that is present at higher pressures. The flame temperature itself is quite insensitive to pressure variations (for pressures from 0.5 to 3.0 atm) for a swirling turbulent flame, but the pressure variations change a chemical reaction timescale called the Damköhler number. Kubayashi (2002) observed a decrease in the Kolmogorov length scale with increasing pressure for a Bunsen burner. In their experiment, integral scales stayed constant as pressure was increased up to 3 MPa. Results of Soika et al. (2003) showed a broadening in the flame front curvature distribution by increasing pressure, which is the result of increased wrinkling in the flame surface.

4.2 Instability Maps

In this section the blow-off limits for methane flame and methane-hydrogen mixture flame at different pressures, bulk velocities and equivalence ratios are calculated. The percent of hydrogen may be defined in terms of the hydrogen (V_{H2}) and methane (V_{CH4}) volumetric flow rates as $\alpha = V_{H2} / (V_{H2} + V_{CH4})$. The reaction of the fuel mixture is written as:

$$(1 - \alpha)CH_4 + \alpha H_2 + \tfrac{1}{2}(4 - 3\alpha)\, O2 \rightarrow (1 - \alpha)CO_2 + (2-\alpha)H_2O \qquad (4.1)$$
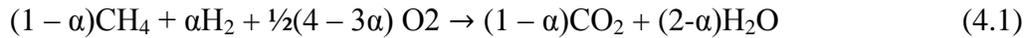
And the stoichiometric fuel-oxidant volume ratio $(F/O_2)_{st}$ in the methane-hydrogen-air mixture may be modeled as follows:

$$(F/O_2)_{st} = 2/(4 - 3\alpha) \qquad (4.2)$$

Finally, the equivalence ratio (ratio of actual fuel-oxidant ratio to the stoichiometric fuel-oxidant ratio) is defined in equation (4.3) below.

$$\varphi = (F/O_2)_{act} / (F/O_2)_{st} \qquad (4.3)$$

In this thesis all the equivalence ratios are calculated based on (4.3). Figure 4.1 displays the blow-off limit of methane flame at atmospheric conditions for various velocities. It is obvious by increasing the bulk velocity, the blow-off occurs at slightly higher equivalence ratios and it does not alter the blow-off limit significantly. This behavior is observed at higher pressures too. Figures (4.2) to (4.4) show the blow-off limits at 2, 3 and 4 bars. In this burner the turbulence intensity is roughly 10 % of the mean flow for stable flame operation. Turbulent intensities increase as a result of bulk velocity increase and their interaction with the flame in a confined geometry entrain the flame surface and cause quenching in some parts of the flame. And when these turbulent fluctuations are strong enough they can cause blow-out in the system. However at 4bar it seems increasing the bulk velocity improves the stability map. This contradictory effect is due to enhanced heat transfer from the flame to the burner as a result of flame attachment to the burner exit. In this condition burner has the role of flame holder.
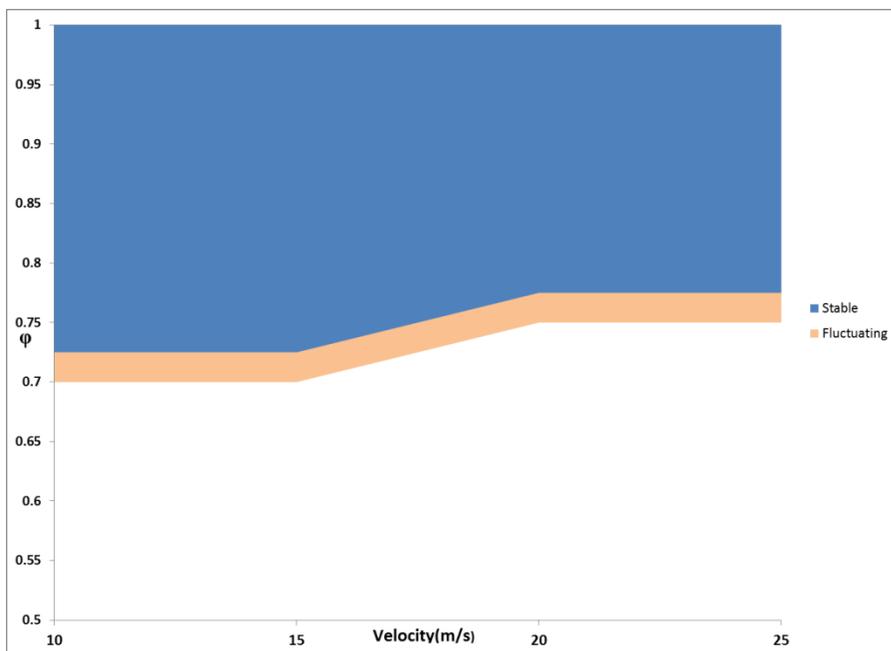
Figure 4.1 Stability map for the 3.81cm burner at 1 bar (100% Methane)
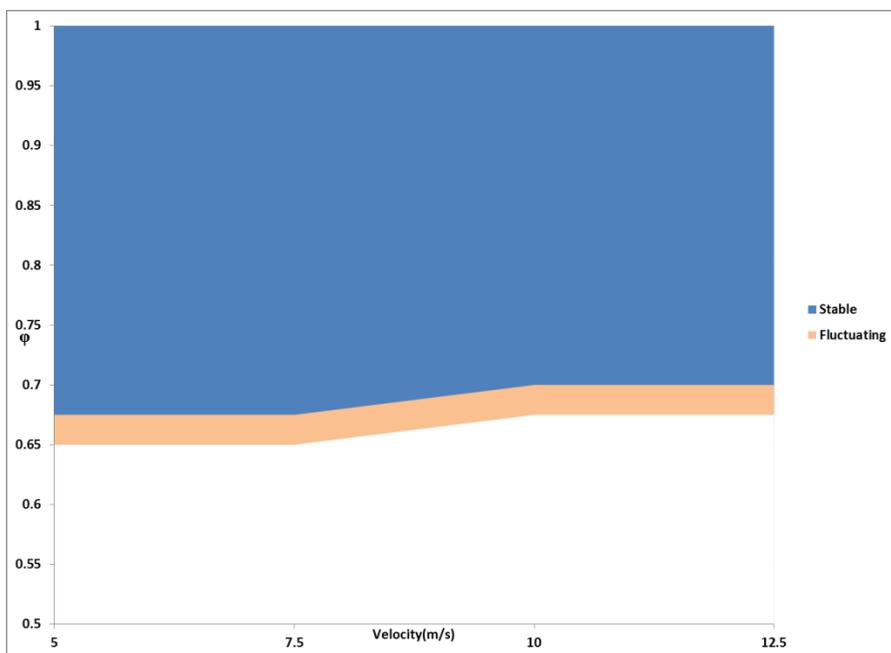
Figure 4.2 Stability map for the 3.81cm burner at 2 bar (100% Methane)
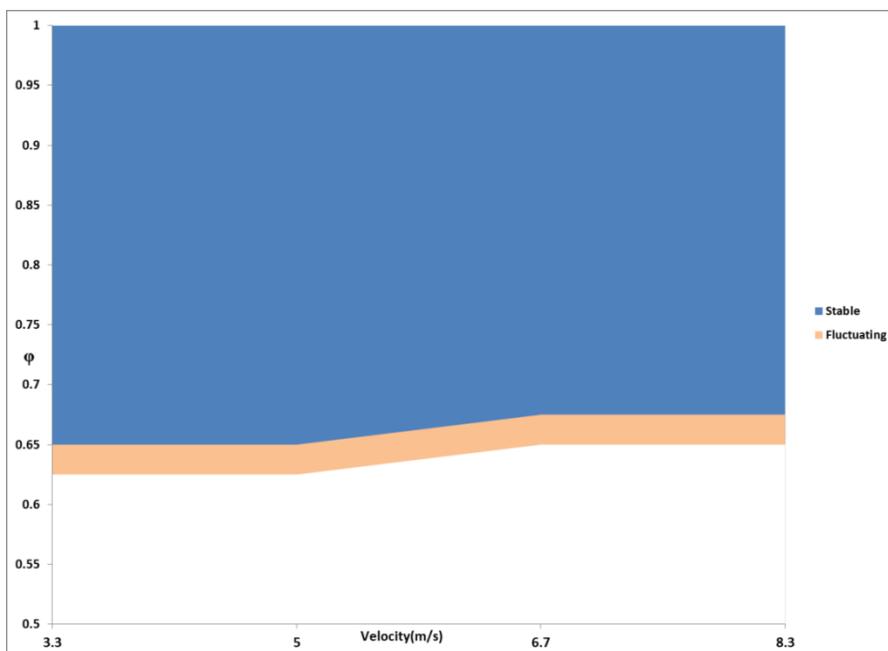
Figure 4.3 Stability map for the 3.81cm burner at 3 bar (100% Methane)
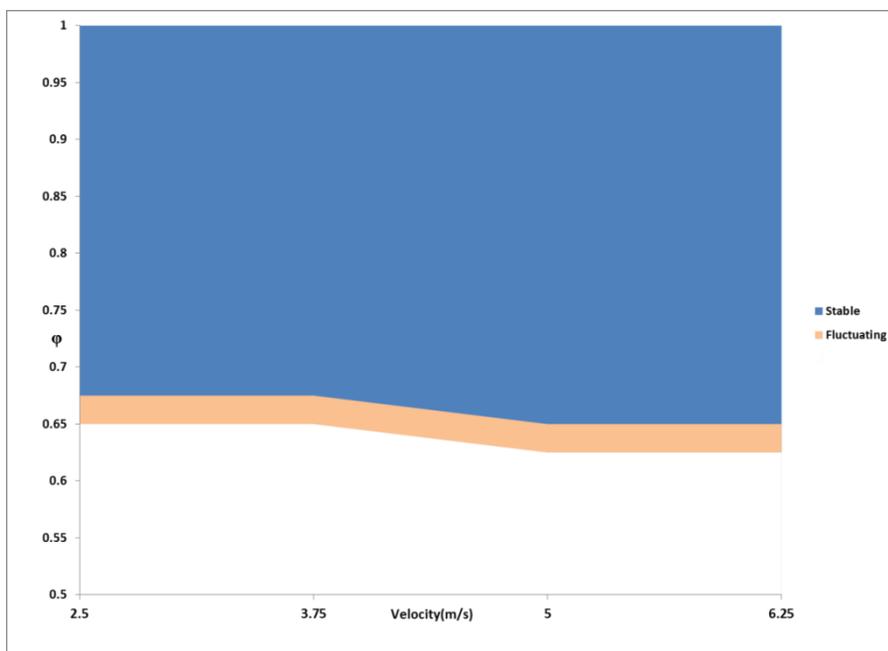
Figure 4.4 Stability map for the 3.81cm burner at 4 bar (100% Methane)

Temperature measurements show that at 4 bar, the burner temperature is about 65 C approximately double that of the 35 C that was observed 3 bar and three times of the 22 C that measured at one and two bar. Compared to other pressures, the bulk velocities tested relatively low.

Littlejohn et al. (2010) measured the lean blow-off limit of a low swirl burner in an unconfined geometry at atmospheric conditions. They observed that the lean blow-off occurs around φ=0.5 for velocities from 7.5 to 20 m/s, and that by increasing the velocity, the blow-off limit increases slightly. The trend of their observation is in agreement with the results of this study, but the stability map in the confined geometry is narrower. In a confined chamber blow-off takes place close to φ=0.7 which is 30 % higher than the blow-off in Littlejohn's results.

The stability map for 20 % hydrogen and 80 % methane fuel is also calculated; the results are illustrated in Figures 4.5 through 4.8.
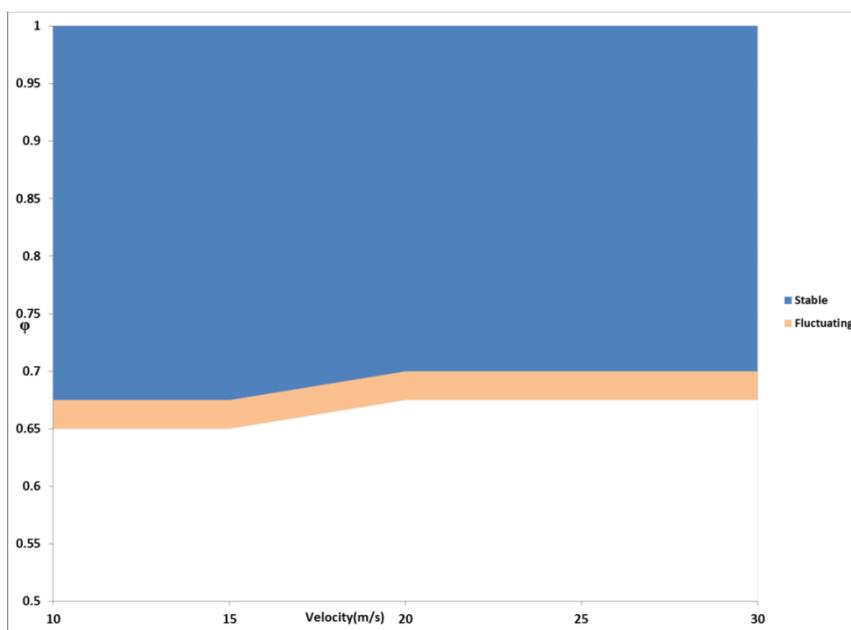
Figure 4.5 Stability map for the 3.81cm burner at 1 bar (80% Methane, 20% Hydrogen)
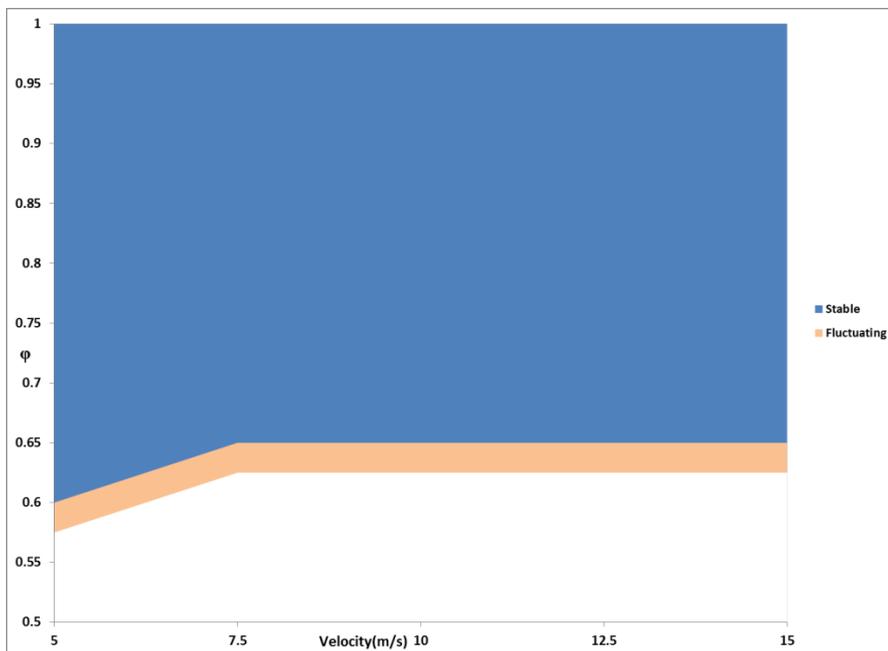
Figure 4.6 Stability map for the 3.81cm burner at 2 bar (80% Methane, 20% Hydrogen)
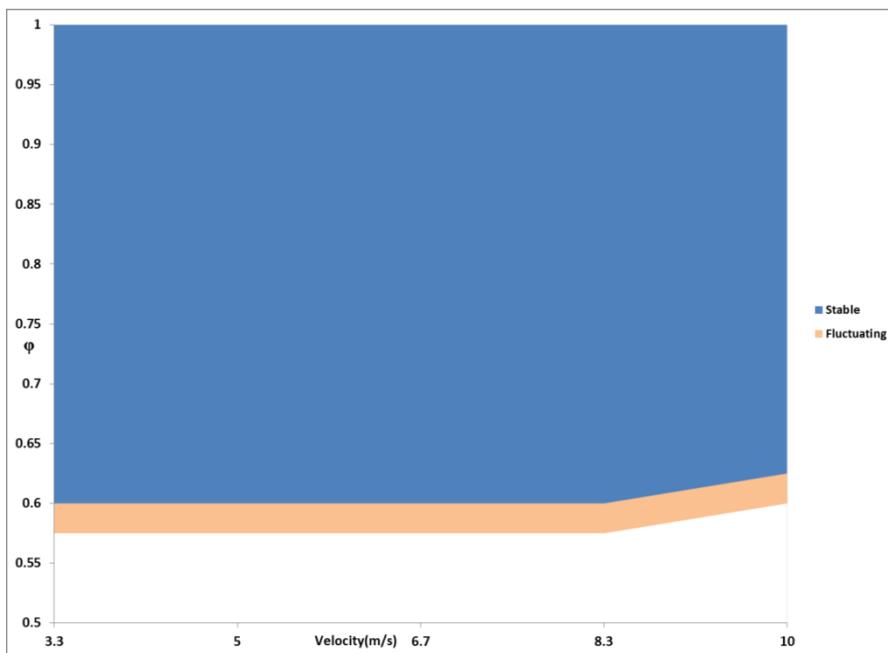
Figure 4.7 Stability map for the 3.81cm burner at 3 bar (80% Methane, 20% Hydrogen)
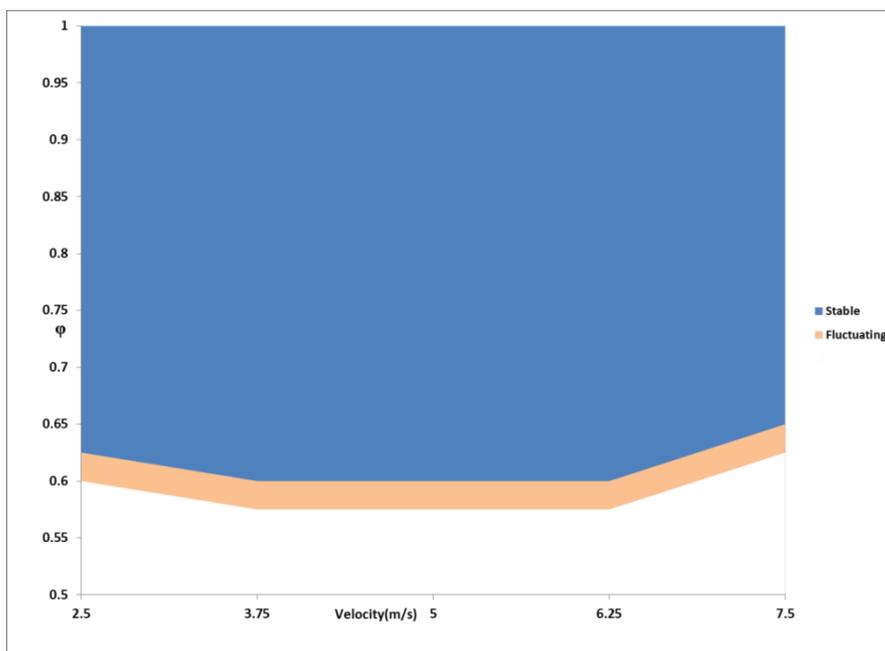
Figure 4.8 Stability map for the 3.81cm burner at 4 bar (80% Methane, 20% Hydrogen)

The stability maps of hydrogen-methane mixture are similar to the methane cases and the blows off curves follow the same trends. However the mixture fuel can operate in broader range of equivalence ratios. Based on the result presented above, 20 % hydrogen enrichment of the fuel improves the blow-off limit between 7 (for lower velocities) to 15 (for higher velocities) percent. Boschek et al. in 2007 reported the stability maps of a premixed burner at high pressures. The showed at high pressures hydrogen enrichment of methane fuel improves lean blow out limits around 9 % which is within the range observed in this study.

In the next step the effect of pressure and hydrogen enrichment of the fuel on the flame stability at constant bulk velocity was examined. Lean blow-off-limits for pure methane and hydrogen-methane mixtures at three different pressures (1, 2 and 3 bar) were determined. In all tests, bulk velocity was kept constant at 10 m/s. In Figure 4.9, the stability map of a 3.81 cm low swirl burner is shown.
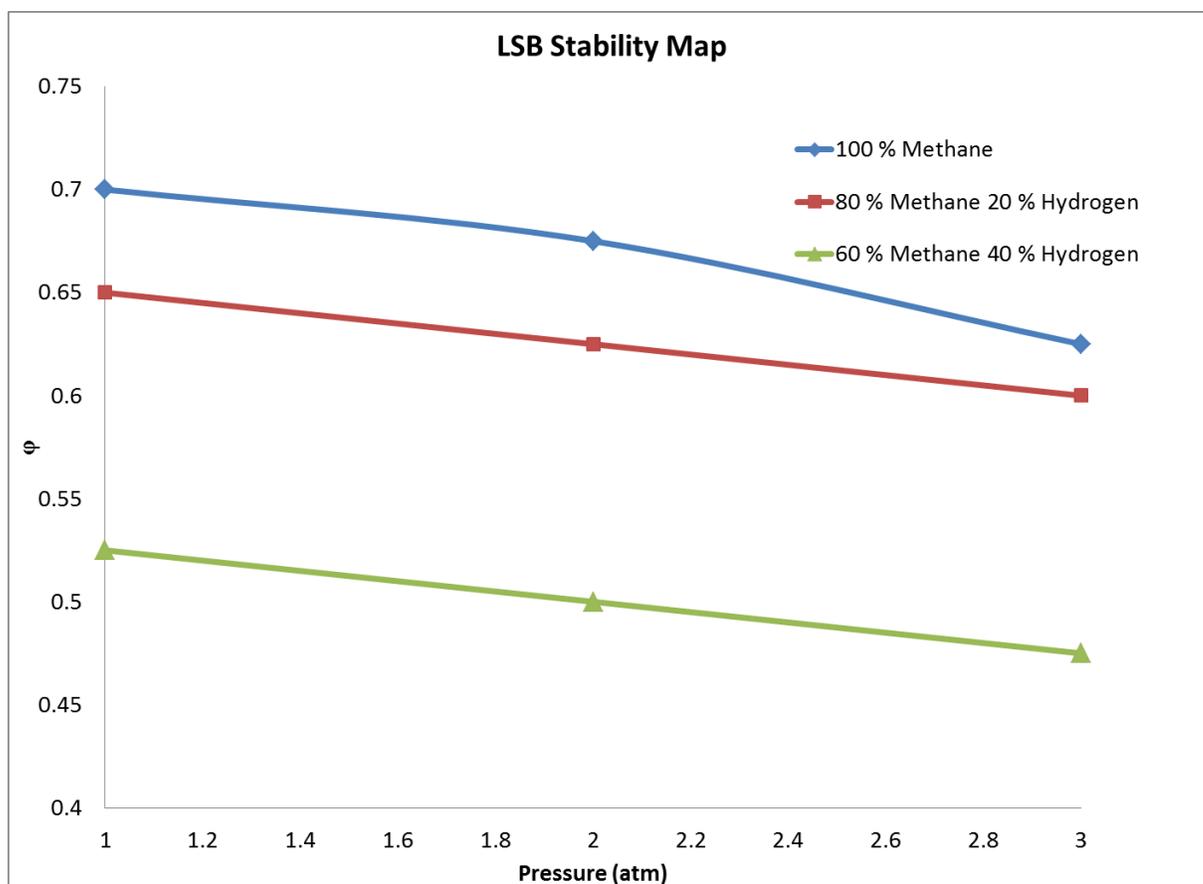
Figure 4.9 Lean blow-off limits determined for low-swirl burner at constant bulk velocity

Adding 20 % hydrogen to the methane improves the blow-off limit about 7 % while increasing hydrogen to 40 % causes a 35 % decrease in blow out limit and stabilizes the flame in a wider range of equivalence ratios. Hydrogen enrichment of methane increases the local burning rate, as hydrogen is a more reactive fuel. Higher OH radical concentration, as a result of adding hydrogen, leads to a higher global reaction rate and higher turbulent burning velocity, which in turn causes the blow out to take place at lower fuel to air ratios. The hydrogen-methane mixture has a lower Lewis number than

pure methane, which implies mass diffusion has become dominant while hydrogen is added, and the overall burning rate rises.

Elevating the pressure also improves the stability ranges. As pressure rises from 1 to 3 bar the blow-off occurs at lower equivalence ratios. Results in Figure 4.9 portray the same trend as Grieblel et al. (2007) observed. The stability map of pure methane and methane-hydrogen mixture shows an identical behavior. More interactions between flame and flow in a wider range of turbulent dynamics can increase the overall flame area and increase the burning rate of the flame. At higher pressures it has been observed that the flame base moves slightly closer to the burner exit which indicates an increase in the turbulent burning velocity.

The other parameter that can alter the stability map is the burner shape. In figure 4.10 regular burner and cone burner are shown.
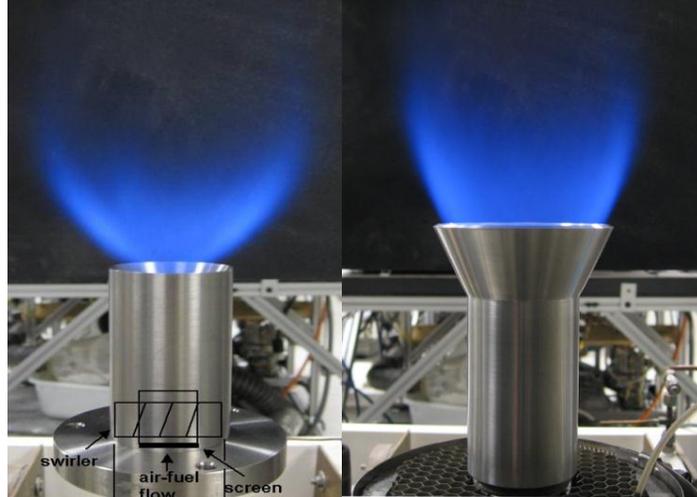
Figure 4.10 Left: Regular burner, Right: Cone burner

The cone burner is designed based on the flow field in the swirler and the flame does not attach to the burner. Because of that the cone temperature even at high pressure

tests does not exceed 100 C. The cone section plays the role of flame holder and stabilizes the flame in a wider range of operating conditions. In figure 4.11 the stability map of the cone burner is shown. It can be observed that the blows off limits are improved 15 to 20 % compared to the regular burner. The same trend was observed at higher pressures for the cone burner. It is expected that a more aerodynamic cone burner design will be able to operate in leaner regime.
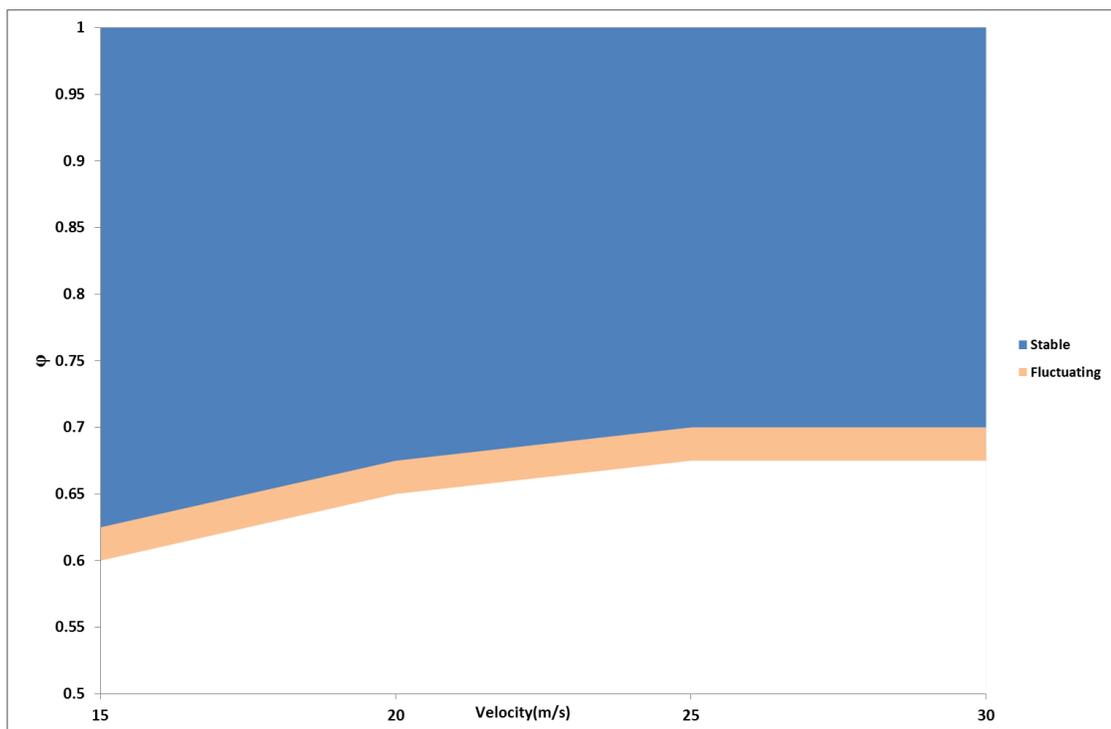
Figure 4.11 Stability map for the cone burner at 1 bar

4.2.1 Pressure Effects on Combustion Dynamics

As mentioned in the introduction, industrial combustion system generally operates at high pressure and this parameter has a significant impact on combustion process. In 2000, Turns suggested that the laminar flame speed can be obtained as:

$$S_L \propto \overline{T}^{0.375} T_u T_b^{-n/2} \exp\left(- E_A / 2R_u T_b\right) P^{(n-2)/2} \tag{4.4}$$

Where S_L is the laminar flame speed, P is the pressure, T_u is unburned gas temperature, T_b is burned gas temperature, E_A is the activation energy and n is the reaction order. In most reactions such as methane combustion, the reaction order is equal to one, so $S_L \propto P^{-0.5}$ and laminar flame speed decrease by increasing the pressure. However the turbulent flame speed seems to be system dependent. Shepherd and Cheng (2001) introduced an empirical relation between the laminar and turbulent flame speed in a low swirl burner.

$$\frac{S_T}{S_L} = \left(1 + C\left(\frac{u'}{S_L}\right)^n\right)^{1/n} \tag{4.5}$$

In this equation C is an empirical constant and u' is the turbulent velocity fluctuations. As noticed before the reaction order for most of the reactions considered in this study is equal to one. In this case equation (4.5) implies a linear dependence of turbulent flame speed on u'/S_L. Littlejohn et al. (2010) showed that this linear relationship is valid for methane, hydrogen and several other syngas in a low swirl burner.

Pressure elevation cause a reduction in laminar flame speed, but turbulent velocity fluctuations are not sensitive to the pressure. So base on the equation (4.5) turbulent flame speed should increase at higher pressures which can results in stabilizing the flame in a broader range of equivalence ratios. Also at elevated pressures the flame stabilizes at a lower position than that observed at atmospheric conditions. In low swirl burner turbulent fluctuation are usually 10 % of mean bulk velocity and the laminar flame speed of methane and methane hydrogen speed can be extract from the literature (Lachaux et al., 2005; Boschek et al., 2007). So for instance for pure methane flame at 10 m/s bulk velocity, u'/S_L is around 8. These values, for the atmospheric conditions, put the low swirl flame in the Corrugated Flamelets region and thin reaction zone of the Borghi

diagram shown in Figure 4.12. In Borghi diagram, L_T is the integral length scale and δ_L is the flame thickness. The thin reaction zone is characterized by a thick preheat zone and a thin inner reaction layer. In this region combustion takes place in a thin region and the measured domain can be segmented into burned and unburned regions. In the Corrugated Flamelets region the flame front is thin and it has an inner structure close to laminar flame and wrinkles by turbulence motion of flow field. And fresh reactant pockets can be formed due to interaction of flame surface and turbulence.
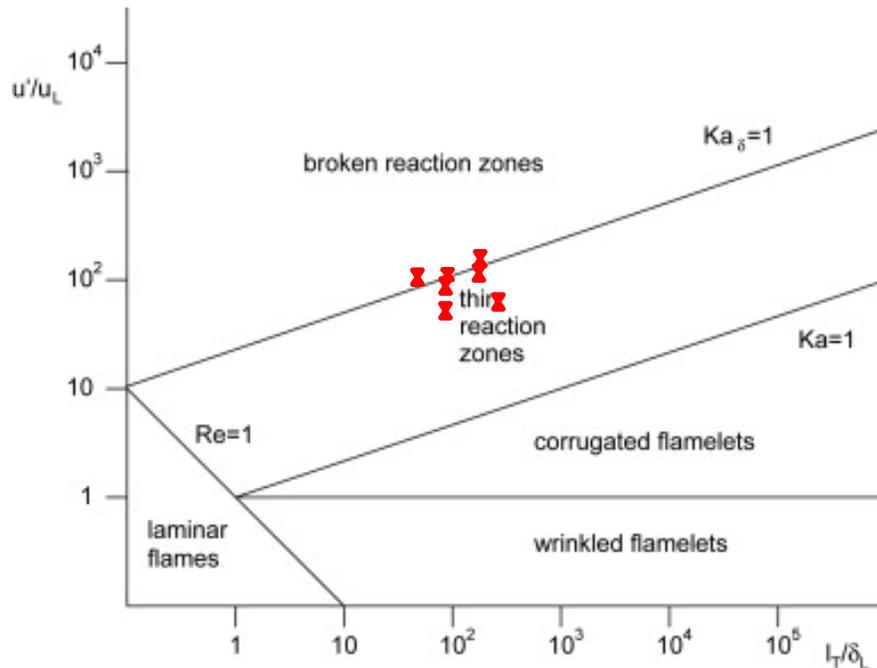
Figure 4.12 Borghi diagram for premixed turbulent combustion

4.2.2 Hydrogen Enrichment Effects on Combustion Dynamics

Lean hydrogen enriched flames exhibit a higher laminar flame speed and a greatly enhanced resistance to strain as noticed in the introduction section. Little john et al. showed that the hydrogen and methane mixture flame also follows the linear form of

equation (4.5), but the value for *C* is higher than pure methane combustion. As a result, turbulent flame speed of hydrogen-methane mixture flame becomes larger than 100% methane fuel. This improves flame stabilization in the low swirl burner and a wider flammability limits achieved by the hydrogen containing fuels. Adding hydrogen also helps to reduce the pollutant emissions. The experiment studies showed that the CO concentration decrease with hydrogen addition .The direct numerical simulation results also showed lower CO emissions per unit fuel consumption are observed for the hydrogen containing methane (Hawk and Chen, 2004).

4.3 Flame Front Curvature

OH PLIF images of methane-hydrogen flames at different conditions (table 4.1) were recorded and analyzed to calculate 2-D flame front curvature. For each case, 300 images were examined. For all the cases bulk velocity is kept constant equal to 10 m/s. Pressure, equivalence ratio and Hydrogen percent are the only parameters changed in these tests.

Table 4.1 Various measurement parameters

Case	Bulk Velocity (m/s)	Pressure (atm)	Equivalence Ratio (φ)	Percent Hydrogen (α)
A	10	1	0.75	0
B	10	2	0.75	0
C	10	3	0.75	0
D	10	1	0.65	20
E	10	2	0.65	20
F	10	3	0.65	20
G	10	1	0.55	40
H	10	2	0.55	40
I	10	3	0.55	40

Figure 4.13 shows the instantaneous images of these flames at different conditions (equivalence ratios from top to bottom: 0.75, 0.75, and 0.55). Although the equivalence ratios are different, increasing the equivalence ratio for a specific fuel only increases the wrinkling even further. Clearly, the increase in pressure and ratio of hydrogen corresponds to an increasingly wrinkled flame.

To analyze the OH images, an edge detection algorithm (Canny-edge detection algorithm) is applied to each image and the OH layer boundaries are found using the software package MATLAB. To find the flame front curvature, h, the edge coordinate (x, y) is defined as:

$$h = \frac{\frac{d^2 y}{dx^2}}{\left(1 + \left(\frac{dy}{dx}\right)^2\right)^{3/2}} \tag{4.6}$$
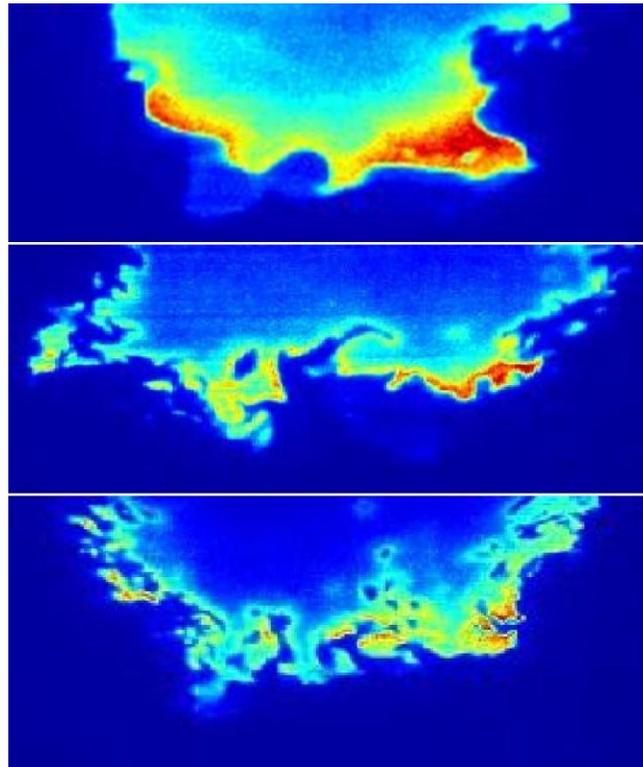
Figure 4.13 Top: 100% methane at 1 atm, middle: 100% methane at 3 atm, bottom: 60% methane, 40% hydrogen at 3 atm

Here, positive curvature is defined as being convex to the reactant gases and negative curvature is being concave to the reactants. In Figures 4.14 and 4.15 the PDF distributions of flame front curvatures are shown. The mean and variance of the curvature distributions are calculated in Table 2. Also included are the magnitudes (or absolute value) of the average radius of curvature of the wrinkled flamelets at different pressures and fuel mixtures. These values indicate the inverse of the mean absolute curvature, $\bar{r} = 1/|\bar{h}|$.

The mean value of curvature for all cases is close to 0, however positive (negative). Adding more hydrogen causes the flame front to wrinkle more and the PDF of curvature distributions becomes broadened (larger variance), which indicates the higher probability of larger curvatures. This effect seems to be stronger at higher pressures.

Broadening of flame front curvature distributions, when methane is enriched with hydrogen, might be due to a decrease in Lewis number of the fuel mixture as well as an enhancement of smaller scale flame front wrinkling (Adding hydrogen to the methane causes a decrease in Lewis number of the mixture fuel). One of the effects of a reduction in Lewis number is that the mass diffusion becomes dominant and the local burning rate of these flames increases and the flame sensitivity to strain rate reduces.

The effect of equivalence ratio on this trend was also examined, and a result is displayed in Figure 4.15. It can be seen that increasing the equivalence ratio from 0.55 to 0.65 reduces the probability density peak by approximately 7 %. The average radius of curvature for the 40 % H_2 case was calculated to be 1.3 mm. This calculated value allows a comparison of hydrogen fuel fraction while maintaining a constant equivalence ratio. It is then found that increasing from 20 % to 40 % H_2 at a constant equivalence ratio of 0.65 resulted in a nearly 20% decrease in radius of curvature.
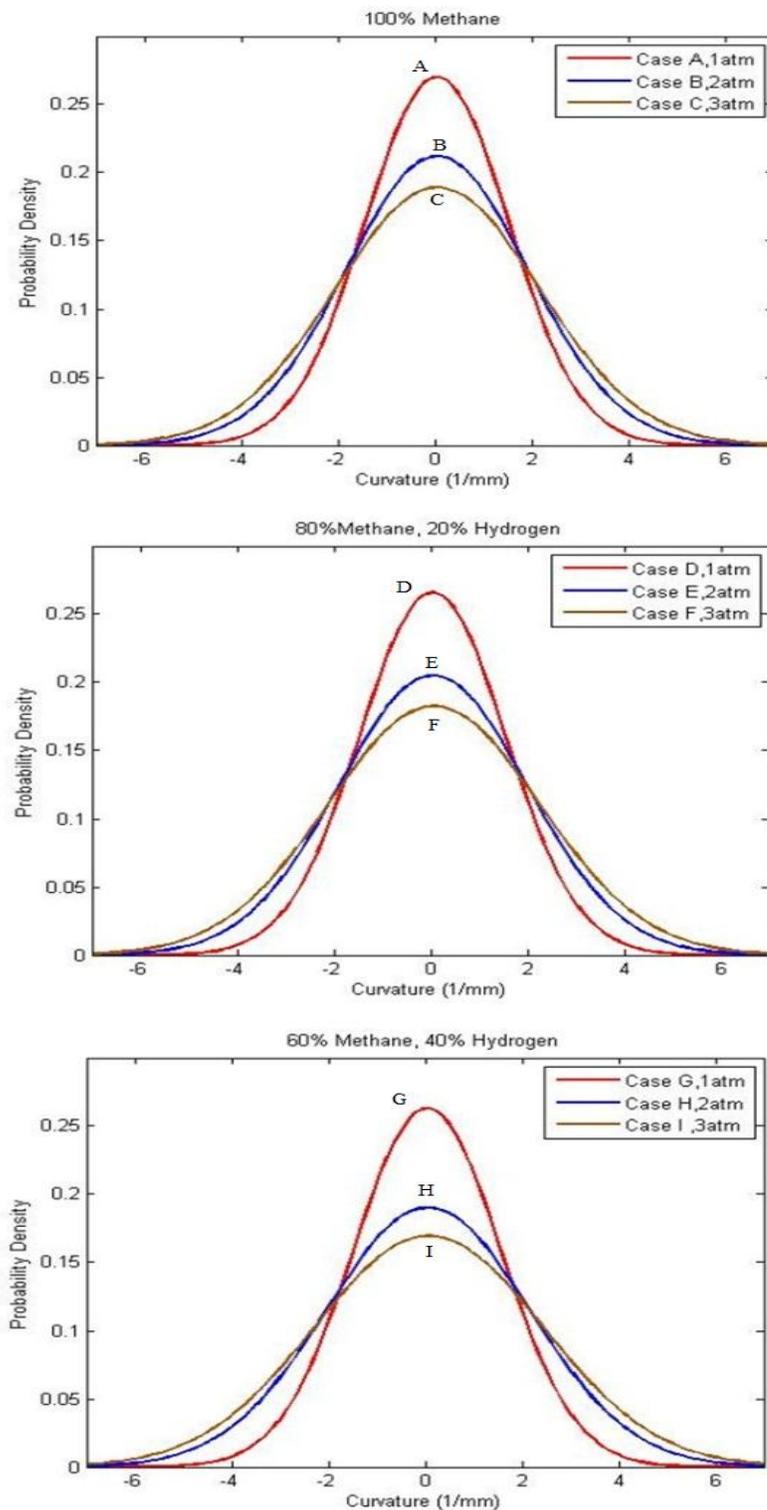
Figure 4.14 PDF of flame front curvature distribution for 100% methane flame, 80% methane-20% hydrogen flame and 60% methane-40% hydrogen flame 1, 2 and 3 atm

Table 4.2 Mean, variance, and average absolute radius of flame front curvature

CH$_4$	Pressure (atm)	Mean	Variance	Avg. Abs. Radius Curv. (mm), $\bar{r}$
100%	1	0.045	2.18	1.7
100%	2	0.048	3.54	1.2
100%	3	0.058	4.45	1.1
80%	1	0.040	2.25	1.6
80%	2	0.049	3.79	1.1
80%	3	0.068	4.78	1.0
60%	1	0.044	2.30	1.4
60%	2	0.058	4.40	1.0
60%	3	0.076	5.54	0.9
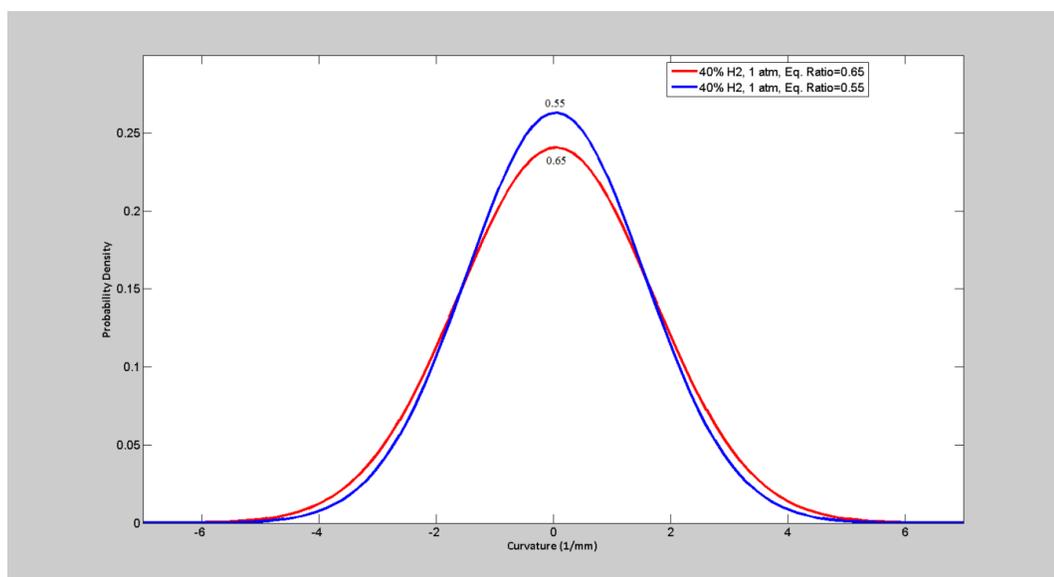
Figure 4.15 PDF of flame front curvature distribution for 60% methane, 40% hydrogen at 1 atm for equivalence ratios of 0.55 and 0.65

Extrapolating the 40 % H$_2$ data to determine the average absolute radius of curvature at an equivalence ratio of 0.75 resulted in a 30 % decrease in curvature (calculated to be 1.2 mm) as compared to the pure methane case (curvature of 1.7 mm). This is in agreement with previous results and supports the notion that either increasing

the fraction of hydrogen or increasing the pressure results in the flame becoming increasingly wrinkled.

In addition, increasing the pressure has a stronger effect on the curvature distribution. By elevating the pressure, the laminar flame velocity and the kinematic viscosity both decrease. As a result, smaller scales are generated but the integral scales seem to be insensitive to the changes in pressure (Kobayashi, 2002). This causes an increase in the dynamic range of turbulent structures and the difference between small scales and large scales becomes larger. So in this range of turbulent scales, the flame interacts with the flow and the turbulent small scales of the flow can alter the flame surface and cause it to wrinkle more.

4.4 Flame Surface Density

As Driscoll [24] mentioned in his review paper, measurements of flame structure such as flame surface density, Σ, are important because both the turbulent burning velocity, s_T, and the stability mechanism which governs the combustion process depend on the flamelet wrinkling process, which are geometrically dependent. To calculate flame surface density, OH PLIF images have again been used. As done previously, 300 images were analyzed with MATLAB. First, the flame front was detected and then binarized images were generated from the boundaries of the OH radical field, summed, and averaged to produce mean progress variable $\langle c \rangle$ maps (figure 4.16). These $\langle c \rangle$ contours represent the probability of OH boundaries (flame front) being at a given location within the flame brush. The instantaneous OH layer edges are superimposed on the $\langle c \rangle$ map and the lengths of the edge falling within a given $\langle c \rangle$ range (in this analysis $\langle c \rangle$ is from 0 to 1 and this range is divided into 0.1 intervals) are summed and the following formula is applied:

$$\Sigma = \frac{L(\langle c \rangle)}{n_f A(\langle c \rangle)} \tag{4.7}$$

In Equation 4.7, $A(\langle c \rangle)$ is the area between adjacent $\langle c \rangle$ contours, $L(\langle c \rangle)$ is the total length from all the edges falling within this area and n_f is the number of analyzed images.
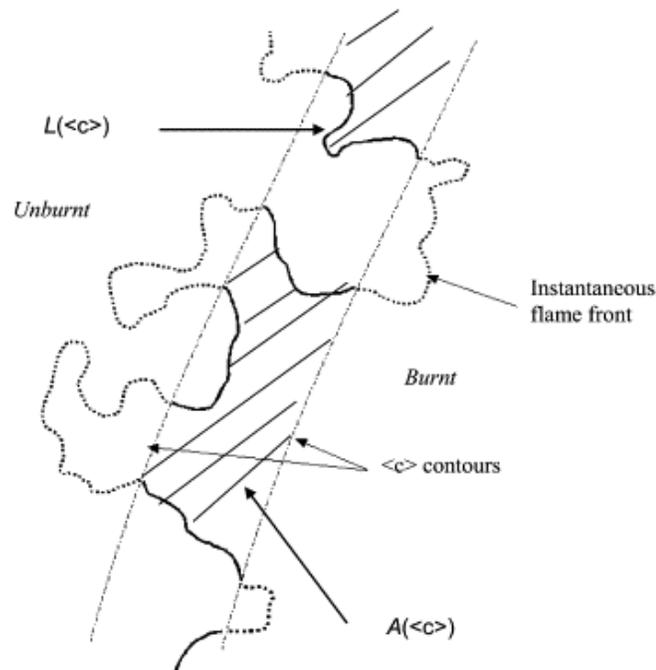
Figure 4.16 Flame Surface Density calculations

Source: Tang, 2006

In Figure 4.17, flame surface densities of various mixed flames are shown. For all cases, the graph of flame surface density vs. progress variable shows a parabolic behavior. This trend has been seen by others as well (Halter et al., 2005; Guo et al. 2010). In figure 4.18 flame surface density at 3 atm for three different percent of hydrogen are shown (results at 1 and 2 atm show the same trend).
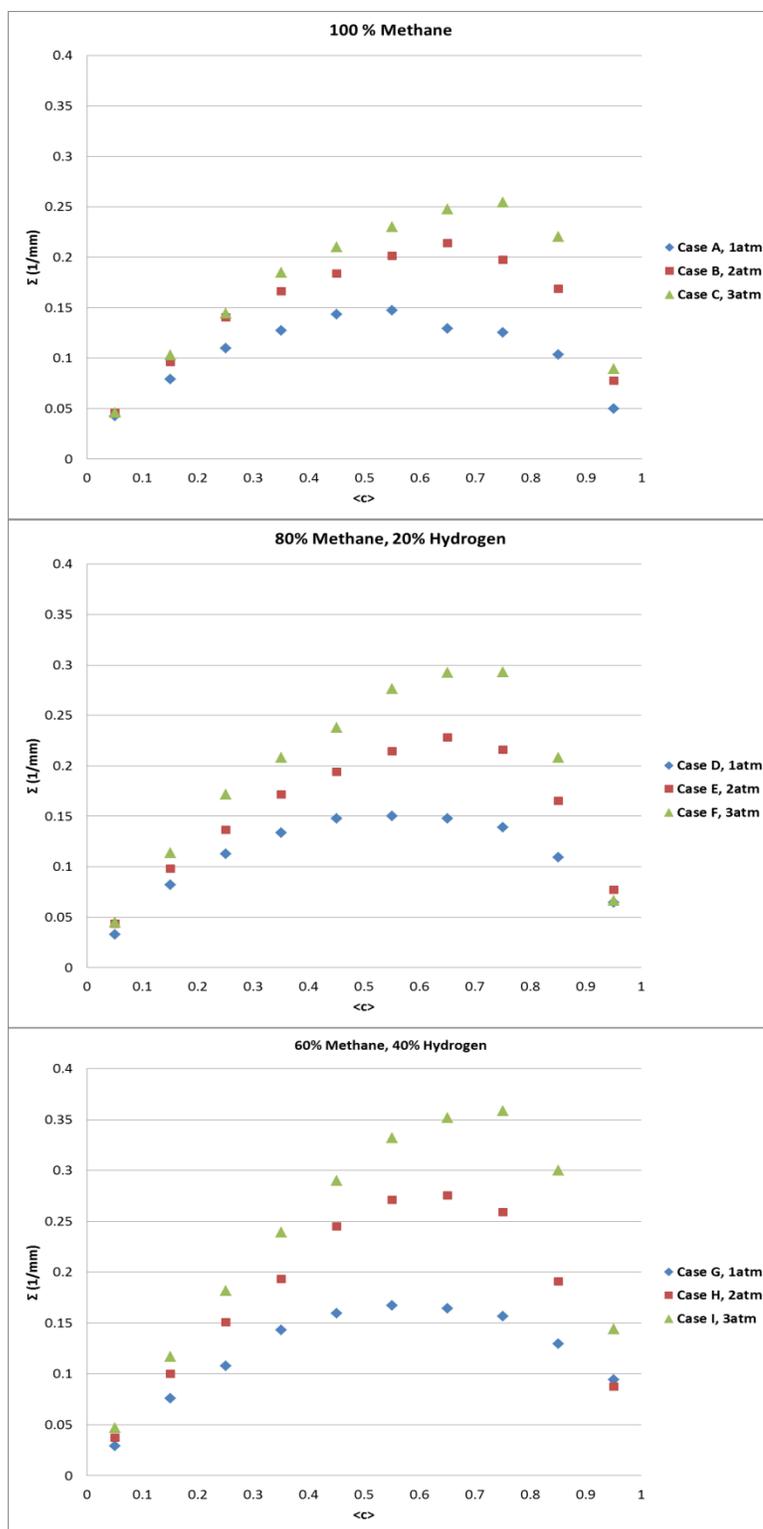
Figure 4.17 Flame surface densities at different conditions

Adding hydrogen slightly increases the flame surface density which is in agreement with the results reported by Halter in a Bunsen burner and Zhu (2010) in a swirl-stabilized flame. However, Guo observed a completely different trend. In their V-shape flame the density shows a decrease as hydrogen is added to methane. This contradictory behavior illustrates the dependency of flame structures to the geometry of the burner.
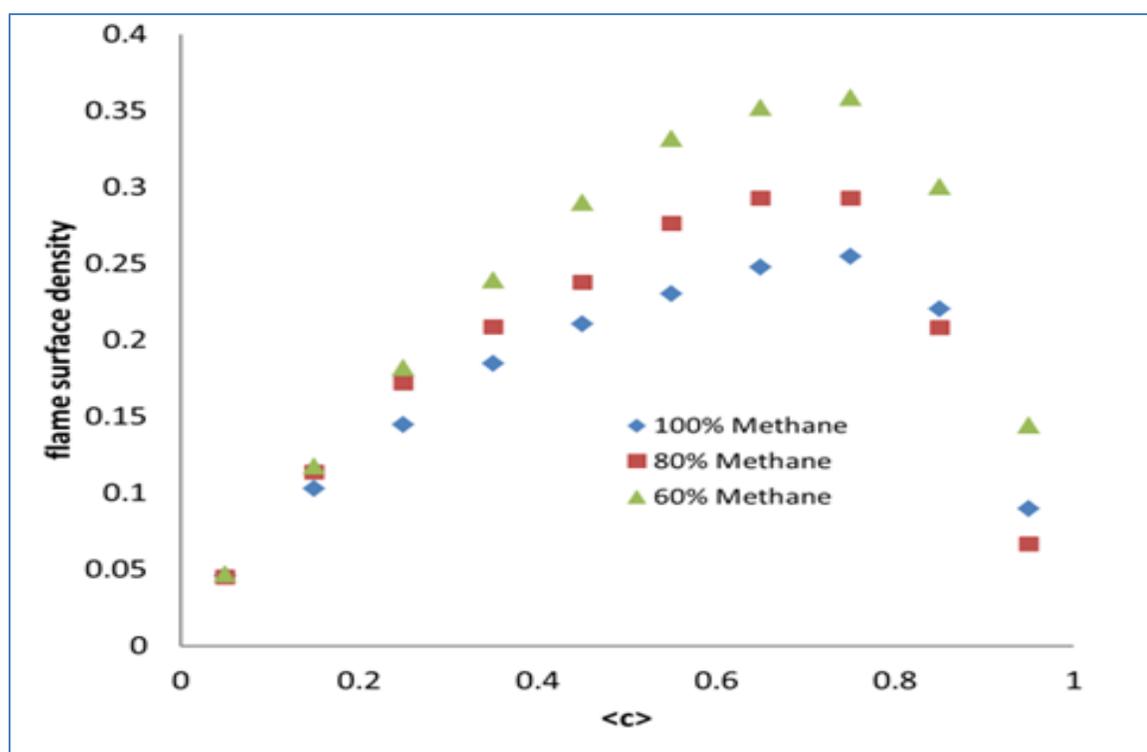
Figure 4.18 Flame surface density at 3 atm for different hydrogen enrichment

Figure 4.20 shows the dependency of the flame surface density on equivalence ratio. At 40 % H_2, the flame surface density is plotted for equivalence ratios of 0.55 and 0.65. The plot shows that the increase in equivalence ratio results in an increase in the

flame surface density by about 7 %. The same trend would also be expected at elevated pressures, which is in agreement with the radius of curvature results.
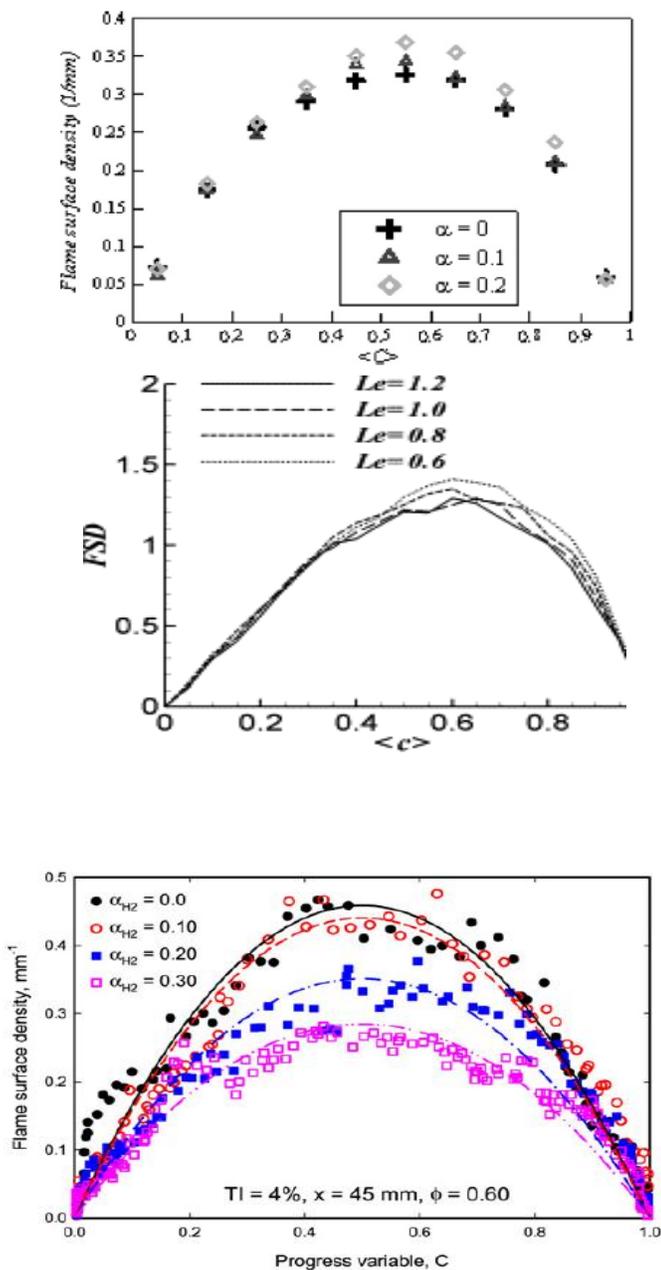
Figure 4.19 Flame surface density measured by Halter (top left), Insuk (top right) and Guo (Bottom),
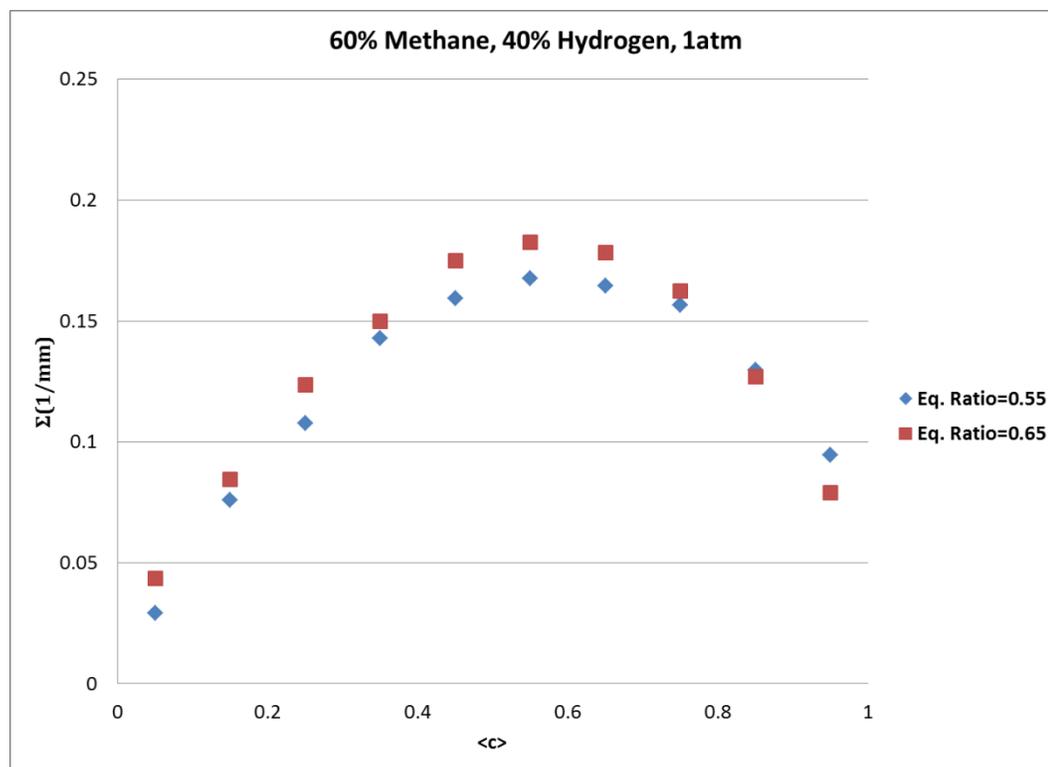
Figure 4.20 Flame surface densities for 60% methane, 40% hydrogen at 1 atm for equivalence ratios of 0.55 and 0.65

By elevating the pressure, the maximum flame surface density increases more, as larger amounts of hydrogen are mixed with methane, which is in agreement with the curvature plots. In Figure 4.21, the maximum values of flame surface density are plotted at three different pressures. As the concentration of hydrogen increases, the slope of the maximum flame surface density increases; this indicates more wrinkling at higher pressures than at lower pressures. This effect may be due to a faster reaction rate of hydrogen at higher pressures. Based on the previous results, maintaining a constant equivalence ratio for each mixture, to say 0.75, would result in an increase in the slope of the 80 % methane case, and an even further increase in the slope of the 60 % methane case.
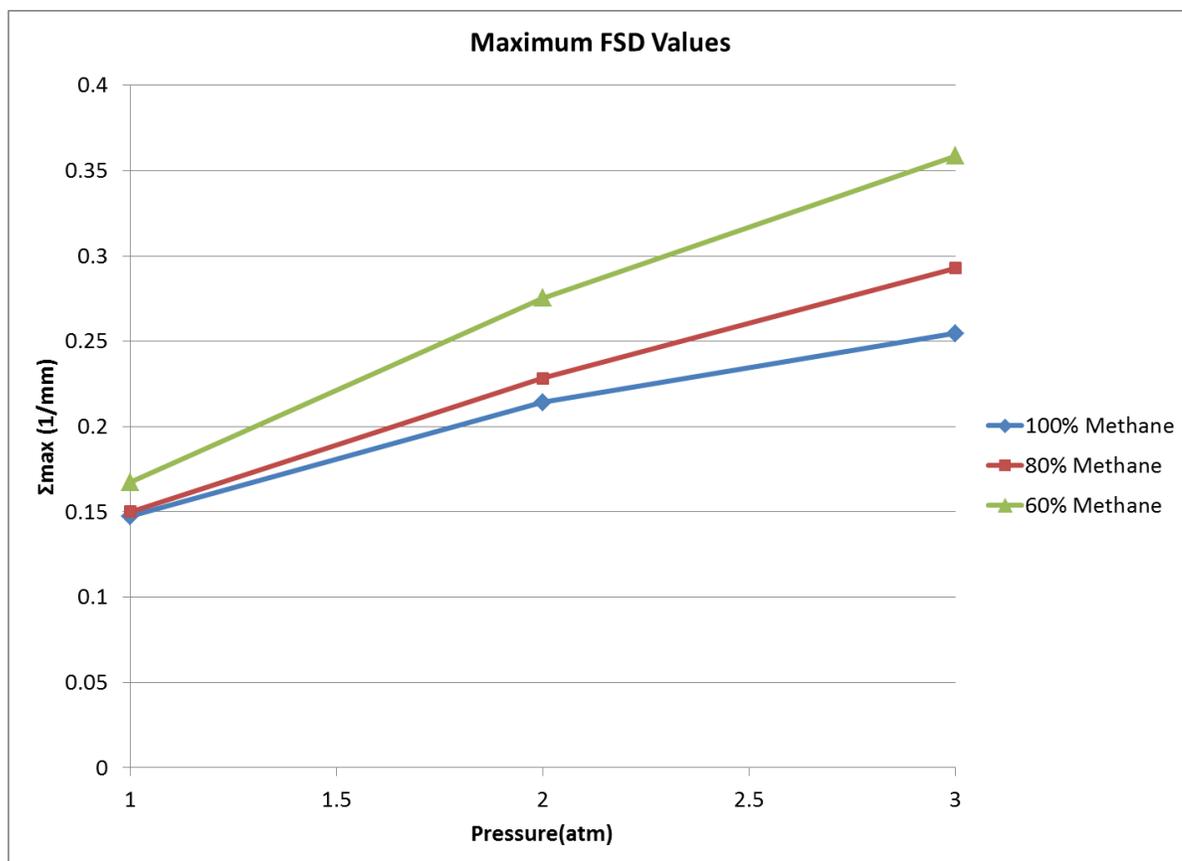
Figure 4.21 Maximum flame surface densities

As mentioned before, by raising the pressure, turbulent small scales (Kolmogorov scales) become even smaller, while there is no corresponding change for the integral scale. This allows the flame to interact with the turbulent flow in a wider range of scales, and these small scales wrinkle the flame surface more than at atmospheric conditions. The other effect of pressure is shifting of the Σ maximum to higher values of $\langle c \rangle$. This behavior has not been seen in Bunsen burner flames or other papers, but it is in agreement with the DNS simulations of Han et al. (2008). Based on their simulation, the maximum is shifted toward the edges of the flame, close to the products region, due to convection, and the flame area produced by strain throughout the flame brush is then convected downstream and rapidly destroyed. This destruction is due to the propagation

term in the flame surface density transport equation when downstream of the flame brush. At high pressures, the turbulent structure of the flow is changing and turbulent fluctuations can penetrate through the flame brush and convect the OH layer towards the products. The difference between the results of this study and Halter's results might be due to different approaches in measuring the flame surface density. Halter measures the temperature in order to calculate the flame surface density while OH concentration is used in this study. It seems a variation in flow turbulence does not have a significant effect on thermal layers while simultaneous measurement of temperature and OH radicals can help clarify the ambiguities.

4.5 Pressure Fluctuations

Pressure fluctuations inside the chamber for the test conditions in table 4.1 are measured by using a piezoelectric pressure transducer. Figure 4.22 shows the normalized root mean square of pressure data (P_{rms}) for each condition. Atmospheric pressure is used to normalize all the pressure fluctuations. The P_{rms} do not vary noticeably from 1 to 2 atm, but at 3 atm the amplitude of fluctuations increases significantly (about 30% compared to 1 and 2 atm) which shows a change in combustion dynamic from 2 to 3 atm.

Also figure 4.23 shows that adding hydrogen may cause to decrease in the level of pressure fluctuations, however in this figure the equivalence ratios of pure methane flame and the mixtures are not the same. So hydrogen enrichment of methane has the benefit of reducing the pollutant emissions and also can cause noise reduction (3 to 4 dB reduction) in the combustor.
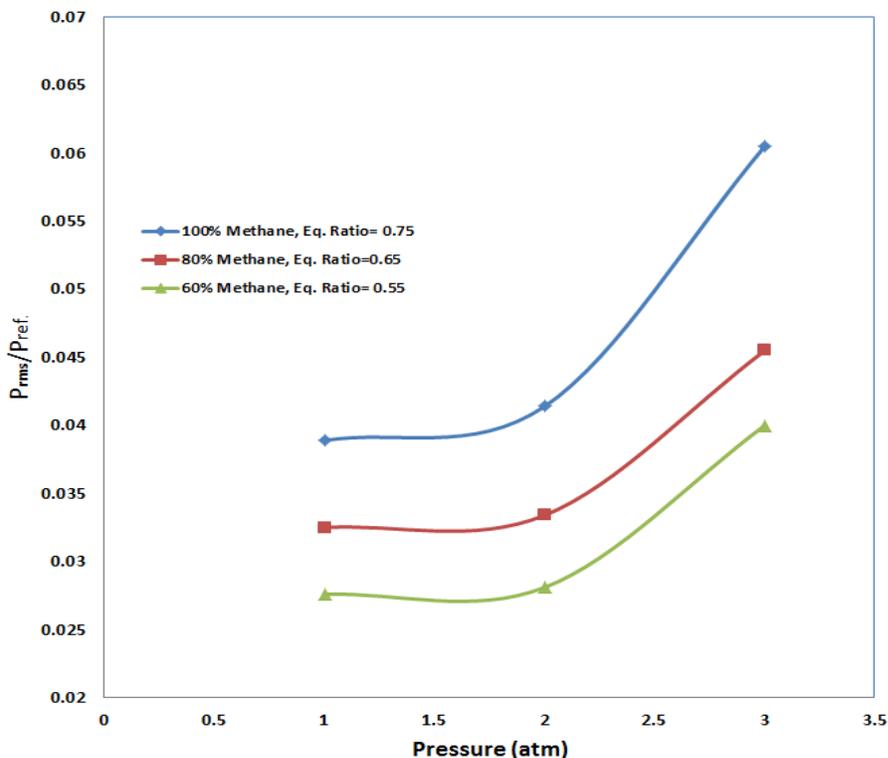
Figure 4.22 Normalized P_{rms} at different conditions

4.6 Summary and Conclusion

In this chapter instability map of a 3.81cm low swirl burner, at different operating conditions with various fuels was calculated. Also the effect of geometry on flame stabilization by applying a cone burner was investigated. Also images of OH radical concentrations are taken with PLIF techniques and analyzed to calculate the flame front curvature and flame surface density.

Hydrogen enrichment of methane fuel along with an increase in the pressure causes the blow-off limits to occur at a lower equivalence ratio, broadening the range of stability. The 2D flame front curvature measurements show increased wrinkling of the flame front at higher pressures and ratios of hydrogen. Interactions of the turbulent small scales with the flame surface, a decrease in Lewis number, and an increase in the local and overall burning rates of fuel due to the faster reaction rate of hydrogen all seem to

contribute to the increase in the flame area and flame front wrinkling. Similarly, as the ratio of hydrogen increases, mass diffusion becomes the dominant term in the transport equation as a result of the reduction in Lewis number, thereby wrinkling the flame surface even more.

Finally, the flame surface density also increases as a result of increased wrinkling of the flame surface when hydrogen is added or the pressure is raised. It appears that hydrogen has a stronger effect on flame wrinkling at elevated pressures (this effect is reduced at atmospheric pressures). Also, the flame surface density ($\sum$) vs. mean progress variable ($<c>$) graph shows a parabolic behavior which has been observed by other researchers. Shifting of the maximum flame surface density at high pressures towards the products of combustion due to convection is also observed, along with its rapid destruction.

CHAPTER 5

FLAME AND ACOUSTIC INTERACTION

In this chapter flame interaction with imposed acoustic pressure fluctuation in the range of 45 Hz to 195 Hz are studied. In the first section the methodology for constructing the Rayleigh index maps is reviewed. The results exhibit two different modes of coupling between heat release and acoustic forcing. Also the flame structures under acoustic excitation condition are calculated and the effect of frequency variation on the flame surface density and curvature is addressed.

5.1 Rayleigh Index Maps

5.1.1 Pressure Signal and Flame Images

Pressure power spectrum density in the 2.54 cm low swirl burner shows that there is no self-induced acoustics. Only three weak modes were observed between 85 to 125 Hz, but their amplitudes were very low, close to the broad band noise level. These weak natural modes might be due to large chamber space compared to the flame size. In this case, fluctuations can dissipate in the chamber and no strong mode can be formed. Also the swirl intensities in this burner are smaller than other conventional high swirl burner and the flame is stabilized more through the flow divergence rather than the swirl mechanism (Huang, 2008). However in 3.81 cm burner the pressure power spectrum is different. Figure 5.1 shows both pressure power spectrum of 2.54 cm and 3.81 cm low swirl burners. As the size of burner diameter is change, it is expected that the dominant modes shift to the lower frequencies ($f \propto c/D$), but the pressure signal shows a contradictory behavior. The three modes observed in 2.54 cm burner are shifted 10 to 20 % towards higher frequency in 3.81 cm burner. It shows that the combustion process and the chamber acoustics are actively interacting, otherwise shifting should be observed in other direction.
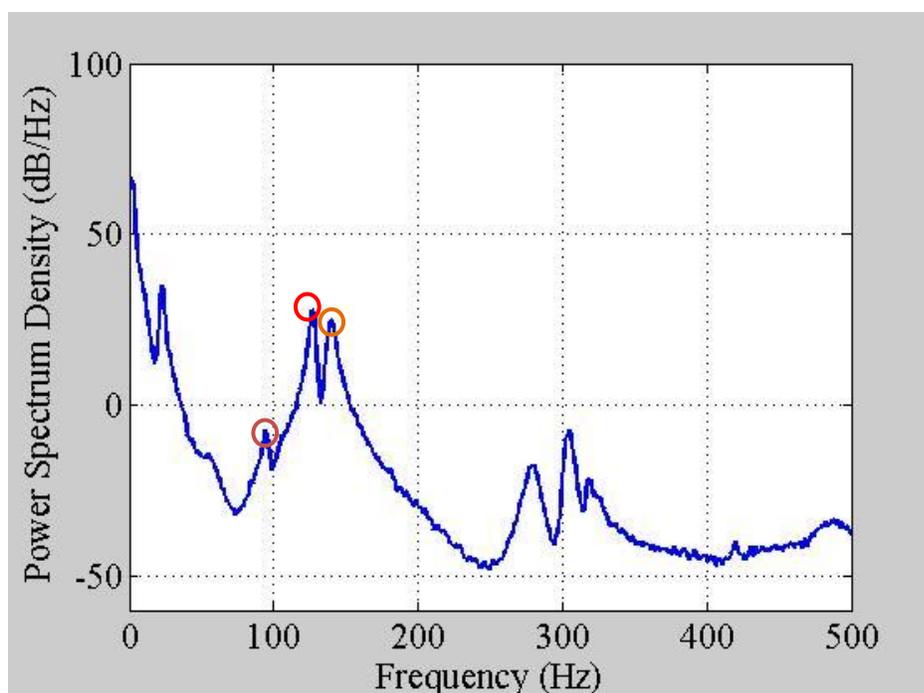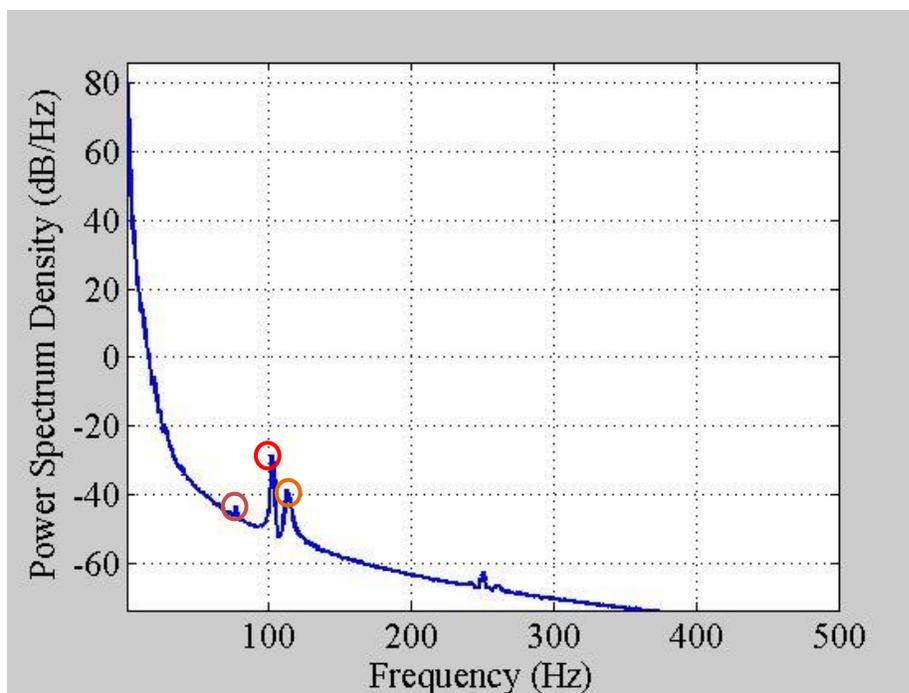
Figure 5.1 Power spectrum density of pressure oscillations, reacting flame with no excitation. Top: 3.81 cm burner. Bottom: 2.54 cm burner.

The first natural mode in 3.81 cm burner is 95 Hz which is weaker than the two other modes, but still stronger than the modes in smaller burner. The second and third modes are 125 and 135 Hz which have the same strength. These modes are stronger than the peaks in the 2.54 cm burner, because of higher flow rates of reactants and as a result more heat release inside the combustion system. Also, based on the shape of the peaks in figure 5.1 it can be deduced that the acoustic energy can be pumped to these natural modes in a broader range of frequencies. The P_{rms} for the 2.54 cm burner was 0.003 % of mean pressure compared to 0.025 % for the 3.81 cm burner. Based on the pressure power spectrum, combustion coupling with acoustic field in the range of 45 Hz to 195 Hz is examined in this chapter. A sample of pressure signal and its power spectrum density at forcing condition is displayed in figure 5.2.
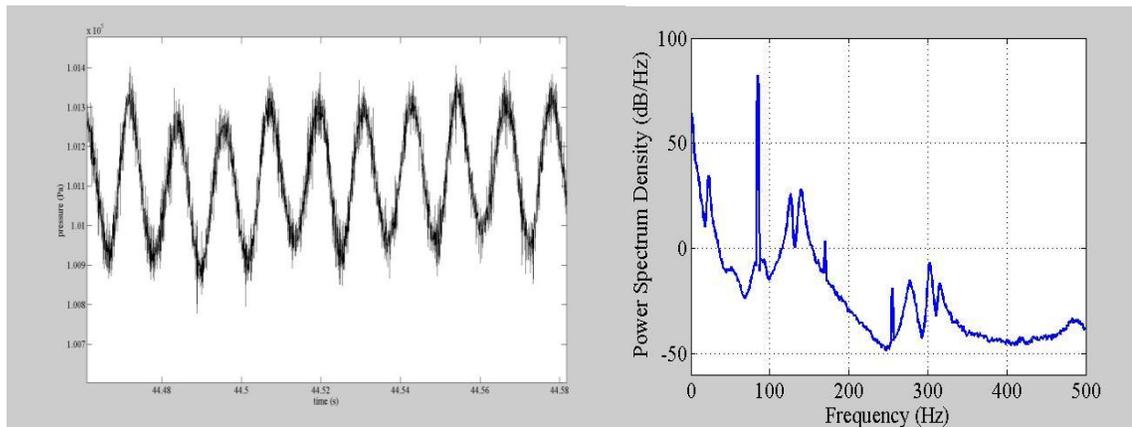
Figure 5.2 Pressure signal and power spectrum density of pressure oscillations at 85 Hz excitation

Flame images in this work are captured by using an ICCD camera and PLIF technique. In figure 5.3 a sample of instantaneous flame image under the influence of acoustic forcing and the average of 900 instantaneous images along with the flame picture taken by the normal camera are shown.
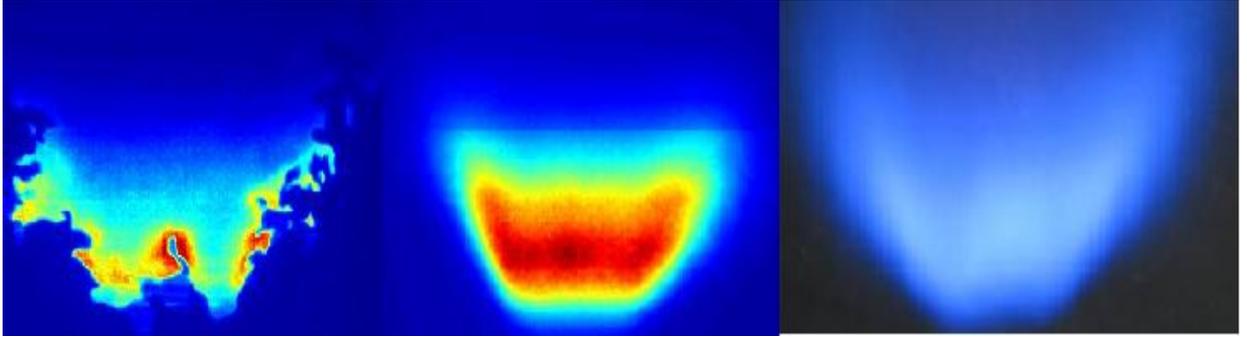
Figure 5.3 Left: instantaneous OH image, Middle: average of 900 instantaneous images Right: flame picture taken by normal camera

As can be seen in 5.3, LSB flame has a blue color bowl shape. The blue color of LSB methane flame is due to the no soot production in this burner.

5.1.2 Rayleigh Index Map Construction: Methodology

In chapter 2 several instability criteria were introduced. The most common criterion applied to predict combustion instability initiation is the Rayleigh criterion. Rayleigh index maps are constructed based on this criterion and they show where in the combustion zone, heat release fluctuations are coupled with the pressure perturbations. In this work equation 5.1 is used to calculate the Rayleigh index (R) at each point.

$$R = \int_0^1 \frac{p'q'}{p_{rms}\bar{q}}\,dt \qquad (5.1)$$

Here p' is the pressure oscillation, p_{rms} is the root mean square of the pressure oscillation for each set of images, q' is the oscillation of the heat release, $\bar{q}$ is the mean heat release, and dt indicates an integral over time. This formulation has been used by Culick (1976), Kang et al. (2007), Huang and Ratner (2009), Yilmaz et al. (2009) to study unstable heat release coupling with acoustic forcing.

To calculate Rayleigh index, pressure signal and OH images are recorded simultaneously. Then the OH images are averaged and for each of them, OH fluctuations

are calculated by subtracting each image from the average one. Pressure fluctuations are obtained following the same procedure. And at last, the Rayleigh maps are constructed as a function of calculated *p'* and *q'*. Figure 5.4 graphically displays the procedure explained here.
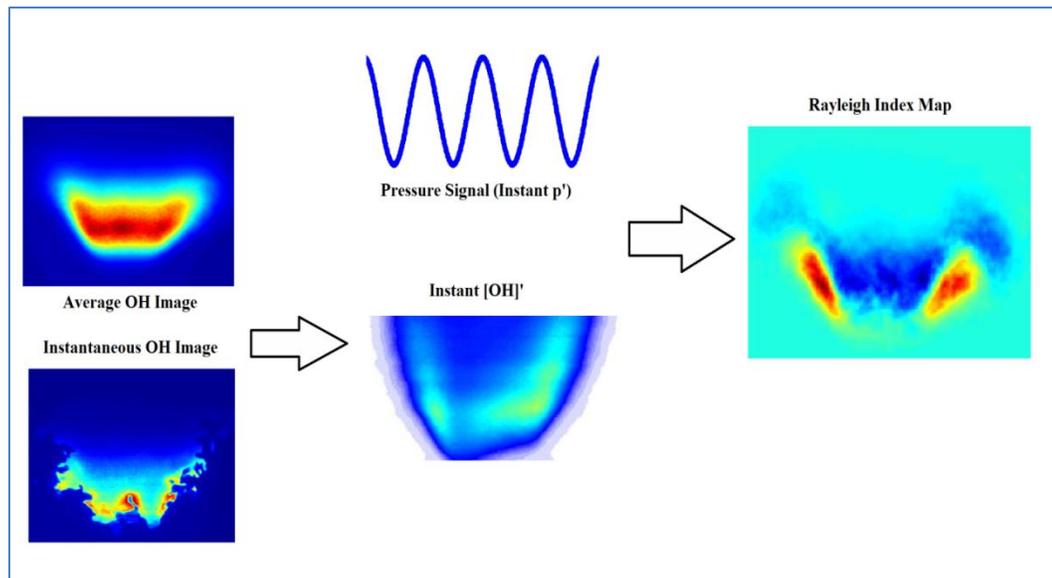
Figure 5.4 Procedure of construction of Rayleigh index maps

5.1.3 Rayleigh Index Map: Results and Discussion

Rayleigh index maps of flame response to the acoustic forcing of 45 Hz to 195 Hz are calculated. The tests conditions are summarized in table 5.1. For all the frequencies, the amplitude of pressure forcing are kept is the range of 0.05 to 0.2 % of mean pressure. The results are shown in figures 5.4 through 5.6.

Table 5.1 Experiment conditions

Re(D)	Φ	CH$_4$(SLPM)	Air(SLPM)	Pressure(atm)	Q(kW)
25231	0.85	56.01	627.96	1	30.26
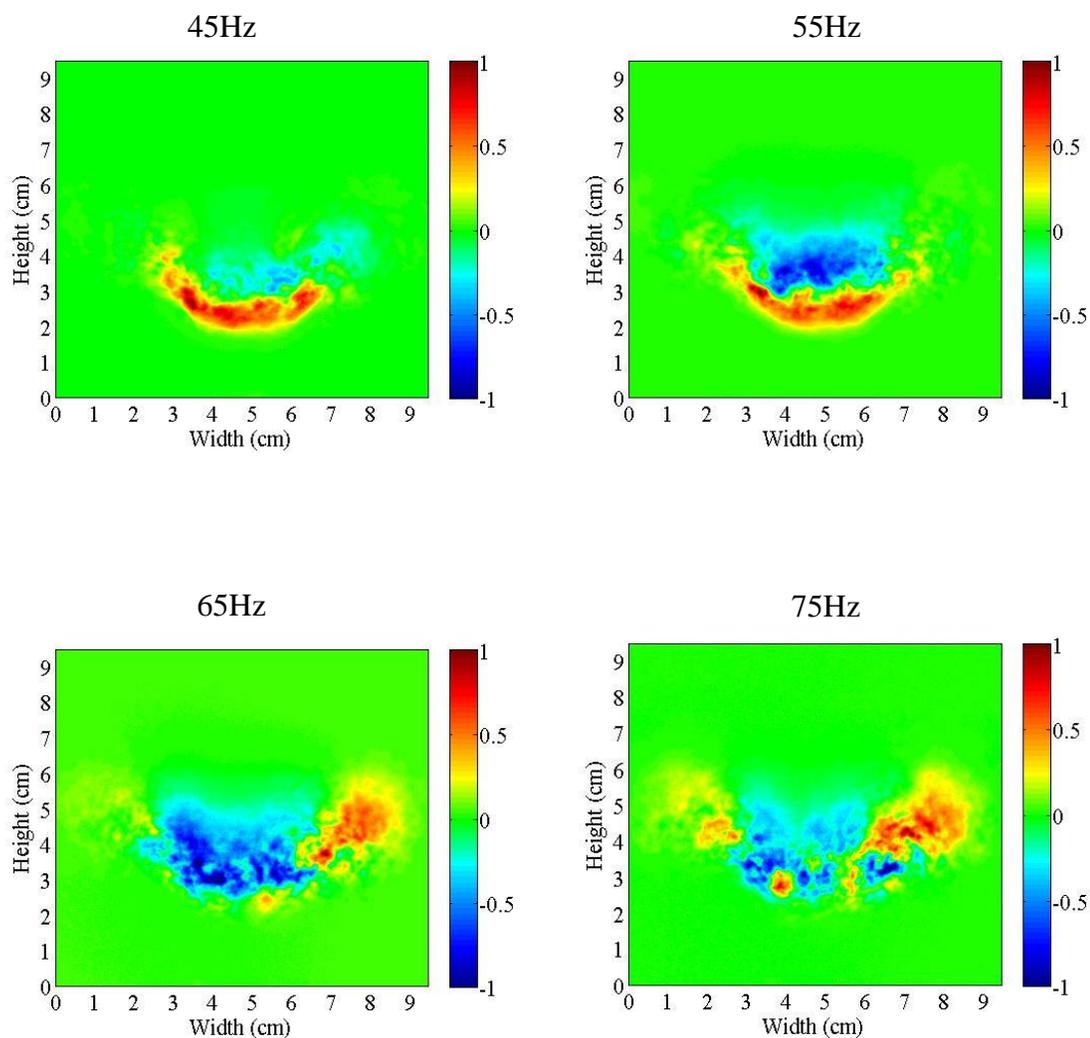
Figure 5.5 Rayleigh Maps for 45, 55, 65 and 75 Hz
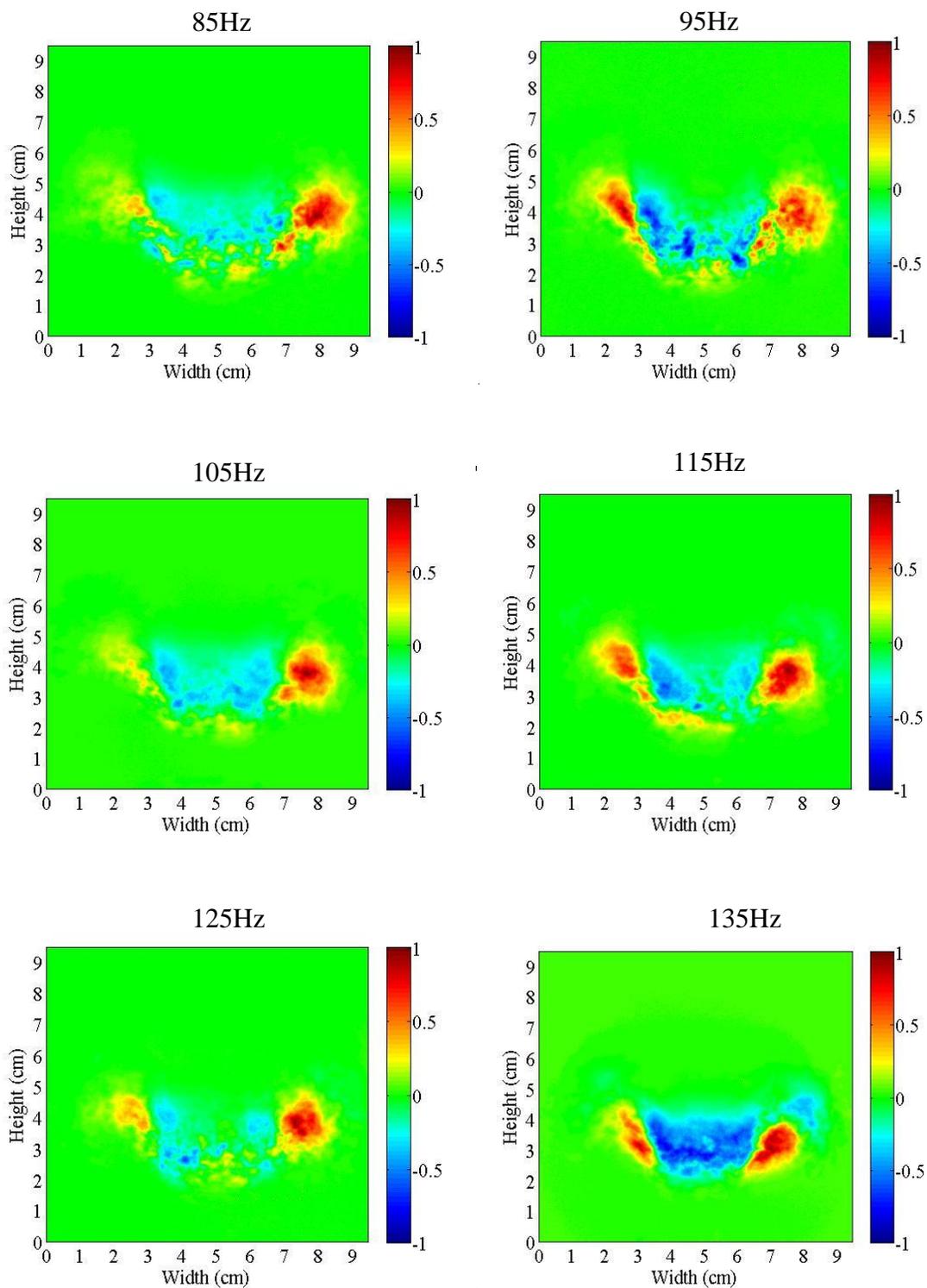
Figure 5.6 Rayleigh Maps for 85, 95, 105, 115, 125 and 135 Hz
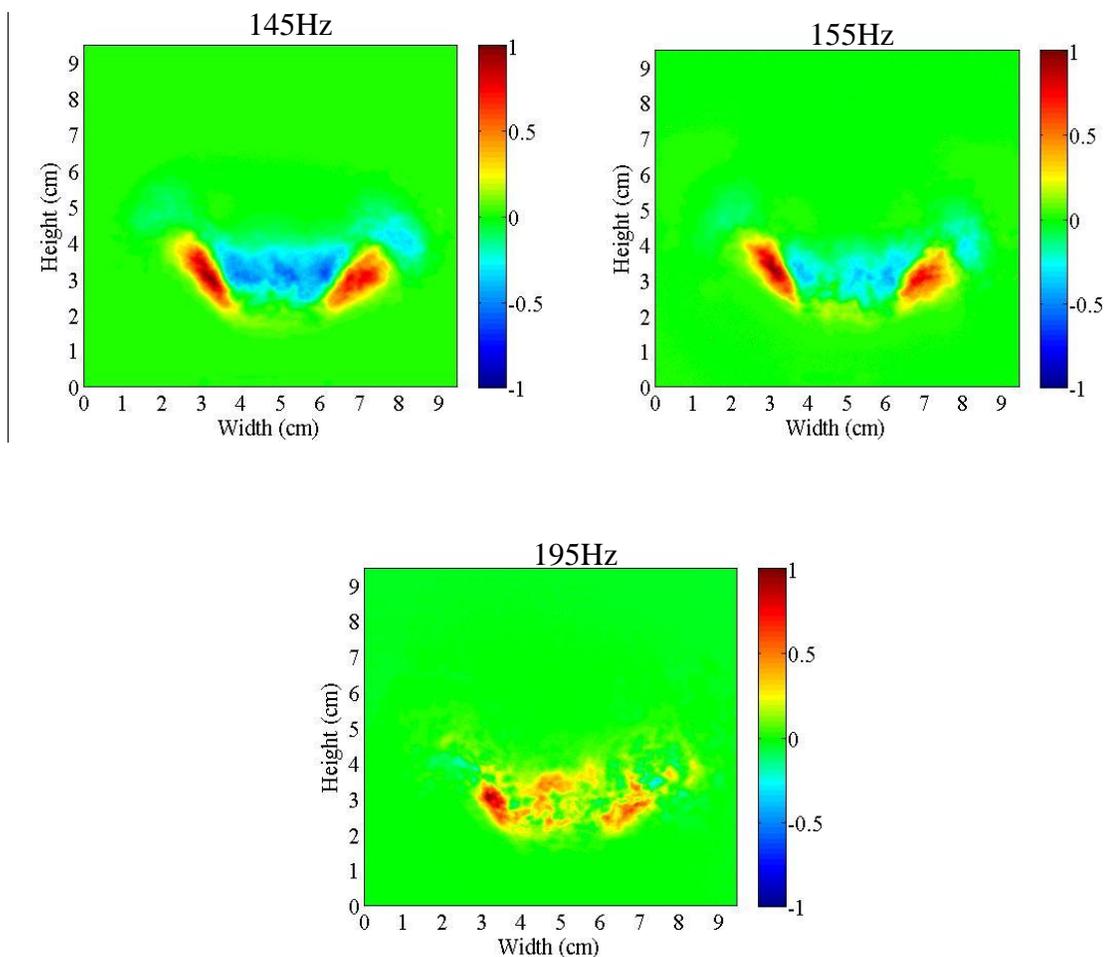
Figure 5.7 Rayleigh Maps for 145, 155 and 195 Hz

All the Rayleigh index maps evaluated are normalized by their maximum values. The positive regions in Rayleigh maps are where the heat release and pressure oscillation are coupled and instability tends to grow and the negative regions are where the heat release and pressure oscillations are out of phase and the instability is inhibited. The results for 45 Hz case show a strong coupling at the flame base as does that of the 55 Hz case. The pressure fluctuations at these low frequencies are inducing bulk velocity

fluctuation resulting in flame base coupling. At these two forcing conditions, the flame base bouncing was observed.

For cases 65 Hz through 105 Hz, the frequency of excitation is close to one of the natural modes of the chamber (~95 Hz), some coherent structures are initiating but are not clear in comparison with that of the 135 Hz and 145 Hz cases. It seems a transition occurs between two modes of coupling, one which is associated with the flame base coupling and the other associated with a shear-layer triggered coupling mechanism.

From 115 – 155Hz, the acoustic driving induces fluctuations of velocity near and at the burner exit resulting in shear-layer triggered coupling. These fluctuations trigger the developing shear- layer and the resulting shear layer vortex pattern causes variation in flame surface which results in unsteady heat release which then gives off pressure waves that close the feedback loop. The test case of 195Hz does not show any coherent coupling.

Huang (2008) saw similar trends in flame response to acoustic perturbation in a 2.54 cm diameter burner, shown in figures 5.7 and 5.8. For 55Hz, the observed acoustic coupling at the flame base is similar to that of the 3.81 burner. The range of frequencies that the shear-layer mode was observed by Huang was narrower than that reported here.

The widening of the range of frequencies which the shear layer is triggering the thermoacoustic coupling is a result of the 3.81 cm burner setup allowing acoustic energy to be pumped into the system at a broader range of frequencies compared to 2.54 cm burner.

The global Rayleigh might measure by summing the local Rayleigh values in the whole combustion zone. Results for all the forcing conditions show that the global Rayleigh value is close to zero. It indicates the combustion process is stable. Also the pressure inside the chamber does not grow with time. In addition the coherent structures don't appear without the excitation, so it could be deduced that the shear layer is convectively unstable for a sub-range of acoustic excitation frequencies.
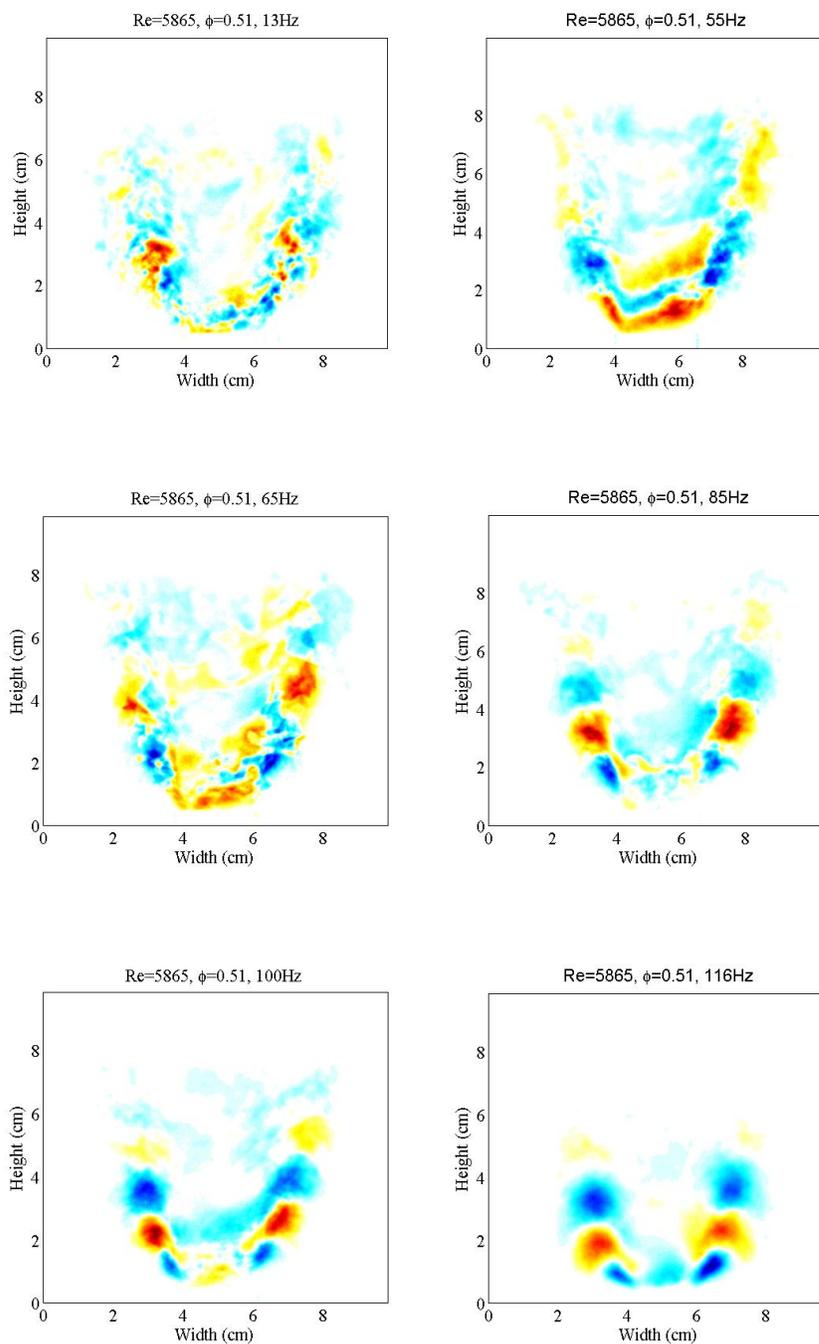
Figure 5.8 Rayleigh Maps in the 2.54 cm low swirl burner (13, 55, 65, 85, 100 and 116 Hz)

Source: Huang, 2008
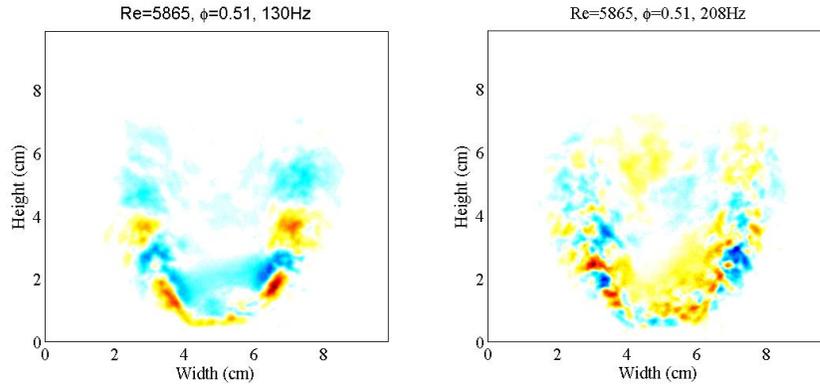
Figure 5.9 Rayleigh Maps in the 2.54 cm low swirl burner (130 and 208Hz)

Source: Huang, 2008

Interaction between Acoustic excitation and flame dynamics has been investigated before (Gutmark et al., 1989; Renard et al., 2000; Huang and Ratner, 2009) and it was found that frequency of vortex rollup can lock onto the frequency of acoustic fluctuations if the amplitude of the acoustic oscillations is large enough to trigger the shear layer and its frequency is close to the natural frequency of vortex shedding. Samaniego et al. (1993) observed this coupling for a propane flame in a side-dump combustor occurs at Strouhal number of the order of one. In 1999 Paschereit et al. reported *St=0.58* is the critical Strouhal number in a premixed swirl burner. Huang (2008) observed that the coupling between the acoustic field and the flame in a low swirl burner occur in the range from 0.27 to 0.87. In this work the St Number is calculated based on both burner diameter (St_D) and momentum thickness (St_θ).

$$St_\theta = \frac{f\theta}{U} \quad , \; St_D = \frac{fD}{U} \tag{5.2}$$

Where f is the frequency of excitation, U is the bulk velocity, D is the diameter of the burner and θ is the shear layer momentum thickness. To calculate the momentum thickness the flow-field measured by Littlejohn et al. (2007) at 10 m/s for low swirl burner and equation 5.3 are used.

$$\theta = \int\limits_{0}^{D/2} \frac{u(r)}{U}(1 - \frac{u(r)}{U})dr$$

(5.3)

Where r is the distance from the center of the burner and u is velocity. The calculated St Number is summarized in table 5.2.

Table 5.2 Summary of Strouhal numbers

	f(Hz)	45	55	65	75	85	95	105	115	125	135	145	155	195
Re=25231 (Φ=0.85)	St_D	0.17	0.21	0.25	0.29	0.32	0.36	0.40	0.44	0.48	0.51	0.55	0.59	0.74
	St_θ	.027	.034	.040	.046	.052	.057	.064	.070	.076	.082	.088	.095	.119

Birbaud et al. (2006) showed that acoustic forcing might induce three motions of a free-jet, a convective motion, an acoustic propagation zone, and a mixed zone of the first two modes which are governed by the St Number values. In this study it is observed that the acoustic and flame coupling occurs at St_D and St_θ less than one. And the large coherent structures are seen in the range of St_D =0.40 - 0.60 and St_θ=0.06-0.1. In compare to 2.54 cm burner, large scale vortical structures are constructed at lower St Number values, which suggest the jet mode effect in the 3.84 burner is stronger than the smaller burner.

5.1.4 Flame Response

The flame response to the acoustic forcing is measured as follow:

$$C_R = \frac{q'/\overline{q}}{p'/\overline{P}}$$

(5.4)

In figure 5.10 the logarithm of equation 5.4 multiplied by 20 is plotted versus exciting frequency. The magnitude in this figure is in decibels (dB). Flame response is almost identical, varying slightly with forcing frequency. At the natural modes frequencies the flame response is stronger than other frequencies. Comparing the flame response with the Rayleigh index maps, it may be deduced that the coherent structures in Rayleigh maps are related to the global response of the flame to the acoustic forcing.
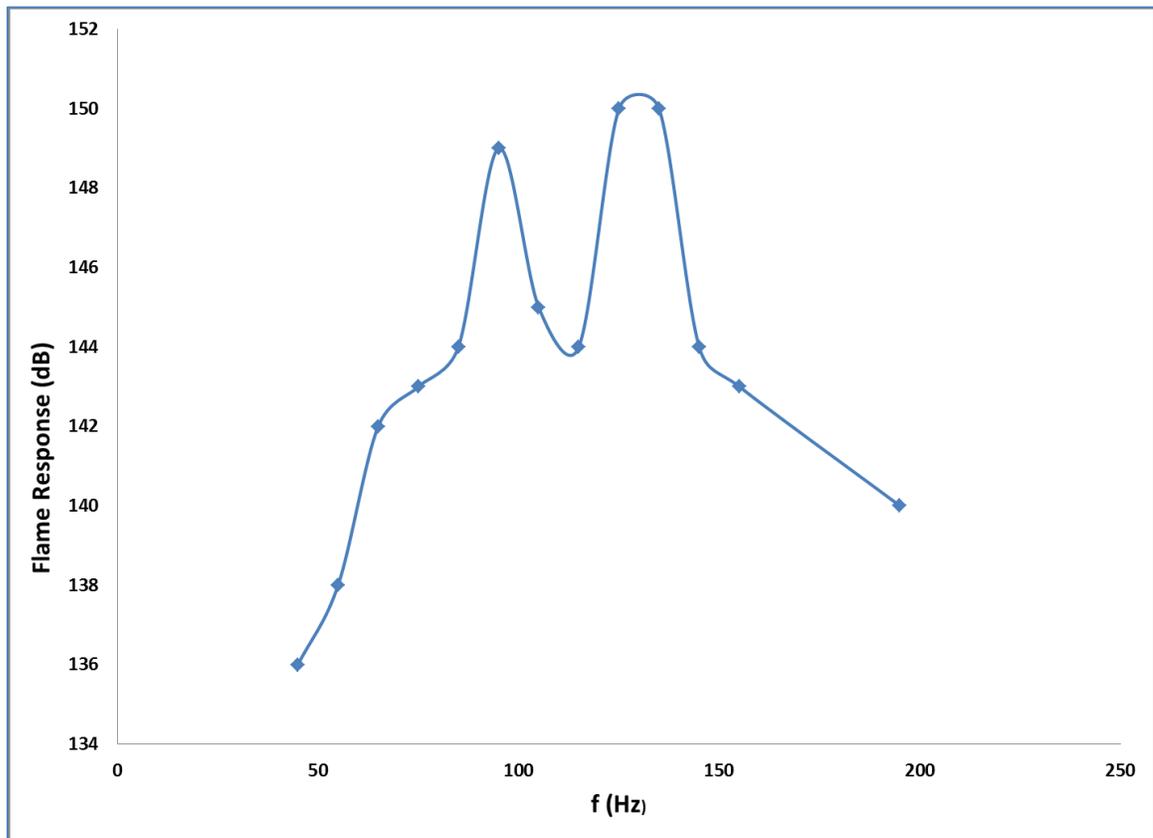
Figure 5.10 Magnitude of flame response to the acoustic forcing.

5.2 Effects of Acoustic Forcing on the Flame Structures

For all the forcing conditions introduced in previous sections the flame shape, flame surface curvature and flame surface density are calculated. The results show that acoustic forcing interacts with the flame surface and cause variation in the structure of the flame as well as the flame shape. The effect of frequency and amplitude of pressure forcing on the flame structures and shape are addressed in this section.

5.2.1 Flame Angle

For each of the forcing condition, the average of 900 OH images is calculated to study the effect of acoustic excitation on the flame shape. Figure 5.11 shows an example of average flame image for 85 Hz. The angle between the flame wing and the flame base as shown in the figure 5.11 is measured for each test condition and plotted in figure 5.12. Two distinct regions can be observed in 5.12 which may refer to the coupling modes introduced in previous section. At frequencies close to the natural mode of the chamber the flame is more compact, Θ is larger, and as frequency moves away from this natural chamber mode the flame widens.
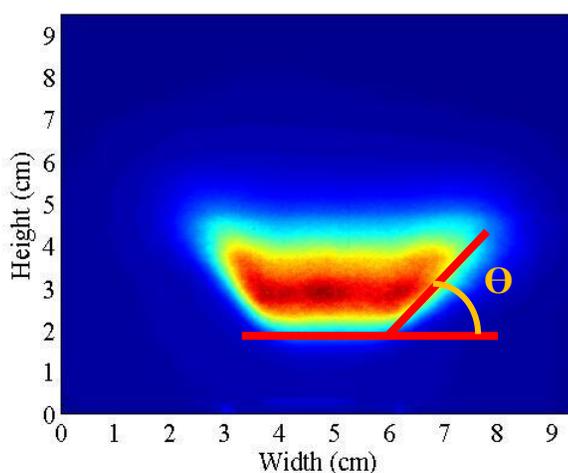
Figure 5.11 Averaged PLIF images of flame (P=1atm, φ=0.85, f=85 Hz).
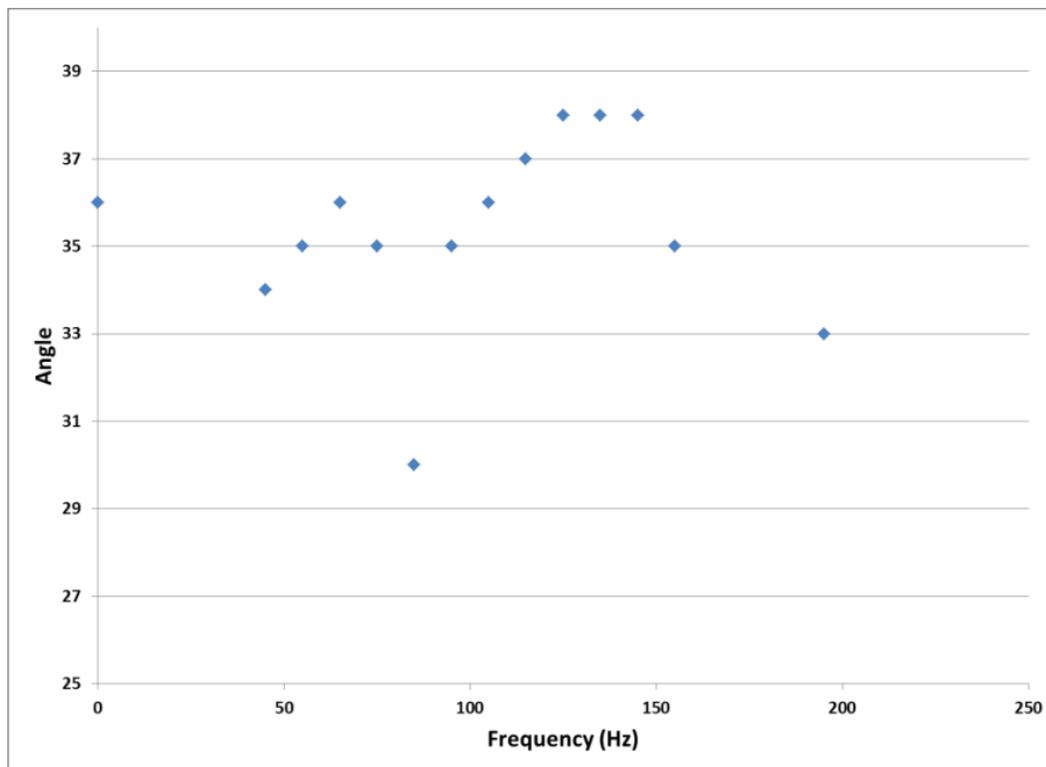
Figure 5.12 Flame angle of average PLIF images.

5.2.2 Effects of Acoustic Forcing on the Flame

Structures

2D flame surface curvature is measured using the procedure explained in chapter 4. For each case 300 images are used to construct the distribution of curvature. Figure 5.13 shows the results of flame surface curvature and figure 5.14 displays results only for selected frequencies of acoustic forcing: 0Hz, 45Hz, 95 Hz, and 135Hz.

These frequencies represent the three different modes of coupling observed in this study.   All of the cases, from 45Hz to 195Hz, the pressure fluctuations induced by forcing are observed to interact with the flame surface. As a result of this interaction the PDF of distribution of curvature is broader than the no excitation case.
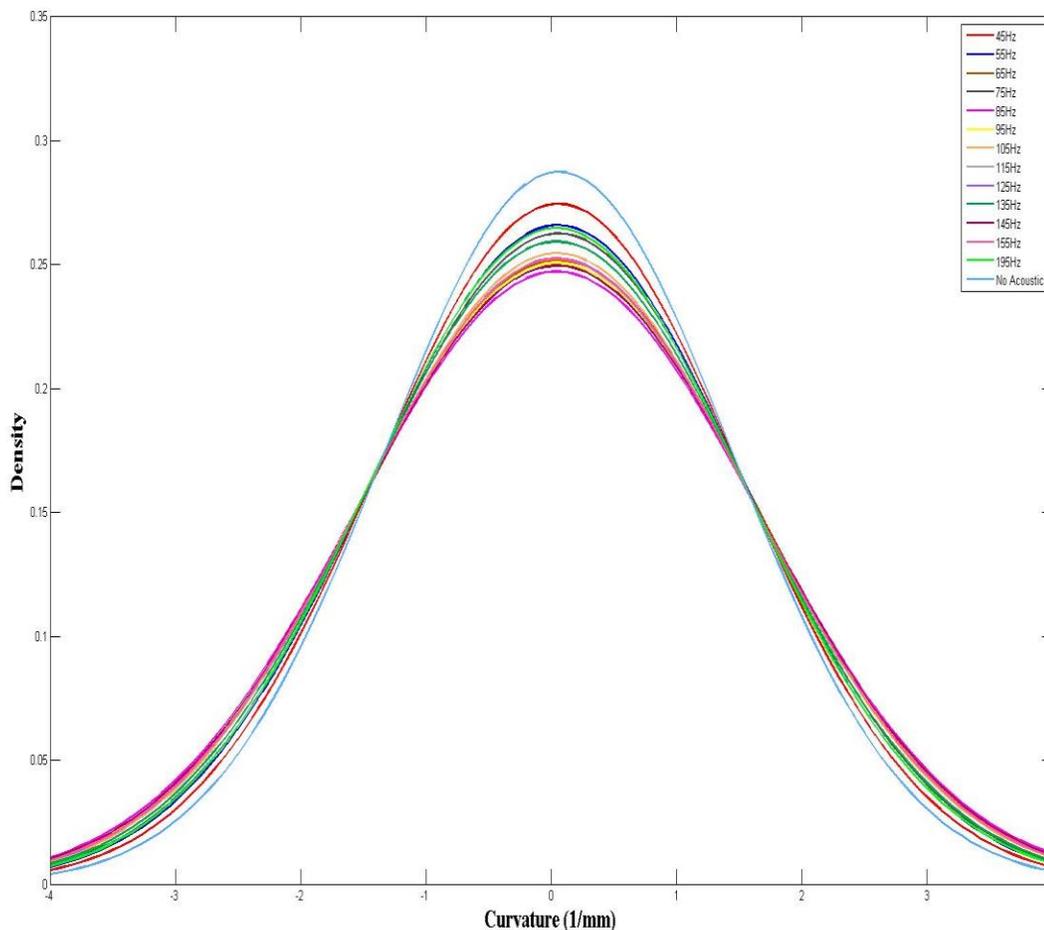
Figure 5.13 Flame surface curvature distribution.

The base mode coupling seems to wrinkle less than that of the shear-layer mode and transition mode which wrinkles most. In the base mode the flame base bouncing dissipate the turbulent fluctuations in the reactants flow and does not allow them to affect the flame wings and stretch the flame surface at the higher positions. However in the shear-layer mode coupling, the flame base motion is not sufficiently strong to dissipate the turbulent fluctuations and also the pressure wave interacts with the flame wings and causes the flame surface to be stretched more and as a result the flame surface wrinkles more.
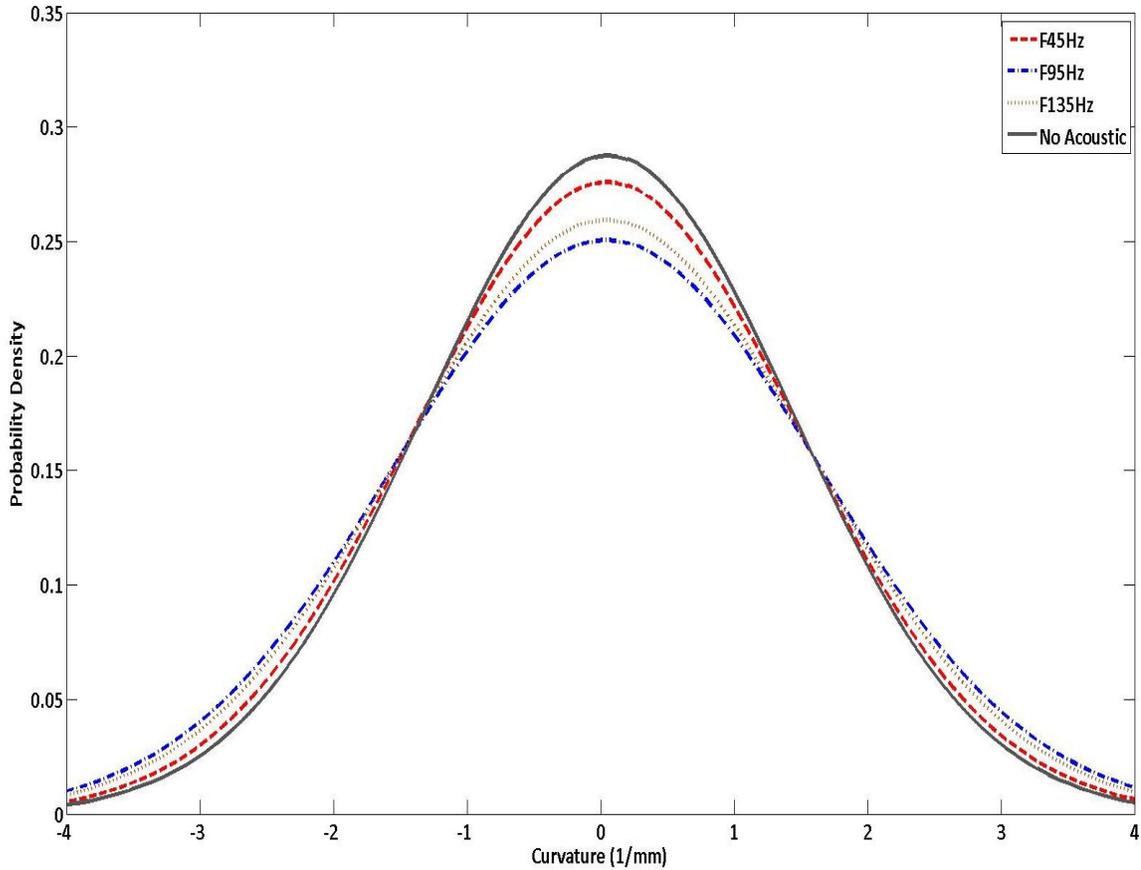
Figure 5.14 Flame surface curvature distribution for selected test conditions.

In table 5.3 the mean value of curvature, variance and mean absolute radius of curvature are calculated. The mean curvature for all the test cases is close to zero, however positive. The mean absolute radius of curvature decreases as the acoustic forcing is applied which shows the PDF of curvature is broadened. The lowest mean absolute radius of curvature occurs between 85 Hz through 145 Hz of pressure excitation, which relate to the shear-layer coupling mode. Shear-layer coupling seems to decrease the radius of curvature about 10-15%, however the base mode just decrease it 6% which is even less than the 195 Hz forcing case. The Rayleigh map of 195 Hz forcing presented in previous sections did not show any coherent coupling and only some random structures were observed.

Table 5.3 Mean, variance, and average absolute radius of flame front curvature

Frequency (Hz)	Mean	Variance	Avg. Abs. Radius Curv. (mm), $\bar{r}$
0	0.058569	2.00541	1.78
45	0.054873	2.11106	1.68
55	0.052709	2.24946	1.68
65	0.057683	2.50715	1.64
75	0.055583	2.30775	1.63
85	0.042564	2.60355	1.58
95	0.043953	2.53118	1.59
105	0.046455	2.45459	1.6
115	0.043006	2.49874	1.59
125	0.04577	2.49354	1.59
135	0.044096	2.36579	1.6
145	0.045506	2.55318	1.59
155	0.043684	2.4988	1.61
195	0.043919	2.27072	1.64

But this frequency decreases the radius more than the base mode frequencies. So it can be deduced that close to the natural modes of the combustor, the mean absolute radius of curvature become smaller than the other forcing frequencies. Also when base mode coupling occur in the system, it works like a Helmholtz resonator and damp the fluctuations and as a result the PDF of flame curvature distribution is narrower than the other forcing cases.

The flame surface density also shows similar trend. Figure 5.15 exhibits the flame surface density calculated for all the test cases. All the curves show a parabolic behavior as was observed before. Two distinct parabolas are observed, the top parabola is representative of the shear-layer mode and the bottom the base mode. The maximum FSD, plotted in figure 5.16, for cases 45Hz and 55Hz experience lower values than that of the other test cases. It seems this behavior is a result of the base mode is dissipating turbulent effects at the exit of the burner. During the test for these two frequencies flame bouncing was observed. These fluctuations at the flame base washes out small scale

turbulent structures this small scale eddies cannot reach the flame wings and interact with the flame surface. Because of this the maximum flame surface density for these cases is smaller than that of the no acoustic case. The flame surface density of the base mode is smaller than other cases.
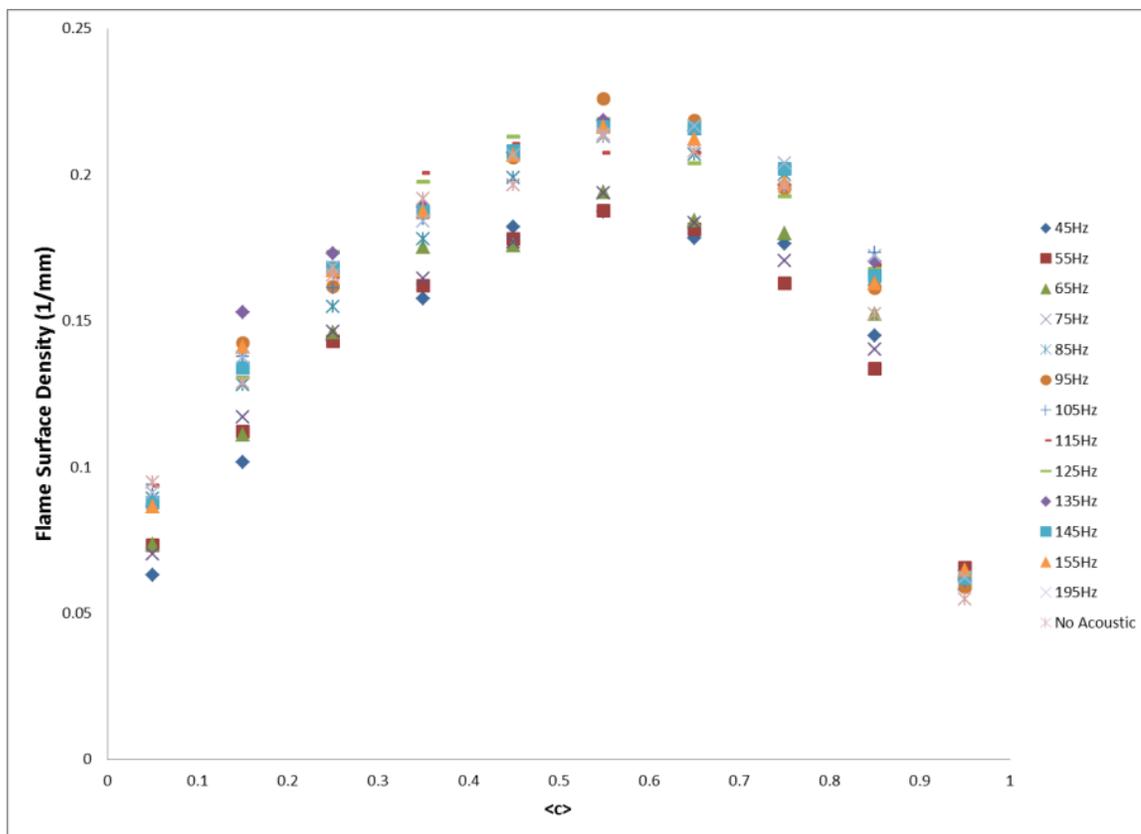
Figure 5.15 Flame surface density at various forcing frequencies

The maximum flame surface density of the shear-layer mode seems to be 15% greater than that of the base mode. At these frequencies the base fluctuation was not as strong as the 45 and 55 Hz cases and cannot dissipate the turbulent structures exiting the burner very well this structure can be convected downstream and interact with the flame surface.
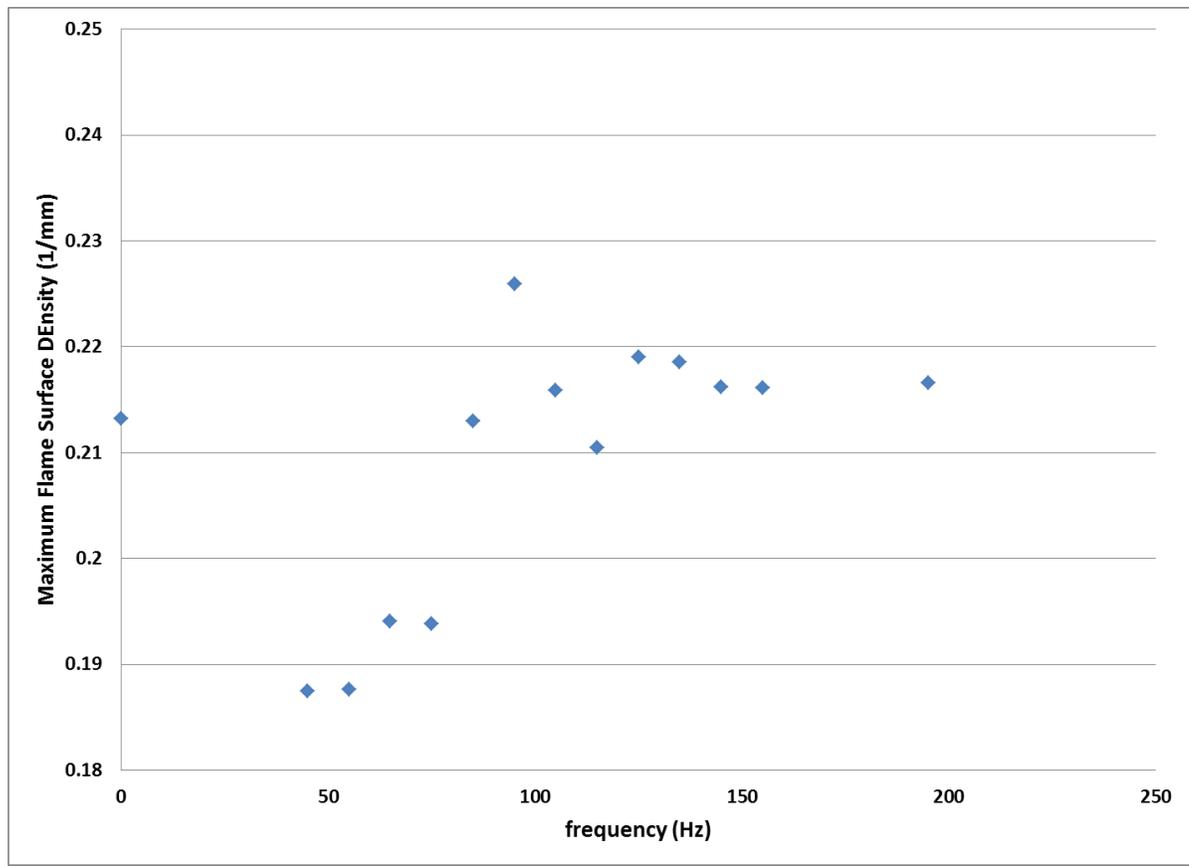
Figure 5.16 Maximum flame surface density at various forcing frequencies

5.3 Effects of the amplitude of Acoustic Forcing on the

Flame

The amplitudes of pressure forcing for all the Rayleigh maps constructed in previous sections, were kept between 0.05 to 0.2 % of the mean pressure (atmospheric pressure). When the amplitude of the pressure waves is less than 0.05% of the mean pressure, it seems the driving amplitude is not high enough to excite coupling with the heat release oscillations to form toroidal structures. In 2.54 cm burner this critical amplitude was observed to be 0.034% of mean pressure. It shows that in the larger burners with higher flow rates of reactants, the critical amplitude of forcing becomes

larger and the flame will be less sensitive to the acoustic perturbations. Figure 5.17 compares the Rayleigh map at 95Hz for two different forcing amplitudes.
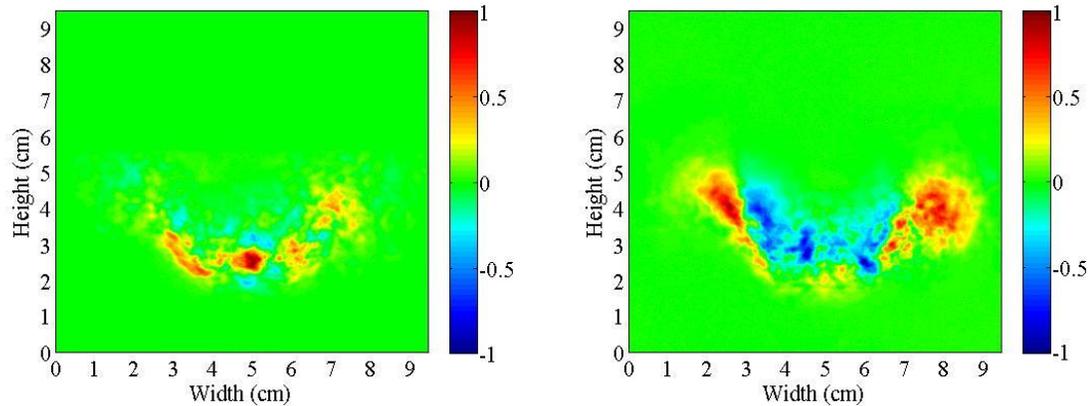
Figure 5.17 Rayleigh index map at 95 Hz, Left: 0.04% of mean pressure, Right: 0.11% of mean pressure

Low amplitude forcing Rayleigh map (left) shows random coupling and no coherent structure can be seen. However in the other map (right) the coherent toroidal structures are easily can be recognized. At these two regions of forcing the overall flame shape does not change significantly and these acoustic triggering just the flame surface wrinkling and the flame wings angle.

For amplitudes higher than 0.2% of mean pressures, the flame response to the acoustic forcing with the frequencies far from the natural modes does not change. Also the flame shape doesn't vary with increasing the amplitude, however at the natural modes of the combustor it seems the amplitude alter the flame shape significantly and it becomes more like an "M" shape flame rather than a bowl shape flame.
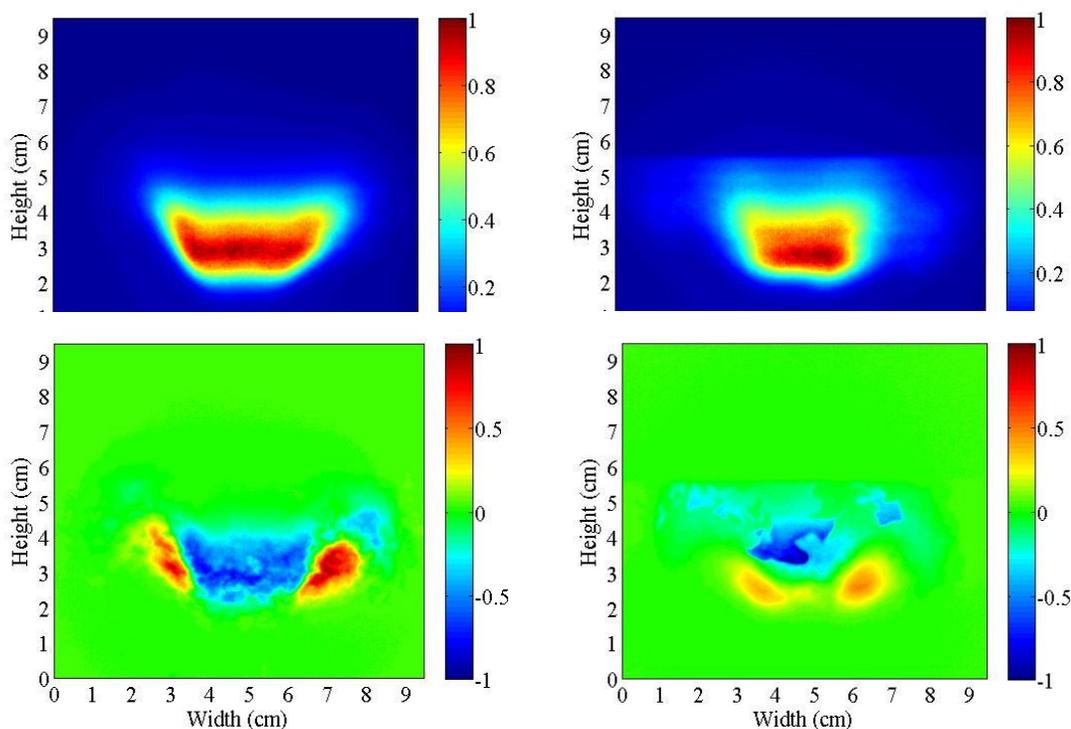
Figure 5.18 OH averaged image of Flame and Rayleigh index map at 135 Hz, Left: Pressure amplitude is 0.09 % of the mean pressure, Right: Pressure amplitude is 0.24% of the mean pressure

Figure 5.18 shows the averaged OH image of methane flame at 135Hz for two different amplitudes of acoustic forcing and also the Rayleigh maps of each case. The flame shape is changed due to the strength of acoustic forcing and the flame base become smaller than the normal shape. Also the shear-layer coupling seems to be weaker at higher amplitude and coherent toroidal structures moved toward the flame base. However in 2.54 cm burner this effect wasn't observed. Increasing the amplitude of pressure excitations, even at natural modes of the combustor didn't change the flame shape significantly. Raising the amplitude above 0.04% also had little effect on the flow

structures, although large amplitude pressure forcing (0.7%) would induce flash-back or blowout.

5.4 Conclusion

OH PLIF data was used to calculate Rayleigh index maps and to construct averaged OH PLIF intensity fields at different acoustic excitation frequencies (45-155, and 195Hz). Based on the Rayleigh index maps, two different modes of coupling between heat release and pressure fluctuation were observed: the first mode, which occurs at 44Hz and 55Hz, shows coupling to the flame base due to the effect of pressure fluctuation on the bulk velocity while the second mode observed was seen close to the natural modes of the chamber. In the first mode, it seems the flame becomes wider and the flame base couples with the acoustic of the chamber. This coupling caused the flame base to bounce on the top of burner exit and dissipate the turbulent fluctuations in the reactants flow field coming from the premixer. This damping mechanism slightly alters the flame shape and structures.

In the second mode, the acoustic driving induces fluctuations of velocity near and at the burner exit. These fluctuations trigger the developing shear layer and the resulting shear layer vortex pattern causes variation in flame surface which results in unsteady heat release. This unsteady heat release then couples with the acoustics that closes the feedback loop. The results also show the flame shape is more compact for this shear layer vortex mode. The flame surface density and flame curvature results support the observation of two distinct coupling modes. The shear-layer coupling mode seems to increase the flame surface density and curvature compared to the base mode.

The coupling between heat release and acoustic fluctuation seems to be a function of acoustic driving amplitude as well. If P_{rms} is less than 0.05 % of mean pressure the fluctuations are not sufficiently strong enough to trigger instability in the 3.81 cm low swirl burner. Between 0.05 to 0.2 % of mean pressure, the results are as described above

in the 5.1.3. In data collected above 0.2% mean pressure forcing, there was a significant change in flame topology at frequencies close to the natural modes of the combustor and it becomes more like an "M" shape flame. However, far from the natural modes (like 45 and 55 Hz) the flame shape and the coupling mechanism do not change by increasing the amplitude.

CHAPTER 6

METHANE-HYDROGEN FLAME AND ACOUSTIC INTERACTION

In this chapter hydrogen-methane flame interaction with imposed acoustic pressure fluctuation in the range of 45 Hz to 195 Hz are studied, and compared with the methane flame response to the acoustic forcing. The results exhibit two different modes of coupling between heat release and acoustic forcing similar to the pure methane flame coupling, which suggests that the driving mechanism of instability for pure methane flame and also hydrogen-methane mixture flame are identical.

6.1 Rayleigh Index Maps

6.1.1 Pressure Signal and Flame Images

In this section the acoustic behavior of two different fuels (100% methane fuel at φ=0.85 and a mixture of 60% methane and 40% hydrogen fuel at φ=0.65) is studied. Bulk velocity for both fuels is maintained at 10 m/s. For the first step, the pressure signal of each flame was recorded in a period of 100 s and then was analyzed and compared. Figure 1 shows the pressure power spectrum density for each fuel case. The results show that the noise level in the mixture flame is lower than the pure methane flame. The root mean square of pressure fluctuations for the mixture flame is 0.023 % of mean pressure, however for the pure methane P_{rms} is 0.028% of mean pressure. Part of the pressure fluctuations in LSB is coming from the breaking down of vortical structures generated by to velocity perturbations at the flame front. But adding hydrogen to the fuel increases the flame resistance to the stretch (Gauducheau et al., 1998); also mass diffusion will become dominant in compare to the thermal diffusion (adding hydrogen to the methane causes a decrease in the Le number), and as a result the vortices formed at the flame surface become weaker and smaller and their break down generates less pressure perturbations in compare to the pure methane fuel.
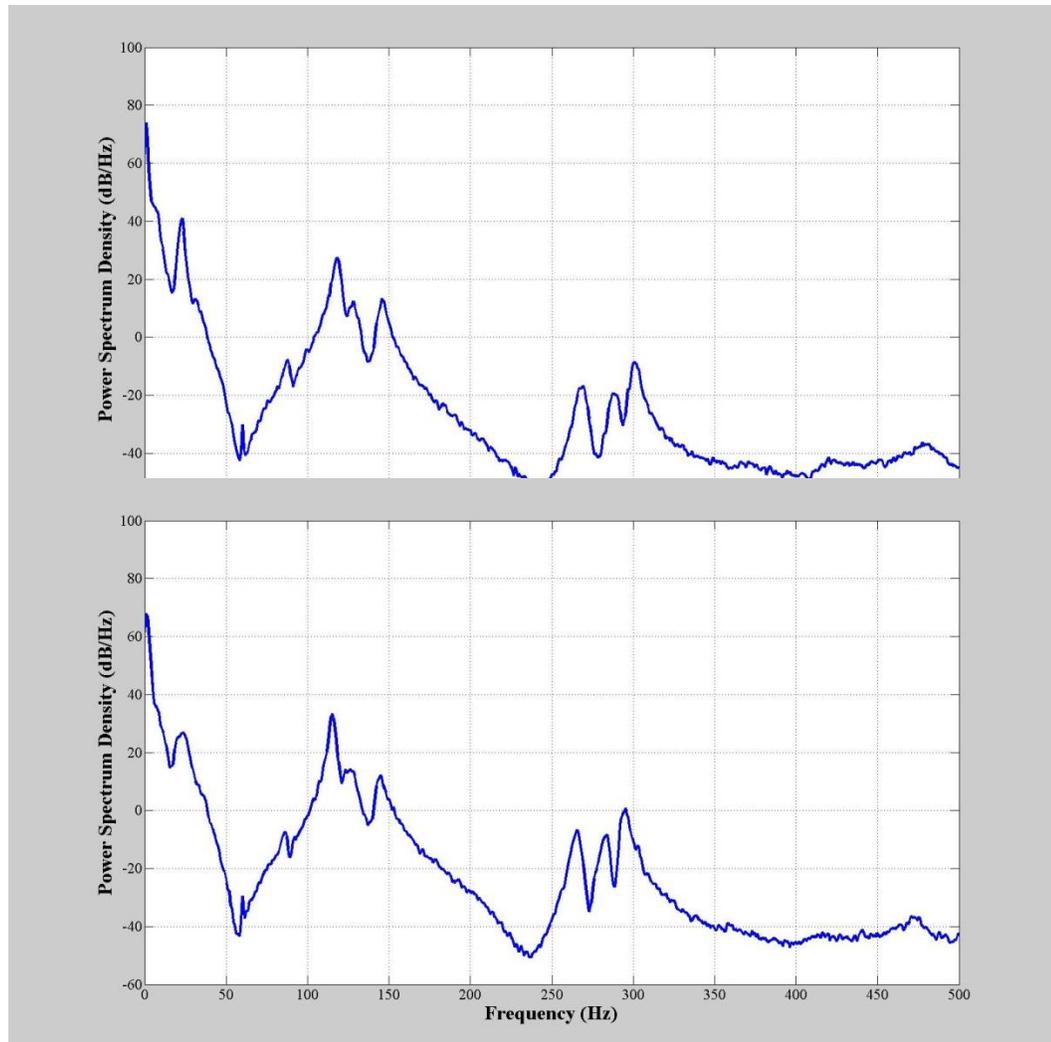
Figure 6.1 Power spectrum density of pressure signal for no forcing cases, Top: 100% methane at 10 m/s and φ=0.85, Bottom: 60% methane and 40% hydrogen at 10 m/s and φ=0.65

In figurer 6.1, pressure signal in both graphs demonstrates similar trends. The only difference is the slight shift of natural modes towards left while methane fuel is enriched by hydrogen. However, if the tests were run at the same equivalence ratios, it was expected to observe the natural modes for the mixture fuel shift positively, but

because the difference between equivalence ratios, the frequency of dominant modes are identical.
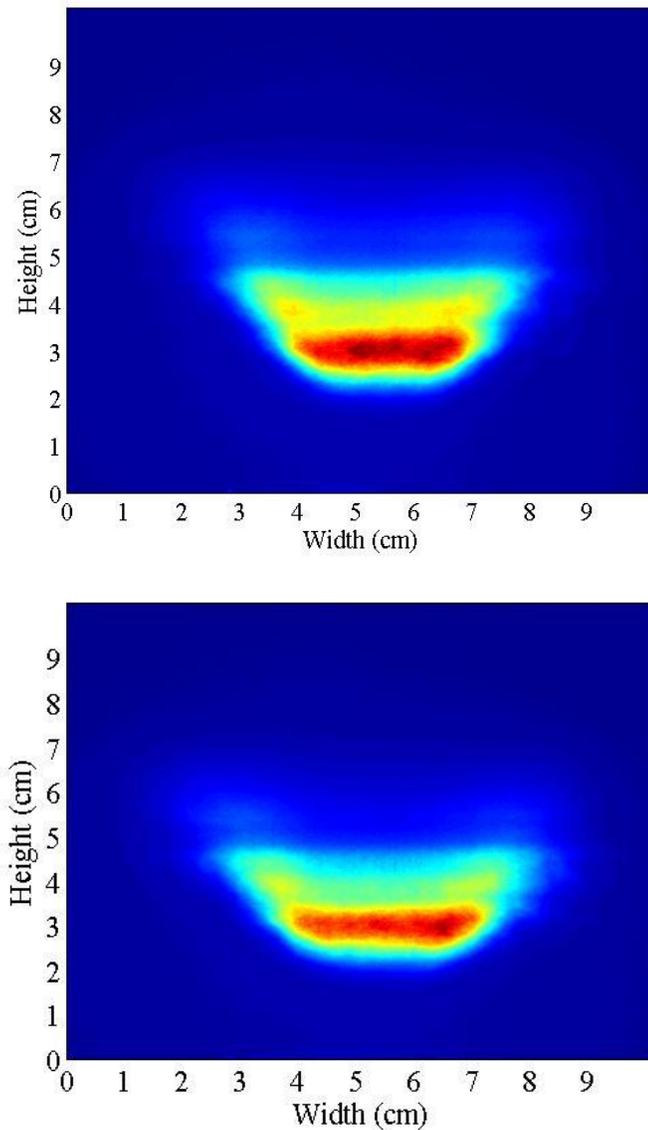
Figure 6.2 Averaged PLIF images of flame, Top: 100% methane at 10 m/s and φ=0.85, Bottom: 60% methane and 40% hydrogen at 10 m/s and φ=0.65

For each fuel flame, 300 OH PLIF images are captured. Figure 6.2 shows the average of flame images for methane and the hydrogen-methane flames. It can be observed through this figure, that the mixture flame is wider than the pure methane flame. Also the mixture flame base is positioned 0.8-1 mm closer to the burner exit than the methane flame base. As hydrogen is added to the fuel, the turbulent flame speed is increased as a result of high reactivity of hydrogen and to match this slight increase in flame velocity with the reactants velocity the flame moves closer to the burner exit and also becomes wider. Without any precise measurement and just by watching the flame, it seems the hydrogen-methane flame length becomes shorter than the methane flame, which is in agreement with Halter and coworkers' observation (2007). They reported that adding hydrogen to a premixed flam causes flame shortening.

If both set of tests were conducted at the same equivalence ratios of 0.85, it would be expected that the methane-hydrogen flame becomes wider and the flame base stabilized at a position closer to the burner exit, because more hydrogen would be introduced to the flame and the flame speed would increase.

6.1.2 Rayleigh Index Map: Results and Discussion

Similar to chapter 5, the flame response to acoustic forcing for both methane-hydrogen and methane flames for selected frequencies between 45 Hz to 195 Hz was measured to construct the Rayleigh index maps. The amplitude of acoustic forcing for both flames was maintained in the same range. For all the acoustic forcing cases, the coupling mechanics which triggers the amplification or damping seems to be identical for both fuels, just for some forcing frequencies slight changes in the structure of coupled region is observed for the mixture flame which is the result of change in the heat release pattern and flame speed. Here only the results for the main natural modes of LSB which are 125 Hz and 135 Hz are presented. Figures 6.3 and 6.4 show the Rayleigh index maps for 125 Hz and 135 Hz excitations.

For 125 Hz acoustic forcing case, the amplitude of pressure fluctuations inside the chamber was maintained 0.12% of mean presser (atmospheric pressure) for both fuels. Figure 6.3 shows the Rayleigh index maps. The acoustic coupling for methane flame is more coherent than the mixture fuel. However, for the mixture case the flame base is also positively coupled with pressure fluctuations. This difference might be due to the effect of hydrogen on heat release pattern. Adding hydrogen increases the reactivity of the reactants and turbulent flame speed (Halter et al., 2007); therefore weaker heat release perturbations will be induced into the system by acoustic forcing. So the coupling between acoustic perturbations and unsteady heat release for methane-hydrogen mixture are not as clear as methane flame.

However, Yilmaz et al. (2009) observed a contradictory behavior in the 2.53 cm LSB. He mentioned by increasing hydrogen volumetric flow rate, more coherent structures develop in the shear layer. The difference between these two observations is a result of difference between the flame speeds and turbulent intensities. In his experiments because of small bulk velocity the hydrogen flow rate was so small and it could not alter the heat release pattern significantly. Also at natural modes of the 2.53 cm burner, the change in the structure of coupled regions by increasing the hydrogen ratio from 7% to 30% is minor.

For 135 Hz forcing case, the amplitude of pressure fluctuations is for methane flame is 0.1% of mean pressure and for the methane-hydrogen flame it is 0.08% of mean pressure. The Rayleigh index maps for both flames show similar coupling structures and the acoustic driving induces fluctuations of velocity near and at the burner exit resulting in shear-layer triggered coupling. These fluctuations trigger the developing shear- layer and the resulting shear layer vortex pattern causes variation in flame surface which results in unsteady heat release which then gives off pressure waves that close the feedback loop.
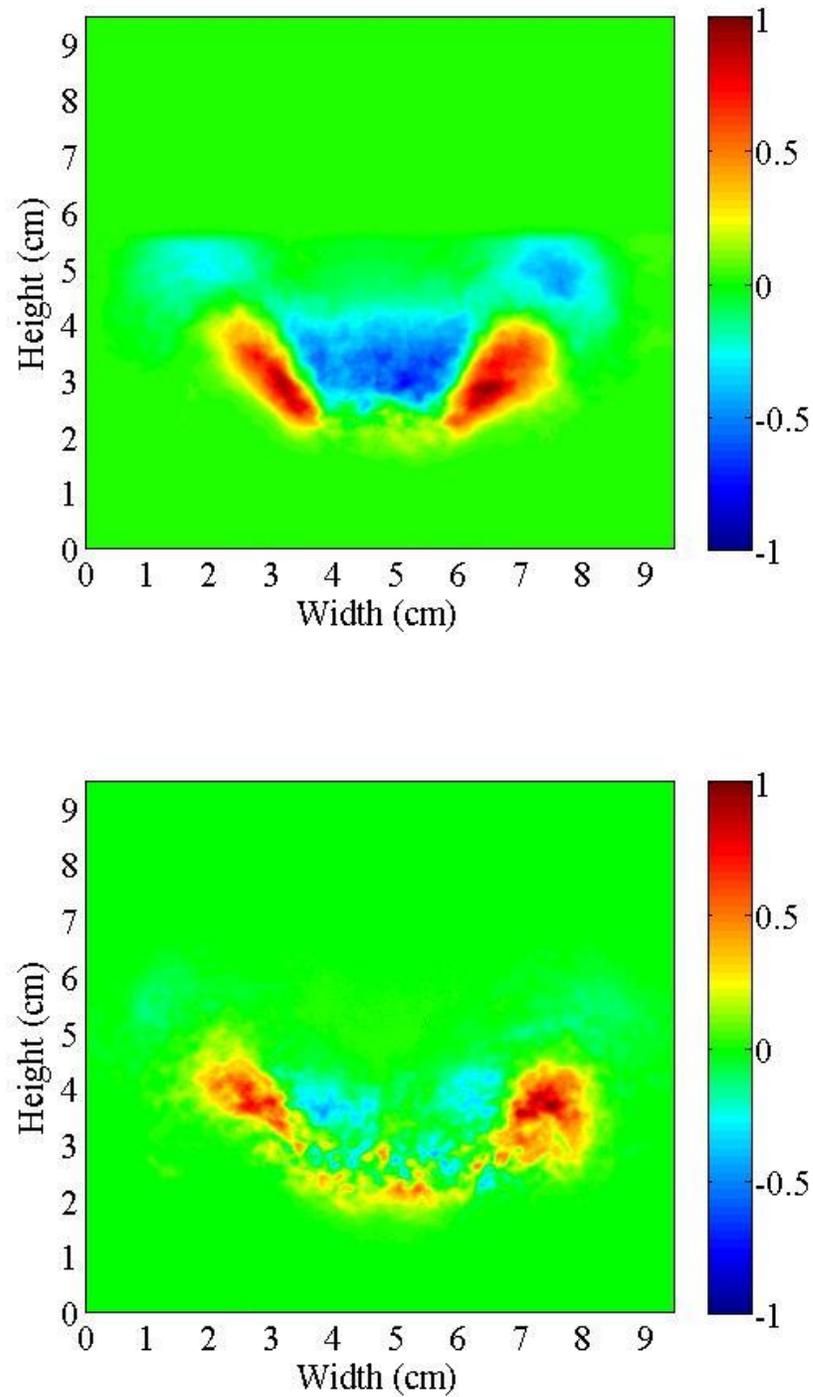
Figure 6.3 Rayleigh Maps in the low swirl burner at 125 Hz, Top: 100% methane at 10 m/s and φ=0.85 (P_rms=0.12% P_mean), Bottom: 60% methane and 40% hydrogen at 10 m/s and φ=0.65 (P_rms=0.12% P_mean)
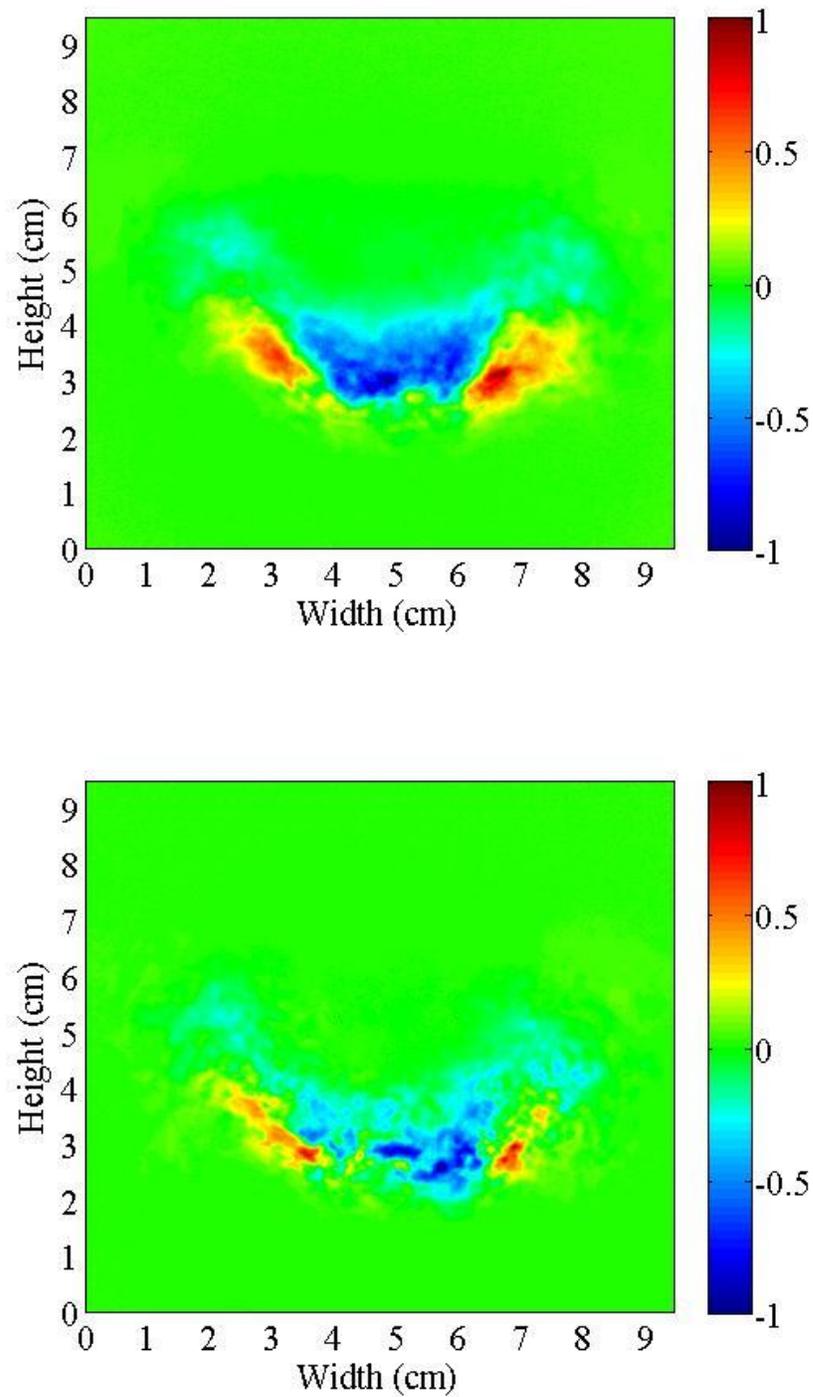
Figure 6.4 Rayleigh Maps in the low swirl burner at 135 Hz, Top: 100% methane at 10 m/s and φ=0.85 (P_{rms}=0.1% P_{mean}), Bottom: 60% methane and 40% hydrogen at 10 m/s and φ=0.65 (P_{rms}=0.08% P_{mean})

However adding hydrogen to the methane similar to the 125 Hz case, results in less coherent couplings, and the region of positive coupling becomes smaller compared to the methane case. One of the reasons could be the negative shift of dominant acoustic modes of hydrogen-methane flame in compare to the pure methane flame. So 135 Hz for the mixture flame is not the peak of power spectrum density graph. The other reason for this phenomenon is similar to what was explained previously for 125 Hz forcing. In all the tests the flame shape did not change noticeably, just the mixture fuel flames are wider, shorter and the flame base is closer to the burner exit similar to the unforced hydrogen-methane flame.

6.2 Hydrogen Flame

In this chapter the pure hydrogen flame is qualitatively studied and also compared with methane flame. Figure 6.5 shows a comparison between methane and hydrogen flames. For both cases the reactants bulk velocity is maintained at 15 m/s. The equivalence ratio of hydrogen flame is 0.3 and for methane flame $\varphi = 0.8$. Equivalence ratios are selected close to the blow out limits. For methane flame the blow out data is reported in chapter 4, and for hydrogen flame blow out limits for only two bulk velocities at atmospheric conditions are measures. At 15 m/s and 20 m/s, blow out occur at 0.275.

It can be observed from instantaneous images that the flame thickened for hydrogen flame is thinner than methane flame and OH radicals are distributed in smaller areas across the flame front in hydrogen flame. The flame surface is wrinkled more for hydrogen fuel and also the flame size is smaller than the methane flame. Moreover the hydrogen flame stabilizes closer to the burner exit. The difference between the methane and hydrogen flames behavior and shape is because hydrogen is a more reactive fuel and its laminar and turbulent flame speeds are higher than methane flame. Also in hydrogen combustion, mass diffusion is dominant in compare to heat diffusion, while in methane combustion mass and heat diffusion are balanced.
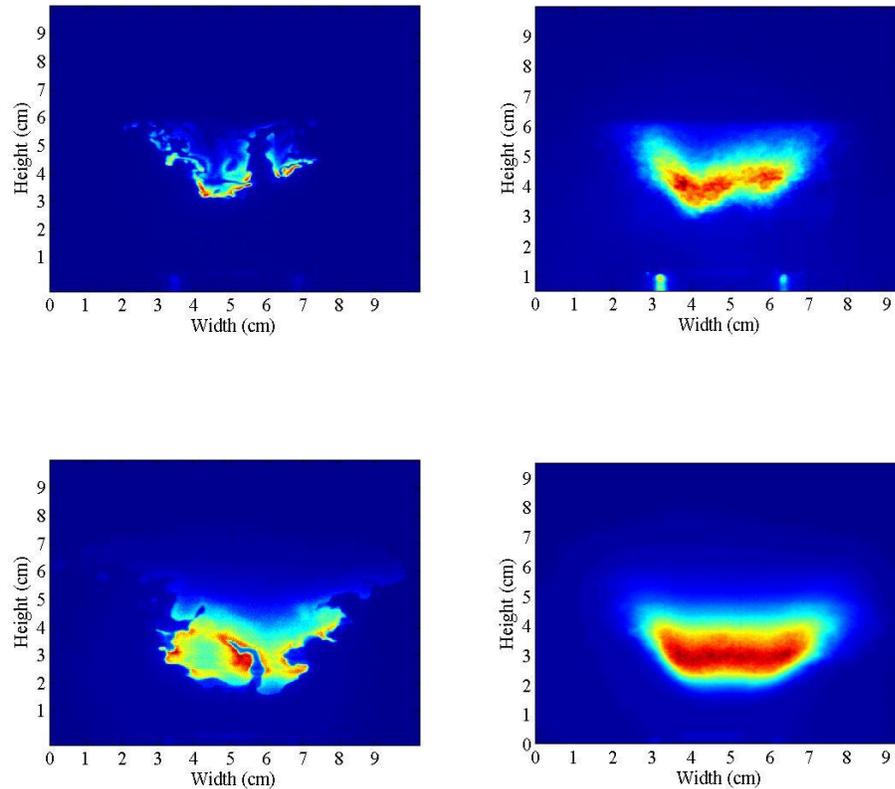
Figure 6.5 Top: Hydrogen flame at 15 m/s and φ=0.3 left: instantaneous image, right: average image, Bottom: methane flame at 15 m/s and φ=0.8, left: instantaneous image, right: average image

6.3 Conclusion

Similar to chapter 5, OH PLIF data was used to calculate Rayleigh index maps and to construct averaged OH PLIF intensity fields at different acoustic excitation frequencies for hydrogen-methane fuel. The results were compared to pure methane fuel case. It seems the coupling mechanisms of pressure oscillations and unsteady heat release for both fuels is the same. The only difference between the two fuels tested in this study is that for the mixture flame, vortical structures are less coherent and the flame size is smaller and wider. Also the flame is stabilizes closer to the burner exit compared to the pure methane flame. Adding hydrogen increases the reactivity of the fuel and turbulent

flame speed; therefore weaker heat release perturbations will be induced into the system by acoustic forcing. So the coupling between acoustic perturbations and unsteady heat release for methane-hydrogen mixture are not as clear as methane flame.

Also, a qualitative comparison between hydrogen and methane flame is done in this chapter which shows hydrogen flame size is smaller than the methane flame.

CHAPTER 7

CONCLUSIONS AND FUTURE WORKS

In this thesis, first the stability maps under different conditions are measured. Also the flame structures are obtained and effects of pressure and hydrogen enrichment of the fuel on flame surface curvature and density were investigated using OH PLIF images. It is found that hydrogen enrichment of methane fuel along with an increase in the pressure causes the blow-off limits to occur at a lower equivalence ratio, broadening the range of stability. The 2D flame front curvature measurements show increased wrinkling of the flame front at higher pressures and ratios of hydrogen. Interactions of the turbulent small scales with the flame surface, a decrease in Lewis number, and an increase in the local and overall burning rates of fuel due to the faster reaction rate of hydrogen all seem to contribute to the increase in the flame area and flame front wrinkling. Similarly, as the ratio of hydrogen increases, mass diffusion becomes the dominant term in the transport equation as a result of the reduction in Lewis number, thereby wrinkling the flame surface even more. Also the flame surface density increases as a result of increased wrinkling of the flame surface when hydrogen is added or the pressure is raised. It appears that hydrogen has a stronger effect on flame wrinkling at elevated pressures (this effect is reduced at atmospheric pressures). The flame surface density ($\sum$) vs. mean progress variable ($<c>$) graph shows a parabolic behavior which has been observed by other researchers. Shifting of the maximum flame surface density at high pressures towards the products of combustion due to convection is also observed, along with its rapid destruction.

In these experiments, acoustic perturbations are imposed on a low swirl stabilized methane-air flame using loudspeakers. The flame response is examined and quantified with OH planar laser induced fluorescence. Rayleigh index maps of the flame are computed for each frequency and operating condition. Based on the Rayleigh index

maps, two different modes of coupling between heat release and pressure fluctuation were observed: the first mode, which occurs at 44Hz and 55Hz, shows coupling to the flame base due to the effect of pressure fluctuation on the bulk velocity while the second mode observed was seen close to the natural modes of the chamber. In the first mode, it seems the flame becomes wider and the flame base couples with the acoustic of the chamber. This coupling caused the flame base to bounce on the top of burner exit and dissipate the turbulent fluctuations in the reactants flow field coming from the premixer. This damping mechanism slightly alters the flame shape and structures.

In the second mode, the acoustic driving induces fluctuations of velocity near and at the burner exit. These fluctuations trigger the developing shear layer and the resulting shear layer vortex pattern causes variation in flame surface which results in unsteady heat release. This unsteady heat release then couples with the acoustics that closes the feedback loop. The results also show the flame shape is more compact for this shear layer vortex mode. The flame surface density and flame curvature results support the observation of two distinct coupling modes. The shear-layer coupling mode seems to increase the flame surface density and curvature compared to the base mode.

The coupling between heat release and acoustic fluctuation seems to be a function of acoustic driving amplitude as well. If P_{rms} is less than 0.05 % of mean pressure the fluctuations are not sufficiently strong enough to trigger instability in the 3.81 cm low swirl burner. Between 0.05 to 0.2 % of mean pressure, the results are as described above in the 5.1.3. In data collected above 0.2% mean pressure forcing, there was a significant change in flame topology at frequencies close to the natural modes of the combustor and it becomes more like an "M" shape flame. However, far from the natural modes (like 45 and 55 Hz) the flame shape and the coupling mechanism do not change by increasing the amplitude.

Also, the thermoacoustic coupling mechanism for two fuels, pure methane and a mixture of 60% methane and 40% hydrogen are compared. The results show that the

triggering mechanism is similar for both fuels, and the only difference is that the acoustic coupling for methane flame is more coherent than the mixture fuel. Adding hydrogen increases the reactivity of the reactants and turbulent flame speed; therefore weaker heat release perturbations will be induced into the system by acoustic forcing. So the coupling between acoustic perturbations and unsteady heat release for methane-hydrogen mixture are not as clear as methane flame. Adding hydrogen increases the reactivity of the reactants and turbulent flame speed; therefore weaker heat release perturbations will be induced into the system by acoustic forcing. So the coupling between acoustic perturbations and unsteady heat release for methane-hydrogen mixture are not as clear as methane flame.

7.1 Future Works

For future works, PIV measurements of velocity fluctuations for methane and hydrogen-methane flames under acoustic forcing are recommended. Also Rayleigh index maps should be constructed in a wider range of frequencies and amplitudes. Testing the effect of amplitude in the range of 1-10 % of mean pressure could be useful. Also, repeating these tests at higher pressures is helpful to investigate the effect of mean pressure on the coupling mechanism.

Hydrogen combustion is another interesting research topic which could be developed in the combustion lab. Studying the flame structures variations as a function of operating conditions like pressure, bulk velocity and equivalence ratio and making a data base is another recommendation for future works on LSB.

REFERENCES

Ainsworth, R. W., Thorpe, S. J., and Manners, R. J., "A new approach to flow-field Measurement-A view of Doppler global velocimetry techniques" *International Journal of Heat and Fluid Flow*, *Volume 18, Issue 1*, *February 1997*, *Pages 116-130*

Allen., M.G., Mcmanus, K.R., Sonnenfroh, D.M., and Paul, P.H., "Planar Laser-Induced-Fluorescence imaging measurements of OH and Hydrocarbon fuel fragments in High-Pressure Spray-Flame combustion," *Applied Optics*, Vol. 34, No. 27, 1995, pp. 6287-6300

Anderson, J.D., Computational Fluid Dynamics, McGrawllHill, 1995

Balachandran, R., Ayoola, B.O., Kaminski, C.F., Dowling,A.P., "Experimental investigation of the nonlinear response of turbulent premixed flames to imposed inlet velocity oscillations," *Combustion and Flame*, Vol. 143, 2005, pp. 37-55

Baillot, F., Durox, D., Ducruix, S., "Parametric response of a conical flame to acoustic waves," *Combustion Science and Technology,* Vol. 142, No. 1, 1999, pp. 91-109

Barenblatt, G. I., Zel'dovich, Ya. B., and Istratov, A. G., *Prikl. Mekh. Tekh. Fiz.*, No. 4, 21–26 (1962).

Bastiaansy, R. J. M, Vremanz, A. W., AND Pitsch, H., "DNS of lean hydrogen combustion with amelet-generated manifolds", Center for Turbulence Research, Annual Research Briefs 2007

Battles, B.E., and Hanson, R.K., "Laser-induced fluorescence measurements of NO and OH mole fraction in fuel-lean, high-pressure (1-10 atm) methane flames: fluorescence modeling and experimental validation," *Journal of Quantitative Spectroscopy and Radiative Transfer,* Vol. 54, No. 3, 1995, pp. 521-37

Bellows, B.D.1., Neumeier, Y.1., and Lieuweir, T.1., "Forced response of a swirling, premixed flame to flow disturbances," *Journal of Propulsion and Power,* Vol. 22, No. 5, 2006, pp. 1075-84

Birbaud, A.L., Durox, D., and Candel, S., "Upstream flow dynamics of a laminar premixed conical flame submitted to acoustic modulations," *Combustion and Flame,* Vol. 146, No. 3, 2006, pp. 541-552

Bisio, G., and Rubatto, G., "Sondhauss and Rijke oscillations- thermodynamic analysis, possible applications and analogies", Energy 24 (1999) 117–131

Boschek, E., Griebel, P., Erne, D., Jansohn, P., "Lean blow out limits and NOx emissions of turbulent, lean premixed, high pressure CH4/H2/AIR flames," Eighth International Conference on Energy for a Clean Environment: cleanair 2005 27-30 June, 2005 Lisbon – Portugal

Boschek, E., Griebel, P., Jansohn, P., "Fuel variability on turbulent, lean premixed flames at high pressures", Proceeding of GT2007, ASME Turbo Expo 2007: Power for Land, Sea and Air, May 14-17, 2007, Montreal, Canada

Boughanem, H., Trouve, A. *Proceedings of the Combustion Institute* 27 (1998) 971

Candel, S., "Combustion dynamics and control: progress and challenges," *Proceedings of the Combustion Institute*, Vol. 29, 1991, pp.561-606

Cheng, R.K., Littlejohn, D., Nazeer, N., Smith, K.O., "Laboratory studies of the flow field characteristics of low-swirl injectors for adaption to fuel-flexible turbines," *2006 ASME Turbo Expo, GT2006-90878*

Cheng, R.K., Yegian, D.T., Miyasato, M.M., Samuelsen, G.S., Benson, C.E., Pellizzari, R. and Loftus, P., "Scaling and development of Low-Swirl burners for low emission furnaces and boilers," *Proceedings of the Twenty-Eighth Symposium on Combustion,* The Combustion Institute, Pittsburgh, 2000, pp. 1305-1313

Chigier, N.A., Beer, J.M., "Velocity and static pressure distributions in swirling air jets issuing from annular and divergent nozzles," *Trans ASME J Basic Eng 86D*, 1964, 788-796

Cho, J.H., and Lieuwen, T.C., "Modeling the response of premixed flames to mixture ratio perturbations," *2003 ASME Turbo Expo,* Vol. 2, American Society of Mechanical Engineers, New York, NY 10016-5990, United States, Atlanta, GA, United States, 2003, pp. 67-76

Chu, B.T., "Mechanism of generation of pressure waves at flame fronts," *National Advisory Committee for Aeronautics -- Technical Notes,* 1956, pp. 20

Clanet, C., Searby, G., "First experimental study of the Darrieus-Landau instability," *Physical Review Letters*, 80, 1998, pp.3867-3870

Clavin, P., Pelce, P., He, L.T., "One-dimensional vibratory instability of planer flames in propagating in tubes," *J. Fluid Mech.*, Vol. 216, 1990, pp. 299-322

Coats, C.M., "Coherent structures in combustion," *Progress in Energy and Combustion Science*, Vol.22, 1996, pp.427-509

Coker, A., Neumeier, Y., Zinn, B.T., "Active instability control effectiveness in a liquid fueled combustor," *Combustion Science and Technology,* Vol. 178, No. 7, 2006, pp. 1251-1261

Conrad, T., Bibik, A., Shcherbik, D., "Control of the stability margin in a liquid fueled combustor using a "smart" fuel injector," *AIAA/ASME/SAE/ASEE 42nd Joint Propulsion Conference,* Vol. 6, American Institute of Aeronautics and Astronautics Inc., Reston, VA 20191-4344, United States, Sacramento, CA, United States, 2006, pp. 4775-4788

Crighton, D., Dowling, A., Ffowcs Williams, J., Heckle, M., and Leoppington, F., "Modern Methods in analytical acoustics", Springer Verlag, New York 1992

Culick, F.E.C., "Nonlinear behavior of acoustic waves in combustion chambers, Part I," Acta Astonautica, Vol. 47, No. 13, 1976, pp.715-734

Culick, F.E.C, "Combustion instabilities in propulsion systems," *American Society of Mechanical Engineers, Noise Control and Acoustics Division (Publication) NCA,* v 4, 1989, p 33-52

Culick, F.E.C, "Dynamics of combustion systems: fundamentals, acoustics, and control", A short course of lectures, 2001

Culick, F.E.C., and Yang, V., "Overview of combustion instabilities in liquid-propellant rocket engines," *Liquid Rocket Engine Combustion Instability,* Vol. 169, Progress in Astronautics and Aeronautics, AIAA, Washington, DC, USA, 1995

Culick, F.E.C., Unsteady Motions in Combustion Chambers for Propulsion Systems, NATO, AG-AVT-039, 2006

Culick, F.E.C., Burnley, V., and Swenson, G.,"Pulsed instabilities in solid-propellant rockets" Journal of Propulsion and Power, Vol. 11, No.4, 1995, pp. 657-665

Dabireau, F., Cuenot, B., Vermorel, O., and Poinsot, T., "Interaction of H2/O2 flames with inter walls", Combustion and Flame, 135 (2003) pp 123-133

Delataillade, A., Dabireau, F., Cuenot, B., and Poinsot, T., "Flame/wall interaction and maximum heat wall fluxes in diffusion burners", Proceeding of Combustion Institute, 29 (2002) pp 775-780

Denet, B., *Physical Review* E 55 (1997) 6911

Docquier, N., Belhalfaoui, S., Lacas, F., Darabiha, N., Rolon, C., "Experimental and numerical study of chemiluminescence in methane/air high pressure flames for active control applications," *Proceedings of the combustion institute*, Vol. 28, 2000, pp.1765-1774

Dowling, A.P., and Morgans, A.S., "Feedback control of combustion oscillations," *Annual Review of Fluid Mechanics,* Vol. 37, 2005, pp. 151-182

Dowling, A.P., and Stow, S. R, "Acoustic analysis of gas turbine combustors," *Journal of Propulsion and Power,* Vol. 19, 2003, pp. 751-764

Driscoll, J. F., "Turbulent premixed combustion: Flamelet structure and its effect on turbulent burning velocities", Progress in Energy and Combustion Science 34(2008) 91-134

Durbin, M.D., and Ballal, D.R., "Studies of lean blowout in a step swirl combustor", *Journal of Engineering for Gas Turbines and Power*, Vol. 118, No.1, 1996, pp.72-77

Durox, D., Ducruix, S., and Baillot, F., "Strong acoustic forcing on conical premixed flames," *Symposium (International) on Combustion,* Vol. 1, 1998, pp. 883-889

Durox, D., Schuller, T., and Candel, S., "Combustion dynamics of inverted conical flames," *Proceedings of the Combustion Institute,* Vol. 30, 2005, pp. 1717-24

Durox, D., Schuller, T., Noiray, N., Candel, S., "Experimental analysis of nonlinear flame transfer functions for different flame geometries," *Proceedings of the Combustion Institute,* Vol. 32, 2009

Duwig, C., Fuchs, L., Griebel, P., "Study of a confined turbulent jet: Influence of combustion and pressure," *AIAA Journal,* Vol. 45, No. 3, 2007, pp. 624-639

Eckbreth, A.C., Laser diagnostics for combustion temperature and species, Gordon and Breach Publishers, 1996

Emadi, M., Karkow, D., Salameh, T., Gohil, A., and Ratner, A., "Flame structure changes resulting from hydrogen-enrichment and pressurization for low-swirl premixed methane-air flames", International Journal of Hydrogen Energy (2012), doi:10.1016/ j.ijhydene.2012.04.017

Fleifil, M., Annaswamy, A.M., Ghoneim, Z.A., "Response of a laminar premixed flame to flow oscillations: a kinematic model and thermoacoustic instability results," *Combustion and Flame,* Vol. 106, No. 4, 1996, pp. 487-510

Fritsche, D., Furi, M., and Boulouchos, K., "An experimental investigation of thermoacoustic instabilities in a premixed swirl-stabilized flame," *Combustion and Flame,* Vol. 151, No. 1-2, 2007, pp. 29-36

Gauducheau JL, Denet B, Searby G. A numerical study of lean CH4/H2/air premixed flames at high pressure. Combust Sci Technol 1998;137:81–99.

Ghoniem, A.F., Annaswamy, A., Wee, D, Yi, T. and Park, Sungbae, "Shear flow driven combustion instability evidence simulation and modeling," *Proceedings of the Twenty-Ninth Symposium on Combustion*, The Combustion Institute, Sapporo, Japan, 2002, pp. 53-60

Ghoniem, A.F., Annaswamy, A., Park, S., and Sobhani, Z., "Stability and emissions control using air injection and H2 addition in premixed combustion", Proceedings of the Combustion Institute 30 (2005) 1765–1773

Ghoniem, A.F., Park, S., Wachsman, A., "Mechanism of combustion dynamics in a backward-facing step stabilized premixed flame," *30th International Symposium on Combustion,* Vol. 30 II, United Kingdom, Chicago, IL, United States, 2005, pp. 1783-1790

Giacomazzi, E., Picchia F. R. And Arcidiacono, N., "A review of chemical diffusion: Criticism and limits of simplified methods for diffusion coefficient calculation", Combustion Theory and Modelling, (2007)12:1, 135-158

Goy, C., James, S., and Rea, S., "Monitoring combustion instabilities: E.ON UK's experience". Chapter 8. In: Lieuwen T, Yang V, editors. Combustion instabilities in gas turbine engines: operational experience, fundamental mechanisms, andmodeling. Progress in Astronautics and Aeronautics 2005;210:163–75.

Griebel,P., Siewert, P., Jansohn, P., "Flame characteristics of turbulent lean premixed methane/air flames at high pressure: Turbulent flame speed and flame brush thickness", *Proceedings of the Combustion Institute*, 31, 2007, 3083-3090

Griffiths, A., Yazdabadi, P., and Syred, N., "Alternate eddy shedding set up by the nonaxisymmetric recirculation zone at the exhaust of a cyclone dust separator" Journal of Fluids Eng. (1998) 120(1):193– 199

Guo, H., Tayebi, B., Glaizzi, C., and Escudie, D., "Burning rates and surface characteristics of hydrogen-enriched turbulent lean premixed methane-air flames", International Journal of Hydrogen Energy 35(2010) pp11343-48

Gupta, A.K., Lilley, D.G., Syred, N., Swirl Flows, Abacus Press, 1984

Gutmark, E., Parr, T.P., Parr, D.M. and Schadow, K.C., "Planar imaging of vortex dynamics in flames," *Journal of Heat Transfer*, Vol. 111, 1989, pp. 148-155

Halter, F., Chauveau, C., Djebaili-Chaumeix, N., and Gokalp, I., "Characterization of the effects of pressure and hydrogen concentration on laminar burning velocities of methane–hydrogen–air mixtures", Proceedings of the Combustion Institute 30(2005) pp201–208

Halter F, Chauveau C, Gökalp I. Characterization of the effects of hydrogen addition in premixed methane/air flames. International Journal of Hydrogen Energy 2007;32:2586-92

Han, I., and Huh, K., "Roles of displacement speed on evolution of flame surface density for different turbulent intensities and Lewis numbers in turbulent premixed combustion", Combustion and Flame 152(2008) pp194-208

Hardalupas Y., and Orain, M., "Local measurements of the Time-Dependent heat Release rate and equivalence ratio using chemiluminescent emission from a flame," *Combustion and Flame*, Vol. 139, 2004, pp188-207

Hassel, E.P., and Linow, S., "Laser diagnostics for studies of turbulent combustion," *Meas. Sci. Technol.*, Vol.11, 2000, pp37-57

Haumann, J., and Leipertz, A., "Flame-temperature measurements using the Rayleigh scattering photon-correlation technique", Optics Letters, Vol. 9, Issue 11, pp. 487-489 (1984)

Hawkes, E., and Chen, J., "Direct numerical simulation of hydrogen-enriched lean premixed methane-air flames", Combustion and Flame 138(2004) pp242-58

Huang, Y., "Combustion dynamics of swir-stabilized lean premixed flames in an acoustically-driving environment" PhD thesis, University of Iowa, 2009

Huang, Y., Ratner, A., "Experimental investigation of thermoacoustic coupling for low-swirl stabilized lean premixed flames," *Journal of Propulsion and Power*, in press, 2009

Huang, Y., "Modeling and simulation of combustion dynamics in Lean-Premixed Swirl-Stabilized gas-turbine engines," Thesis, Pennsylvania State University, 2003

Huang, Y., and Yang, V., "Effect of swirl on combustion dynamics in a lean-premixed swirl-stabilized combustor," *Proceedings of the Combustion Institute,* Vol. 30, 2004, pp. 1775-82

Huang, Y., Wang, S.W., and Yang, V., "A systematic analysis of combustion dynamics in a Lean-Premixed Swirl-Stabilized combustor," *AIAA Journal*, Vol. 44, 2006, pp. 724-740

Hult, J., Burns, I.S., and Kaminski, C.F., "Two-line atomic fluorescence flame thermometry using diode lasers," *Proceedings of the Combustion Institute,* Vol 30, 2005, pp 1535-1543

Johnson, M., Littlrjohn, D., Nazeer, W., Smith, K., and Cheng, R., "A comparison of the flowfields and emissions of high-swirl injectors and low-swirl injectors for lean premixed gas turbines" , Proceedings of the Combustion Institute 30 (2005) 2867–2874

Kang, D.M., Measurements of combustion dynamics with laser-based diagnostic techniques, Thesis, California Institute of Technology, 2006

Kang, D.M., Culick, F.E.C, Ratner, A., "Combustion dynamics of a Low-Swirl combustor", *Combustion and Flame*, Vol. 151, 2007, pp 412-425

Kang, D.M., Fernandez, V., and Ratner, A., "Measurements of fuel mixture fraction oscillations of a turbulent jet non-premixed flame", Combustion and Flame 156 (2009) 214–220

Kaskan, W.E., and Noreen, A.E., "High-frequency oscillations of flame held by bluff body," *American Society of Mechanical Engineers -- Meeting A-66,* American Society of Mechanical Engineers (ASME), 1954, pp. 14

Katharina, K., Meier, U., Brigitte, A., "Laser-induced fluorescence study of OH in flat flames of 1-10 bar compared with resonance CARS experiments," *Applied Optics*, Vol. 29, No. 10, 1990, pp 1560-1569

Keller, J.J., "On the Interpretation of Vortex Breakdown," *AIAA Journal*, Vol.33, No.12, 1995, pp. 2280-2287

Kendrick, D., Anderson, J., and Sowa, W.,"Acoustic sensitivity of lean premixed fuel injectors in a single nozzle rig" ASME, Paper 98-GT-382, 1998

Kiefer, J., Li, Z.S., Zetterberg, J., Bai, X.S., Alden, M., "Investigation of local flame structures and statistics in partially premixed turbulent jet flames using simultaneous single-shot CH and OH Planar Laser-Induced Fluorescence imaging," *Combustion and Flame*, Vol., 154, 2008, pp.802-818

Kobayashi, H., "Experimental study of high-pressure turbulent premixed flames", Experimental Thermal and Fluid Science 26(2002) pp375-87

Kohse-Hoinghaus. K., Barlow, R.S., Alden, M., and Wolfrum, J., "Combustion at the focus: laser diagnostics and control," *Proceedings of the Combustion Institute*, Vol. 30, 2005, pp 89-123

Kojima, J., Ikeda, Y., and Nakajima, T., "Basic aspects of OH(A), CH(A), and C2(d) chemiluminescence in the reaction zone of laminar methane-air premixed flames," *Combustion and Flame,* Vol. 140, No. 1-2, 2005, pp. 34-45.

Kornilov, V.N., Schreel, K.R.A.M., and De Goey, L.P.H., "Experimental assessment of the acoustic response of laminar premixed Bunsen flames," *31st International Symposium on Combustion,* Vol. 31 I, United Kingdom, Heidelberg, Germany, 2007, pp. 1239-1246

Kulsheimer, C., Buchner, H., "Combustion Dynamics of Turbulent Swirling Flames," *Combustion and Flame*, Vol. 131, 2002, pp. 70-84

Landau, D., "Factors influencing wear in machines," *Machine Design,* Vol. 16, No. 9, 1944, pp. 105-108

Lachaux, T., Halter, F., Chauveau, C., Gokalp, I., and Shepherd, I., " Flame front analysis of high-pressure turbulent lean premixed methane–air flames", Proceeding of Combustion Institute 30(2005) pp819–826

Law, C.K, "Combustion Dynamics" Cambridge, 2006

Law, C.K., and Sung, C.J., "Structure, aerodynamcs, and geometry of premixed flamelets," *Prog. Energy Combust. Sci*, Vol. 26, 2000, pp. 459-505

Law, C.K., "Structure, and Limit phenomena of laminar flames at elevated pressure," *Combustion. Sci. Tech*., 178, pp. 335-360

Lawn, C.J., Evesque, S., and Polifke, W., "A model for the thermoacoustic response of a premixed swirl burner, part one: acoustic aspects," *Combust. Sci. and Tech.*, Vol. 176, 2004, pp.1331-1358

Lee, C. L., Jou, C.J.G., Tsai, C.H., "Improvements in the performance of a medium-pressure-boiler through the adjustment of inlet fuels in a refinery plant," *Fuel,* Vol. 86, No. 5-6, 2007, pp. 625-631

Lee, D., and Lieuwen, T.C., "Premixed flame kinematics in a longitudinal acoustic field," *Journal of Propulsion and Power,* Vol. 19, No. 5, 2003, pp. 837-846

Lee, J.G., and Santavicca, D.A., "Experimental diagnostics for the study of combustion instabilities in lean premixed combustors," *Journal of Propulsion and Power,* Vol. 19, No. 5, 2003, pp.735-750

Lee, S.Y., Seo, S., Broda, J.C., Pal, S., and Santoro, R.J., "An experimental estimation of mean reaction rate and flame structure during combustion instability in a lean premixed gas turbine combustor," *Proceedings of the Combustion Institute,* Vol. 28, 2000, pp. 775-782

Lee. J.G., Lee, T.W., Nye, D.A., and Santavicca, D.A., "Lewis number effects on premixed flames interacting with turbulent Karman vortex streets," *Combustion and Flame,* Vol. 100, 1995, pp.161-168

Li, H., Zhou, X., Jeffries, J.B., Hanson, R.K., "Sensing and control of combustion instabilities in swirl-stabilized combustors using Diode-Laser absorption," *AIAA Journal,* Vol. 45, No. 2, 2007, pp. 390-398

Lieuwen, T., "Modeling premixed combustion-acoustic wave interactions: a review," *Journal of Propulsion and Power*, Vol.19, 2003, pp.765-781

Lieuwen, T., and Zinn, B.T., "On the experimental determination of combustion process driving in an unstable combustor," *Combustion Science and Technology,* Vol. 157, No. 1-6, 2000, pp. 111-127

Lieuwen, T., Neumeier, Y., and Zinn, B.T., "Role of unmixedness and chemical kinetics in driving combustion instabilities in lean premixed combustors," *Combustion Science and Technology,* Vol. 135, No. 1-6, 1998, pp. 193-211.

Lieuwen, T.C. and Yang, V.(eds), Combustion Instabilities in Gas Turbine Engines: Operational Experience, Fundamental Mechanisms, and Modeling, AIAA Progress in Astronautics and Aeronautics, Vol. 210,2005, 657 pages

Lieuwen, T.C., "Statistical characteristics of pressure oscillations in a premixed combustor," *Journal of Sound and Vibration,* Vol. 260, No. 1, 2003, pp. 3-17

Littlejohn, D., Majeski, A., Tonse, S., Castaldini, C., and Cheng, R.K., "Laboratory investigation of an ultralow NO_x premixed combustion concept for industrial boilers" Proceedings of the Combustion Institute, Volume 29, 2002/pp. 1115–1121

Littlejohn, D., and Cheng, R.K., "Fuel effects on a low-swirl injector for lean premixed gas turbines," *31st International Symposium on Combustion,* Vol. 31 II, Elsevier Ltd, Oxford, OX5 1GB, United Kingdom, Heidelberg, Germany, 2007, pp. 3155-3162

Littlejohn, D., Cheng, R.K., Noble, D.R., and Lieuwen, T., "Laboratory investigation of low-swirl injectors operating with syngases", Journal of Engineering for Gas Turbine and Power, Vol. 132, 011502, 2010

Locke, R.J., Hicks, Y.R., Anderson, R.C., "Two-dimensional imaging of OH in a lean burning high pressure combustor," NASA, Washington, DC, USA, 1995

Mandilas, C., Ormsby, M., Sheppard, C., and Woolley, R., "Effects of hydrogen addition on laminar and turbulent premixed methane and iso-octane-air flames" Proceedings of the Combustion Institute 31(2007) pp1443–50

Marble, F. E., and Broadwell, J. E., "The coherent flame model for turbulent chemical reactions", Tech. Rep. TRW-9-PU, Project Squid, 1977

Markstein, G.H., Guenoche, H., and Putnam, A.A., "Nonsteady flame propagation," *AGARDograph 75,* 1964, pp. 328

Matalon, M., "Intrinsic flame instabilities in premixed and nonpremixed combustion," *Annu. Rev. Fluid Mech.*, Vol. 39, 2007, pp.163-191

Matalon, M., and Matkowsky, B.J., "On the stability of plane and curved flames," *SIAM Journal on Applied Mathematics,* Vol. 44, No. 2, 1984, pp. 327-43

Matveev, K.I., and Culick, F.E.C., "A model for combustion instability involving vortex shedding," *Combustion Science and Technology,* Vol. 175, No. 6, 2003, pp. 1059-1083

Mcintosh, A.C., "Pressure disturbances of different length scales interacting with conventional flames," *Combust. Sci. and Tech.*, 1991, Vol. 75, pp. 287-309

Najm, H.N., and Ghoniem, A.F., "Coupling between vorticity and pressure oscillations in combustion instability," *Journal of Propulsion and Power,* Vol. 10, No. 6, 1994, pp. 769-776

Nazeer, W., Smith, K., Sheppard, P., Cheng, R., and Littlejohn, D., "Full scale testing of a low swirl fuel injector concept for ultra-low NO_x gas turbine combustion system", Proceedings of GT2006, ASME Turbo Expo 2006: Power for Land Sea and Air May 8-11, 2006, Barcelona, Spain

Nicoud, F., Poinsot, T., "Thermoacoustic instabilities: Should the Rayleigh criterion be extended to include entropy changes?", Combustion and Flame 142 (2005) 153–159

Nori, V., and Seitzman, J., "Evaluation of Chemiluminescence as a Combustion Diagnostic under Varying Operating Conditions", 46th AIAA Aerospace Sciences Meeting and Exhibit, 7 - 10 January 2008, Reno, Nevada

Paschereit, C.O., and Gutmark, E., "Active control of combustion instabilities in gas turbine burners," *2006 ASME 51st Turbo Expo,* Vol. 1, American Society of Mechanical Engineers, New York, NY 10016-5990, United States, Barcelona, Spain, 2006, pp. 161-171

Paschereit, C.O., Gutmark, E., and Weisenstein, W., "Coherent structures in swirling flows and their role in acoustic combustion control," *Physics of Fluids,* Vol. 11, No. 9, 1999, pp. 2667-2678

Petchenko, A., Bychkov, V., Eriksson, L.E., "Flame propagation along the vortex axis," *Combustion, Theory and Modelling,* Vol. 10, No. 4, 2006, pp. 581-601

Peters, N., Turbulent Combustion, Cambridge, 2000

Pocheau, A., *Physical Review* E 49 (1994) 1109

Poinsot, T.J., Trouve, A.C., Veynante, D.P., "Vortex-Driven Acoustically Coupled Combustion Instabilities," *Journal of Fluid Mechanics,* Vol. 177, 1987, pp. 265-292

Poinsot, T., Veynante, D., Theoretical and Numerical Combustion (Second Edition), Edwards, 2005

Pope, S.B., Turbulent flows, Cambridge, 2005

Pun, W., Measurements of Thermo-Acoustic Coupling, Thesis, California Institute of Technology, 2001

Pun, W., Palm, S.L., and Culick, F.E.C., "Combustion dynamics of an acoustically forced flame," *Combustion Science and Technology,* Vol. 175, No. 3, 2003, pp. 499-521

Putnam, A.A., General considerations of autonomous combustion oscillations, The MacMillan Co., New York

Rayleigh, J.W.S., The theory of sound Vol. II, Dover publications, 1945

Renard, P.H., Thevenin, D., Rolon, J.C., Candel, S., "Dynamics of flame/vortex interactions," *Progress In Energy and Combustion Science*, Vol. 26, 2000, pp. 225-282

Richards, G., and Straub, D., "Passive control of combustion dynamics in stationary gas turbines" Journal of Propulsion and Power, 19(2003) 822-829

Roberts, W.L., Driscoll, J.F., Drake, M.C., and Goss, L.P., "Images of quenching of a flame by a vortex-to quantity regimes of turbulent combustion," *Combustion and Flame*, Vol. 95, 1993, pp.58-69

Roberson, J., and Crowe, C., Engineering fluid mechanics, Houghton Mifflin, New York, 1993

Rodriguez-Martinez, V.M., Dawson, J.R., O'Doherty, T., and Syred, N., "Low-frequency combustion oscillations in a swirl burner/furnace," *Journal of Propulsion and Power*, Vol. 22, No. 1, pp217-221

Rogers, D.E., and Marble, F.E., "Mechanism for high-frequency oscillation in ramjet combustor and afterburners," *Jet Propulsion,* Vol. 26, No. 6, 1956, pp. 456-462

Roux, S., Lartigue, G., Poinsot, T., Meier, U., Berat, C., "Studies of mean and unsteady flow in a swirled combustor using experiments, acoustic analysis, and large eddy simulations," *Combustion and Flame*, Vol., 141, 2005, pp. 40-54

Samaniego, J.M, Yip, B., Poinsot, T. and Candel, S., "Low-frequency combustion instability mechanisms in a side-dump combustor," *Combustion and Flame*, Vol. 94, No.4, 1993, pp. 363-380

Santhanam, V., Knopf, F.C., Acharya, S., and Gutmark, E., "Fluorescence and temperature measurements in an actively forced swirl-stabilized spray combustor," *Journal of Propulsion and Power*, Vol. 18, No. 4, 2002, pp855-865

Scarinci, T., Freeman, C., and Day, I., "Passive control of combustion instability in a low emissions aeroderivative gas turbine," *2004 ASME Turbo Expo,* Vol. 1, American Society of Mechanical Engineers, New York, NY 10016-5990, United States, Vienna, Austria, 2004, pp. 487-499

Schadow, K.C., and Gutmark, E., "Combustion instability related to vortex shedding in dump combustors and their passive control," *Progress in Energy and Combustion Science,* Vol. 18, No. 2, 1992, pp. 117-132

Schildmacher, K.-U. , Hoffmann, A., Selle, L., Koch, R., Schulz, C., Bauer, H.-J., Poinsot, T., Krebs, W., Prade, B., "Unsteady flame and flow field interaction of a premixed model gas turbine burner," *Proceedings of the Combustion Institute*, 31, 2007, 3197-3205

Seitzman, J.M., Kychakoff, G., and Hanson, R.K., "Instantaneous temperature field measurements using planar laser-induced fluorescence," *Optics Letters,* Vol. 10, No. 9, 1985, pp. 439-41

Shanbhogue, S.J., Plaks, D.V., and Lieuwen, T., "The K-H instability of reacting, acoustically excited bluff-body shear layers," *43rd AIAA/ASME/SAE/ASEE Joint Propulsion Conference,* Vol. 7, American Institute of Aeronautics and Astronautics Inc., Reston, VA 20191-4344, United States, Cincinnati, OH, United States, 2007, pp. 6631-6647

Shepherd, I.G., and Cheng, R.K., "The burning rate of premixed flames in moderate and intense turbulence," *Combustion and Flame*, Vol. 127, 2001, pp. 2066-2075

Sivashinsky, G.I., "Diffusional-Thermal Theory of Cellular Flames," *Combustion Science and Technology,* Vol. 15, No. 3-4, 1977, pp. 137-146

Smith, D.A., and Zukoski, E.E., "Combustion instability sustained by unsteady vortex combustion," *AIAA/SAE/ASME/ASEE 21st Joint Propulsion Conference,* AIAA, New York, NY, USA, Monterey, CA, USA, 1985, pp. 9

Soika, A., Dinkelacker, F., and Leipertz, A., "Pressure influence on the flame front curvature of turbulent premixed flames: comparison between experiment and theory", Combustion and Flame 132(2003) pp451-62

Sung, H.G., "Combustion dynamics in a model lean-premixed gas turbine with a swirl stabilized injector," *Journal of Mechanical Science and Technology,* Vol. 21, No. 3, 2007, pp. 495-504

Sutton, G., and Biblarz, O., "Rocket Propulsion Elements", Wiley-Interscience (2000)

Swift, G.W., Thermoacoustics: a unifying perspective for some engines and refrigerators, Acoustical Society of America, 2002

Syred, N., "A review of oscillation mechanisms and the role of the precessing vortex core (PVC) in swirl combustion systems," *Progress in Energy and Combustion Science,* Vol. 32, No. 2, 2006, pp. 93-161

Syred, N., and Beer, J.M., "The damping of precessing vortex cores by combustion in swirl generators," *Proceedings of the 3rd Colloquium on Gasdynamics of Explosions and Reactive Systems,* Vol. 17, Marseille, France, 1972, pp. 783-801

Tang, B., and Chan, C., "Simulation of flame surface density and burning rate of a premixed turbulent flame using contour advection", Combustion and Flame 147 (2006) 49–66

Taupin, B., Cabot, G., Martins, G., Vauchelles, D., and Boukhalfa, A., "Experimental study of stability, structure and CH* chemiluminescence in a pressurized lean premixed methane turbulent flame," *Combust. Sci. and Tech.,* Vol. 179, 2007, pp 117-136

Temkin, S., Elements of Acoustics, Wiley, New York, 1981.

Thumuluru, S.K., Bobba, M.K., and Lieuwen, T., "Mechanisms of the nonlinear response of a swirl flame to harmonic excitation," *2007 ASME Turbo Expo,* Vol. 2, American Society of Mechanical Engineers, New York, NY 10016-5990, United States, Montreal, Que., Canada, 2007, pp. 721-731

Turns, S.R., An introduction to Combustion, Mcgraw Hill, 2000

Turrell, MD, Stopford, PJ, Syed, K, Buchanan, E., "CFD simulations of the flow within and downstream of high swirl lean premixed gas turbine combustors," *Proceedings ASME turbo-expo 2004*, vol.1, pp.31-38

Venkataraman, K.K., Preston, L.H., Simons, D.W., Lee, B.J., Lee, J.G. and Santavicca, D.A., "Mechanism of combustion instability in a lean premixed dump combustor," *Journal of Propulsion and Power*, Vol.15, 1999, pp. 909-917

Wang, H., "Oscillation and extinction in flames," PhD thesis, Princeton University, 2007, pp. 6-10

Wangher, A., Searby, G., Quinard, J., "Experimental investigation of the unsteady response of premixed flame fronts to acoustic pressure waves," *Combustion and Flame*, Vol. 154, 2008, pp. 310-318

Wolfrum, J., "Lasers in combustion: from basic theory to practical devices," *Proceedings of the Combustion Institute*, 27, 1998, 1-41

Williams, F., Combustion Theory, Addison-Wesley Pub., Reading, MA, 1985

Wunenburger, R., Andreotti, B., and Petitjeans, P., "Influence of precession on velocity measurements in a strong laboratory vortex", Experiments in Fluids (27) Springer-Verlag (1999)

Yazdabadi, P., Griffiths, A., and Syerd, N., Characterization of the PVC phenomena in the exhaust of a cyclone dust separator", Experiments in Fluids, (1994) Vol. 17, pp 84-95

Yilmaz, I., Ratner, A., Ilbas, M., and Huang, Y., "Experimental investigation of thermoacoustic coupling using blended hydrogen–methane fuels in a low swirl burner", International Journal of Hydrogen Energy 35(2010) pp329-36

Zhang, Y., Ishzuka, S., Zhu, H., Kee, R.J., "Effects of stretch and pressure on the characteristics of premixed swirling tubular methane-air flames," *Proceedings of the Combustion Institute*, 33, 2009

Zhu, S., and Acharya, S., "Effects of hydrogen addition on swirl-stabilized flame properties", Proceedings of ASME Turbo Expo (2010) No. 23686

Zinn, B.T., "Combustion instabilities: problems, solutions, and research needs." *Chemical and Physical Processes in Combustion: 1986 Fall Technical Meeting.* Combustion Inst, Pittsburgh, PA, USA, San Juan Bautista, PR, 1987, pp. 1-12

Zinn, L.T., "A mechanism of combustion instability in lean premixed gas turbine combustors," *Journal of Engineering for Gas Turbines and Power,* Vol. 123, No. 1, 2001, pp. 182-189

Zinn, B.T., and Powell, E.A.,"Non-linear combustion instabilities in liquid-propellant rocket engines" Proceeding of Combustion Institute, Pittsburgh, PA, Vol. 13,1970